Cell-Cell and Cell-Medium Interactions in the Growth of Mouse Embryonic Stem Cells

by

Nikhil V. Mittal

B.Tech. Engineering Physics
Indian Institute of Technology, Mumbai, 2000
S.M. Physics
Massachusetts Institute of Technology, 2003

Submitted to the Department of Physics in partial fulfillment of the requirements for the degree of

Doctor of Philosophy
at the
Massachusetts Institute of Technology

June 2010

Signature of author:_____
Department of Physics
May 14, 2010

Certified by:_____
Professor Joel Voldman
Department of Electrical Engineering and Computer Science
Thesis Supervisor

Certified by:_____
Professor Alexander van Oudenaarden
Department of Physics
Thesis Co-supervisor

Accepted by:_____
Professor Krishna Rajagopal
Associate Head for Education, Department of Physics

Contents

Cell-Cell and Cell-Medium Interactions in the Growth of Mouse Embryonic Stem Cells

by

Nikhil V. Mittal

Submitted to the Department of Physics on May 14th 2010 in partial fulfillment of the requirements for the degree of Doctor of Philosophy at the Massachusetts Institute of Technology

Abstract

Embryonic stem cells serve as powerful models for the study of development and disease and hold enormous potential for future therapeutics. Due to the potential for embryonic stem cells (ESCs) to provide a variety of tissues for use in regenerative medicine, there has been great interest in the identification of factors that govern the differentiation of ESCs into specific lineages. Much of this research builds on previous studies of the role of intercellular signaling in the specification of various cell types in the developing embryo. However, relatively little work has been done on understanding the role of cell-cell communication in the self-renewal of ESCs.

In the first part of this thesis I describe the development and testing of new devices for studying intercellular signaling - the nDEP microwell array and the Bio Flip Chip (BFC). We used the BFC to show that cell-cell interaction improves the colony-forming efficiency and the self-renewal of mouse ESCs. Further, we demonstrate that the interaction is at least partly diffusible.

In the next part of the thesis I describe our use of more traditional assays to validate the results obtained using the BFC and to further explore the role of diffusible signaling in the survival of mouse ESCs. We demonstrate the existence of an optimal density for 2-day culture of mouse ESCs. Further, we demonstrate that the increase in growth with plating density (10^3-10^4 cells/cm^2) is at least partly due to the existence of one or more survival-enhancing autocrine factor(s) in mouse ESC cultures, and that one of these factors is Cyclophilin A.

Finally, we demonstrate that changes in the low molecular weight composition of the medium are likely responsible for the decrease in growth at high plating densities (>10^4 cells/cm^2). We use a numerical model to show that competition between the positive effect (on growth) of autocrine survival factors and the negative effect of nutrient depletion can account for the observed optimal growth density. Our study provides new insight into the processes underlying, and optimization of, growth in cell types that lack contact inhibition such as cancer cells and stem cells.

Thesis Supervisor: Joel Voldman
Title: Associate Professor of Electrical Engineering and Computer Science

Chapter 1: Introduction

This thesis describes the influence of secreted factors, nutrient depletion, and metabolite accumulation on the growth of mouse embryonic stem cells in culture. In this first introductory chapter I will first describe some of the factors that motivated this study. I will begin by providing some background on cell growth and embryonic stem cells.

1.1 Growth of cells in culture

The growth of cells in culture has been studied quantitatively for almost 80 years. Oscar Richards[1] appears to be the first person to attempt to fit microbial (yeast) growth data with numerical models (1928). However, Jacques Monod[2] was the first person to develop mechanistic models of microbial (bacterial) growth that accounted for the effects of nutrient concentrations. In particular, he explored the existence and effects of a "limiting nutrient" in the medium, and showed that the growth of bacteria is well described by the equation: $\frac{d}{dt}n = \mu_m \left(\frac{s}{s+K_s}\right) n$, where n is the concentration of cells, μ_m is the maximum growth rate, s is the concentration of the limiting nutrient, and K_s is the nutrient concentration which supports half the maximum specific growth rate.

Starting around 1990, with the advent of packaged frozen foods, there was much greater interest in understanding the growth of cells, especially bacteria such as *Listeria monocytogenes* (the bacterium responsible for listeriosis, a potentially lethal condition) on various kinds of (food) substrates[3]. Additionally, around the same time, there was growing interest within the biotechnology industry, in the growth of cells for the production of proteins for therapeutic and diagnostic purposes[4, 5]. This production of proteins required the use of large bioreactors and led to increased interest in the use of models to optimize the yield of proteins in these reactors[6]. Most of these models were still Monod-type models except that the availability of computers made it much easier to simulate the effects of depletion of more than one nutrient. Typically, glucose and glutamine were found to be the limiting nutrients. Additionally, models incorporated the effects of the accumulation of metabolites such as lactate and ammonia in the medium, and the (usually) inhibitory effects of these metabolites on cell growth[6]. Such models appear to sufficient for describing the growth of certain types of cells such as bacteria, yeast, Chinese hamster ovary (CHO) cells and hybridomas (the two types of cells often used for producing proteins) etc. However, for most mammalian cells, in addition to nutrient depletion, cell-cell communication/signaling is often an important modulator of cell growth. In the next section I will discuss the various types of cell-cell communication.

1.2 Communication between cells

Cells interact with one another both *in vivo* and *in vitro*. According to the Gene Ontology (GO) database, as of this writing, 454 of 11570 (4%) currently annotated human proteins are directly involved in cell-cell signaling[a]. Cell-cell interactions can be classified into two types:

(i) **Diffusible signaling**. In this type of signaling, one cell produces a molecule (ligand) which is subsequently released from its surface. The ligand then diffuses in the medium or through the extracellular matrix (hence the name diffusible signaling), until it is bound by a receptor molecule on the surface of the same cell, or another cell. The capture of the ligand by the same cell as it is released from is referred to as autocrine capture, while capture by a receptor on a different cell is called paracrine capture. The ligand is sometimes also referred to as a soluble factor, and this type of signaling is therefore also known as soluble signaling.

Autocrine signaling was originally studied in the context of cancer. In the 1980s an autocrine model for cancer growth was widely investigated – i.e. a model that postulated that cancers were caused by cells responding to an excess of growth factors (GFs) that they secrete themselves. This hypothesis is usually ascribed to Sporn and Todaro[7]. One known oncogene, the *sis* oncogene, encodes a protein similar to a growth factor, the platelet-derived growth factor (PDGF) and produces cancers via this mechanism[8]. Some cancers are due to overproduction of GF receptors (Her2 in some breast cancers) which make these cells proliferate rapidly in response to normal levels of growth factors. However, many oncogenic mutations are in proteins downstream from growth factor receptors.

Autocrine signaling via growth factors can modulate the growth rate in two ways[8-10]. The total growth rate is the difference between the rate at which cells divide (proliferation rate), and the rate at which cells die (death rate). Growth factors typically increase the proliferation rate and/or decrease the death rate. Most mammalian cells require the presence of growth factors in the early G1 phase of the cell cycle in order to proceed to the S phase. This mechanism links growth factor concentration and proliferation rate, i.e., growth factors are required for mitosis and therefore such required growth factors are referred to as mitogens. However, in mammalian cells, there appears to be cross-wiring between pathways regulating the cell-cycle and pathways that trigger cell death[9, 10]. As a result, growth factors can also affect the death rate of cell[9, 10].

Paracrine signaling plays a very important role in development where gradients of secreted factors are used to create various regions in an initially homogenous embryo[8]. Paracrine signaling may also play a vital role in the regulation of adult stem cells by niche cells[11] – it is thought that adult stem cells receive cues from surrounding cells that tell them when they need to produce more cells to replace dead cells in the tissue. Endocrine signaling refers to a subset of paracrine signaling where cells from one organ produce a factor that cells in another organ respond to.

[a] The GO database uses the following definition for cell-cell signaling: Any process that mediates the transfer of information from one cell to another. In the mouse genome, 295 of 11165 annotated genes are involved in cell-cell signaling.

(ii) **Contact signaling.** Contact signaling can be further sub-divided into two types –

a. **Signaling through gap junctions.** Gap junctions provide channels through which two cells in contact can exchange small molecules and ions (generally < 1.5 kDa)[12]. The channels consist of two connexons, which are each made up of six connexin proteins (Figure 1.1). In mammals, more than 20 kinds of connexins have been identified. Gap junctional communication is particularly important in the heart, where it serves to transmit ions so as to induce the coordinated contraction of cells[13].

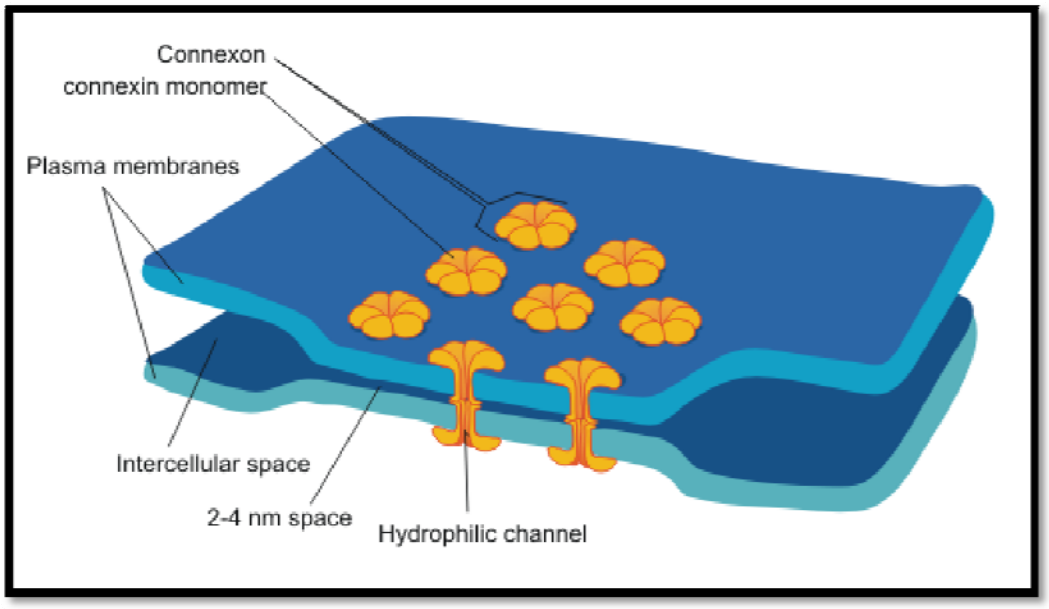

Figure 1.1 Schematic of gap junctions between two cells. Each junction consists of two connexons which are comprised of six connexin molecules each. Image courtesy of Mariana Ruiz (Wikicommons).

b. **Signaling via cadherin molecules.** Cadherins are the molecules that hold cells together. It is these molecules that are believed to be responsible for the well-known phenomenon of contact inhibition seen in cultures of endothelial and epithelial cells[14]. A recent study has shown that some cadherins do this by inhibiting the activity of epidermal growth factor receptors, which are found to be closely associated with cadherins[15]. The name "cadherin" derives from the fact that these molecules need the presence of calcium ions to perform their adhering function.

To summarize, as regards growth in particular, two types of intercellular cell signaling are important modulators: autocrine signaling via growth factors often provides a positive feedback effect on growth, and cadherin interactions often lead to growth inhibition.

In particular, we have investigated the role of cell-cell signaling in the growth of embryonic stem cells (though some results from our studies likely apply to growth in other cell types as well). In the next section I will describe some of the basic properties of embryonic stem cells, and previous work on their growth.

1.3 Embryonic stem cells

Embryonic stem cells (ESCs) are cells that have the potential of being able to produce any cell type in the adult animal. This property is referred to as pluripotency. These cells are derived from the inner cell mass of an early stage embryo, called the blastocyst (Figure 1.2). Human embryos reach the blastocyst stage 4-5 days after fertilization, and consist of 50-150 cells. ESCs have been isolated in a number of different organisms – while mouse ESCs (mESCs) were first isolated in 1981[16, 17], human ESCs (hESCs) were first isolated in 1998[18].

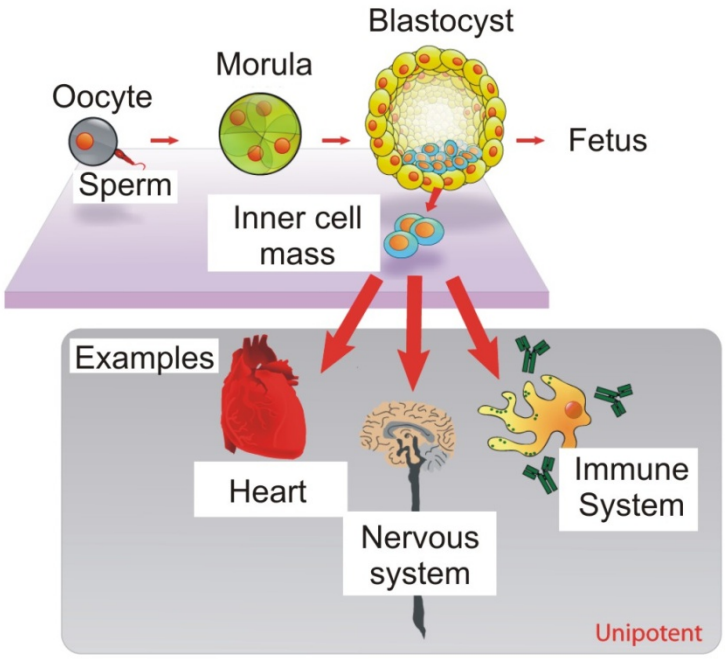

Figure 1.2 ESC derivation and properties. The fertilization of an oocyte by a sperm cell leads to the formation of a zygote. The zygote divides rapidly to form a morula, and then a blastocyst by day 4-5 in humans. The blastocyst consists of two types of cells – inner cells (on the inside) and trophoblast cells (on the outside). Embryonic stem cells are derived from the inner cell mass of a blastocyst. Embryonic cells are pluripotent i.e. they can form any cell type in the adult animal via a process called differentiation. However, ESCs cannot generate the whole organism without the aid of trophoblast cells. Only cells in the morula can form the whole organism and are referred to as totipotent cells. Figure courtesy of Mike Jones (Wikicommons).

ESCs generate organ-specific cells such as neurons, cardiomyocytes etc. via a process called differentiation or commitment. Cells that are partially committed (relative to ESCs) will be able to form some subset of cell types found in the adult animal and are referred to as multipotent cells. Cells that are completely committed will either not divide, or divide to form daughter cells with the same phenotype as the parent (unipotent cells). While ESCs can differentiate to form various cell types, they can also divide to form two daughter ESCs, a process referred to as self-renewal. Self-renewal is obviously crucial for the expansion of ESCs while maintaining their pluripotency.

Given that there are ~36000 known (mouse) genes as of this writing, a complete molecular-level description associated with any state of a cell is challenging to define. Pluripotency is no exception. Several studies have tried to obtain a “molecular signature” associated with pluripotency (for example,

Ivanova *et al.*[19] and Ramalha Santos *et al.*[20]) by comparing the transcriptional profile of ESCs with committed cells such as bone marrow cells using microarrays. Several hundred genes were found to be differentially expressed by ESCs. However, the candidate genes obtained from such experiments will have to be validated. Additionally, the overlap between candidate genes determined by different studies is far from complete[21]. Finally, a recent study has indicated that several proteins are expressed differentially by ESCs as compared to committed cells, but there are no significant differences in RNA concentrations indicating that post-translational regulation may be important for maintenance of a pluripotent state[22].

Nevertheless, smaller-scale studies have implicated a large number of genes as being required for the maintenance of pluripotency. Perhaps not surprisingly, almost all major signal transduction pathways seem to play a role (reviewed in Liu *et al.*[23]). For historical reasons, one pathway that has received considerable attention is the Stat3 pathway. mESCs were initially propagated using a feeder layer consisting of embryonic fibroblast cells[16, 17] (in a medium supplemented with bovine calf serum). Subsequently, it was found that the requirement for the feeder layer could be replaced by adding leukemia inhibitory factor (LIF) to the medium[24, 25]. LIF binds to a heterodimer complex consisting of the LIF receptor (LIF-R) and another receptor subunit called Membrane glycoprotein 130 (gp130). This binding event leads to the activation of several pathways, of which, the activation of Stat3 has been shown to be essential for the maintenance of a pluripotent state in mouse ES cells[26, 27], though not in human ES cells[28]. Besides Stat3, Oct-4[29, 152], Sox-2[30, 31], and Nanog[32-34] are three other transcription factors shown to be essential for developing and maintaining the pluripotent state. These factors appear to be essential in mouse as well as human ES cells (see above references).

1.3.1 Growth of embryonic stem cells

Circling back to self-renewal, note that it actually consists of two processes – maintenance of pluripotency, as well as cell division. While most research on self-renewal has focused on understanding the signaling and transcriptional networks involved in the maintenance of the ESC pluripotent state, comparatively few studies have investigated pathways involved in ESC growth and death under conditions shown to maintain pluripotency. Below I review some of the latter studies.

Cell growth is intimately tied to progression through the cell cycle, and several studies have focused on understanding cell cycle control in mESCs. mESC growth in culture is characterized by a short cell cycle (11–16 hours), primarily owing to a reduction in the duration of G1 phase (as compared to somatic cells, reviewed in Orford and Scadden[35]). This short G1 phase is due to a lack of the mitogen-dependent early G1 phase of the cell cycle, owing to constitutive Cyclin E – CDK2 activity[36]. This constitutive activity of Cyclin E - CDK2 in turn appears to be driven at least partially by a constitutively active Ras protein expressed specifically in ES cells, called Eras[153], which stimulates PI3K, which is upstream of Cyclin E[37].

Very little work has been done thus far on understanding the role of cell-cell signaling in the growth of mESCs. Since these cells appear to lack the mitogen-dependent early G1 phase of the cell cycle, it seems unlikely that cell interactions could modulate the length of the cell cycle. However, it is plausible that cell interactions could modulate the survival of these cells. mESCs typically have survival/colony-forming efficiencies of ~30%[38], while hESCs have survival/colony-forming efficiencies in the range of 1-10%[39].

Studies have shown that the addition of EGF, ANG-2, Activin, or Nodal proteins to mouse ESC (mESC) cultures results in improved growth[40, 41, 154]. However, in these studies they did not test for secretion of these proteins by ESCs, i.e. they did not (attempt to) fully demonstrate that these pathways are constitutively active in mouse ES cultures and that the factors are acting in an autocrine fashion. For example, Ogawa *et al.*[40] demonstrated that addition of Activin or Nodal proteins to a culture improves their growth. Additionally they show that inhibition of Activin-Nodal signaling downstream of the receptor binding event (by Smad7 expression or the specific inhibitor SB-431542), led to decreased growth. However, in this latter assay (especially in the control) it is possible that cells were responding to Activin/Nodal present in the supplied medium and not cell-secreted proteins.

Because ESCs grow as colonies, juxtacrine signaling could also presumably play a growth-supportive role. Todorova *et al.* used pharmacological blockers of gap junctional communication and Connexin-43 small-interfering RNA to inhibit signaling via gap junctions in mESCs[42]. They demonstrated that gap junctional communication enhances either the growth rate or the attachment efficiency (or both) of mESCs. They did not attempt to separate the potential contributions of attachment efficiency and growth rate to the observed decrease in fold growth over 72 hours.

It is clear that an investigation into the role of intercellular signaling in the growth of ESCs is relevant to basic biology. Below I will describe some of the other areas of research that motivated our work.

1.4 Motivation

For my thesis I have investigated the growth of mESCs under conditions supporting self-renewal. Below I highlight some of the issues that motivated this work.

1.4.1 Biophysics of cell growth

In sections 1.1 and 1.2 I described two major factors that influence the growth rate of cells in culture, namely, (i) depletion of nutrients from the medium, and (ii) cell-cell signaling. The depletion of nutrients can also be thought of as a means of indirect communication in that cells are consuming materials out of a common pool. In general, such communication provides a number of positive and negative feedback loops that control cell phenotype. One mechanism for controlling the strength of the feedback is to vary the amount of signal that cells can exchange.

Now let us consider a more concrete example. Most mammalian cell types seem to produce and respond to one or more growth factors in an autocrine fashion[8]. This provides a positive feedback to the rate of growth. Such systems have been studied in considerable detail by the Lauffenburger lab (MIT) and the Shvartsman lab (Princeton). In particular, one can modulate the strength of the feedback by altering the density at which cells are cultured - higher cell densities result in higher densities of the growth factor in the medium, which will result in a higher growth rate (until one reaches a saturation regime). Thus, in general, growth rate increases with cell density[43].

However, eventually one will enter a saturating regime, where additional increases in growth factor concentration do not result in improved growth[127]. Additionally, at high plating densities we expect several kinds of negative feedback to become important – the depletion of nutrients, the consequent

production of metabolites, and contact inhibition of growth[6, 14]. In the simplest case, the combination of a single positive feedback mechanism along with one or more negative feedback mechanisms will result in the existence of a single density at which the growth will be optimal. While it is possible and even likely that biologists have had experimental evidence for this hypothesis for a long time, published observations demonstrating an optimal density for cell cultures have been available only recently[44]. Additionally, while the above mechanisms qualitatively account for such an optimal density, a quantitative assessment is lacking. Our work seeks to fill-in some of the holes in the understanding of factors that determine the optimal density for cell culture.

1.4.2 Potential for the use of ESCs in regenerative medicine

Regenerative medicine includes the study and development of artificial organs, specially-grown tissues and cells (including stem cells), laboratory-made compounds, and combinations of these approaches for the treatment of injuries and disease[45]. According to the 2007 report of the Scientific Registry of Transplant Recipients, every year this decade ~2000 people have died while waiting for a liver transplant. The waiting list for kidney transplants at the end of 2007 consisted of ~80,000 patients. Thus there is clearly a large unmet need for new sources of cells and tissues. However, perhaps the most exciting applications of regenerative medicine will be in developing therapies for conditions for which there are no widely successful, existing therapies. Examples of such conditions include degenerative diseases of the central nervous system (Alzheimer's disease, Parkinson's disease) and spinal cord injury. Another possibility is that tissue-engineered organs may function better than transplanted organs – for e.g., according to the above report, the 5-year survival rate for liver transplant recipients is currently only around 50%.

In most research to-date, researchers have used more committed cells for developing new tissue[46]. For example, in a landmark study in 2006, Atala *et al.* expanded patient bladder cells on bladder-shaped collagen scaffolds and implanted the resulting constructs back into patients, resulting in successful enhancement of bladder volume[47]. Similarly, neonatal cardiac myocytes have been used for developing cardiac tissue constructs[48]. Finally, while embryonic stem cells are derived from an embryo and are pluripotent, adult organisms also contain stem cells (adult stem cells, ASCs) that are multipotent, and several recent studies have used mesenchymal stem cells from adult bone marrow for therapeutic purposes[49]. Mesenchymal stem cells have been shown to have the ability to form bone, cartilage, and fat cells, and, more controversially, skin cells, neurons, and hepatocytes (reviewed by Kuhn and Tuan[50]) .

The advantage of using more committed cell types such as bladder cells or myocytes is that this avoids the process of differentiating less committed cells to the required celltype, processes that are not ready for use in the clinic. An important step forward in this regard is worth noting; Geron Corporation received FDA clearance in early 2009 to begin the world's first human clinical trial of ESC-based therapy for spinal cord injury. The therapy involves the injection of hESC-derived oligodendrocyte progenitor cells directly into the lesion site of the patient's injured spinal cord. However, the trial was placed on hold in mid-August 2009 because "in one preclinical study a higher frequency of animals developed cysts in the injury site than had been seen in numerous foregoing preclinical studies" with their progenitor cells (www.geron.com). Results of this trial are eagerly awaited. Indeed, once differentiation protocols

such as those for oligodendrocyte progenitors have been developed, ESCs may offer some advantages over more committed cells such as adult stem cells (ASCs), for developing tissues[51]:

(i) Most importantly, we do not currently have protocols for obtaining ASCs for several tissue types. Secondly, while tissues can often be developed from "seed" samples of whole tissue, obtaining such a sample, at least from a live individual, is currently extremely impractical for certain kinds of tissue such as CNS tissue.

(ii) More committed cells typically divide slower than less committed ones, if they divide at all. For e.g., the doubling time for mESCs is 11-16 hours[35], while the doubling time for mouse hematopoietic stem cells is approximately 3 days[52], and for mouse mesenchymal stem cells is approximately 2.5 days[164]. Mature hepatocytes do not appear to divide at all (unless injured)[46]. For (more) committed that do divide in culture, this still means that developing tissues from them may take longer, depending on the time required for differentiation of ESCs.

(iii) While conditions for maintaining ESC self-renewal are well established, conditions for the self-renewal of adult stem cells are not. For e.g., ESCs can be propagated practically indefinitely[53], but current protocols allow HSCs to be expanded only ~20-fold in vitro[155].

Certainly, there are many challenges to be addressed before hESCs can be used for developing therapeutic constructs. The most important is the development of reliable differentiation protocols for obtaining functional committed cells. Another is the reliable expansion of hESCs. hESCs are propagated in most labs using a combination of mouse fibroblast feeder layers, and bovine serum-supplemented medium[54]. However, when expanding cell populations for clinical use, it is preferable to do so in feeder-free, serum-free medium, to avoid the risk of transmitting pathogens and immunoreactive substances[55]. Note that the FDA actually does allow the use of bovine serum for culturing cells that may be used therapeutically[b], as long as the following criterion is met: "The residual amount of serum or additives in the final product should be determined, and shall not exceed 1:1,000,000". However, a bigger concern with the use of sera is lot-to-lot variability[56], which may make reproducible differentiation of ESCs very challenging. A third issue is that ESCs seem to be prone to karyotypic instability[57]. Finally, it is very important to exclude undifferentiated cells from the transplanted population, because these cells may form teratomas[16, 17].

The most direct application of this thesis relates to trying to find solutions for the second point mentioned above, i.e. development of media for the expansion of ESCs. Another issue to consider in this regard is the time required for expansion of stem cells to the population size required for therapy. The recent discovery that somatic cells can be "reprogrammed" to ES-like cells[58] (called induced pluripotent stem (iPS) cells) has suggested a route by which autologous grafts could be developed. This approach would circumvent the potential immune rejection of engineered grafts and/or the need for immunosuppressant therapy. Typical organs contain 10^9-10^{11} cells. Given a doubling time of 30-60 hours for hESCs[39], and assuming that iPS cells should have similar doubling times, to grow a clonal population

[b] http://www.fda.gov/biologicsbloodvaccines/guidancecomplianceregulatoryinformation/guidances/cellularandgenetherapy/ucm072987.htm

of 10^{10} cells (i.e. starting for a single cell), and then differentiate them, would take several months. Importantly, this time is a function of the colony-forming efficiency (CFE). If the CFE is 100%, then for a doubling time of 50 hours, it would take approximately 2 months to grow a clonal population 10^{10} cells. However, if the CFE is only 10%, this time would be about 5 months – additional time, which in the real world, a patient may or may not have. Thus, methods for improving the expansion rate of ESCs, while still maintaining pluripotentiality, could be clinically relevant. One way to find ideal media would be to try different growth factors. However, our approach is a more analytical one, where we have tried to find mechanisms already used by mESCs to self-regulate their growth, and see whether these mechanisms can be exploited to obtain faster growth. While we have focused on mESC growth, our approach is easily extendable to the study of hESC and iPS cell growth.

1.4.3 Understanding the development of cancers

In recent years, the notion that cancers may be generated and supported by relatively small populations of cells has gained ground (for a recent review, see Visvader *et al.*[59]). This small population is posited to have stem cell-like properties, and hence the cells comprising this population are referred to as cancer stem cells. One possible origin of these cells is from normal stem cells that have become deregulated, and thus studies of the growth of stem cells may provide clues as to how this deregulation comes about.

1.4.4 Understanding differences between mESCs and hESCs

mESCs have relatively high colony-forming efficiencies (CFE, 30-50% in our studies), and relatively short doubling times (11-16 hours[35]) as compared to hESCs (CFE of 0.1-10%, doubling times 30-60 hours[39]). A deeper understanding of the factors underlying these differences will further our understanding of stem cell biology and mammalian development.

1.4.5 Developing new cell lines in the laboratory

Finally, methods for increasing the growth rate of ESCs especially when growing at low densities will be useful for developing new cell lines in the lab via clonal selection.

1.5 Thesis Aims and Organization

As described above, there are several reasons why the study of the growth of ESCs in culture is interesting, and methods that improve the growth could be potentially useful in the clinic and the laboratory. The main, broad aim of my thesis was to elucidate factors that affect the growth of mESCs in culture. It is known that one of the important factors that affects the growth rate of cells is homotypic cell interactions. The other factors that affect the growth rate of cells are the availability of nutrients and the accumulation of metabolites in the medium, and contact inhibition. However, ESCs are not believed to possess contact inhibition of growth[60]. Thus, my specific thesis aims were as follows:

Aim 1: In support of Aim 2, to develop and test devices for screening for interactions between cells and their effects on particular processes and/or phenotypes. In chapters 2 and 3 I will describe my contributions to the development and of testing of novel devices that can be used to screen for cell

interactions. We used these devices to obtain initial evidence that mESCs communicate with one other via a diffusible signal that improves their survival.

Aim 2: Elucidate and understand factors affecting mESC growth by

a) Measuring culture parameters for mESCs, in particular
   i. Elucidating mechanisms of interaction and quantifying their effects on mESC growth
   ii. Quantifying nutrient depletion, metabolite production, and their effects of mESC growth

   Aim 2a)i. is one of the primary aims of the thesis and experiments related to this aim are described in chapters 2-5. Experiments related to nutrient depletion and related effects are described in chapter 6.

b) Using a numerical model to test the sufficiency of the above measurements. The numerical model and results are described in chapter 6.

And,

Aim 3: Also, in support of Aim 2ai, to determine the identity of signaling proteins in mouse ESC cultures. We performed gel analysis and mass spectrometry of mESC conditioned medium. These experiments are described in detail in chapter 5.

1.6 Summary

In this chapter I provided some basic information about the growth of cells in culture and embryonic stem cells – their origin, properties, and the role they may play in regenerative medicine in the future. I also discussed some of the motivation for studying the growth of ESCs. In addition to making contributions to basic biology we use this as a model system to better understand mechanisms that determine the optimal growth density for cells in culture, and we seek to improve defined media for ESC expansion. Cell-cell communication is one of the key modulators of cell growth, and while technologies for studying intercellular communication exist, they have limitations, especially as screening tools. I will discuss this in more detail in the next chapter. Additionally, in the following two chapters I will describe the development and testing of two novel devices that can be used to screen for the effects of both diffusible and juxtacrine cell interactions in a particular process/phenotype.

Chapter 2: An nDEP Microwell Array for studying intercellular signaling

As mentioned in section 1.5, one of the aims of my thesis research was to develop new technologies to study cell-cell interaction. Below I describe some of the existing technologies for studying this aspect of cell physiology, and unmet needs in this area.

2.1 Technologies for studying homotypic cell-cell communication

Many of the methods used for studying this aspect of cell biology are the same as the methods used for studying other cellular (intracellular) processes. Two examples are:

(a) **Genetic manipulations**: A gene may be deleted ("knocked out"), or additional copies of a gene may be added into a cell ("knocked in"), so as to modulate the levels of the corresponding protein[61]. Finally, the transcription of a gene can be controlled by inserting DNA into the cell, in which the gene is downstream of an inducible promoter.

(b) **RNA interference**: A relatively new technique which is gaining popularity is the disruption of RNA corresponding to a particular gene using either short hairpin RNA (shRNA) or small interfering RNA (siRNA)[62]. This technique is called RNA interference, or RNAi.

The above techniques typically modulate the activity of only one gene at a time. Thus, they are useful for studying the role of a particular gene. On the other hand, these approaches are not useful if one is interested in screening for the existence of an interaction. Alternately, large-scale RNAi screens are performed, which, however, are currently very expensive to perform (see also 7.1.1). Finally, certain signaling proteins have both intracellular and extracellular roles. For example, Cyclophilin A which we will discuss later in this thesis is found in the cytoplasm as well as extracellularly. Intracellularly it aids in the folding of proteins[63] while extracellularly it is a diffusible factor[64]. Similarly, some recent studies suggest that certain connexins such as Connexin43 have intracellular as well as extracellular functions[65]. Use of the above techniques will modulate both - the internal and external concentration of such proteins. Thus it will not be possible to distinguish between the effects of the signaling role and other roles of such proteins using the above methods.

Additional molecules/techniques used by biologists *specifically to study cell interactions* include:

(i) **Antibodies**: Antibodies against particular receptors can be added to the culture medium, which reduce the ability of the natural ligand to then bind those receptors[8]. Note that for such a "blocking antibody" to be useful however, it is important that it does not itself activate the receptor. Similarly, antibodies to cadherin molecules can be used to reduce cadherin-mediated (contact-based) signaling. This approach is again specific and typically used to block one protein per antibody.

(ii) **Density variation**: A common method for varying diffusible signaling is to vary the plating density of cells[43]. However, one has to be careful when using this method because a denser culture will also metabolize the contents of the medium more quickly. This approach is useful

when screening for the presence of a diffusible interaction because changing the density modulates the amount of signal exchanged across all diffusible species.

(iii) **Conditioned medium studies**: Another popular method for studying diffusible signaling involves collecting medium from one culture and then growing a fresh set of cells in this "conditioned medium". This conditioned medium will contain cell-secreted factors. As a control, another set of cells is grown in fresh medium, and thus the effects of the cell-secreted factors can be assayed. Conditioned medium collected from one cell type (say cell type A) could be applied to either a different cell type (cell type B), or a fresh culture of the same cell type (cell type A). In the latter case the idea is that even though the conditioned medium contains the same secreted proteins that the cells in the culture are producing, it takes some time for the concentration of secreted factors to reach physiologically relevant values, so the culture with the conditioned medium has a head start (relative to the control culture). Then by comparing the conditioned medium culture with the fresh medium culture, inferences can be made about the effects of the factors produced by the cells. Here again, as above, one must be careful to distinguish effects of molecules depleted from the original medium versus molecules added into the medium.

(iv) **Microtechnology-based approaches:** Finally, a few microtechnology-based approaches exist for studying cell-cell signaling. Some of these approaches provide means to construct cell pairs[170, 171]. By comparing the phenotype of cell pairs versus single cells, the effect of interactions can be determined. Additionally, our group is investigating the use of fluid flow for modulating diffusible signaling by using the flow to transport secreted molecules away from regions of the device that contain cells[172].

The following observations are worth making:

a) Other than (ii)-(iv) above, all the other methods listed typically require knowledge of proteins – the ligands/receptors/cadherins/connexins produced by the cell. Then the level of that protein can be altered. Additionally, these other methods are primarily designed to modulate one gene at a time.
b) While (ii) and (iii) above can be used to modulate the total diffusible signal, they cannot be used for modulating contact-based signals.
c) Approaches (i)-(iii) above are widely used. The microtechnology-based approaches are recent and have not been widely adopted as yet. We are unaware of any widely used, specialized techniques for studying the effects of contact-based cell interactions. Of course, the more general methods described above can certainly be used to modulate the levels of expression of a particular cadherin or connexin. One technique that is used to determine the existence of gap junctions is to inject a small dye such as luciferase into one cell which is in contact with other cells and then observing whether the dye spreads to the other cells[66].

In the next section I will describe the principle behind a device that builds upon the microtechnology-based cell-pairing approach described above.

2.2 Device principle

My initial research was done in collaboration with Adam Rosenthal, an alumnus of our lab. Adam had been working on this project before I joined the lab, and had started to develop devices that could modulate the amount of interaction between cells[67]. As shown in the schematic below (Figure 2.1a), one way to increase the amount of contact between cells is to create clusters of cells with an increasing number of cells per cluster. Of course, as one does this, one also increases the amount of diffusible signaling between the cells. As a result, the system can be used as a screening tool, to look for the role of both types of signaling in a particular phenotype. A very similar approach has been developed independently by Chris Chen's group (see section 3.4 for a detailed comparison).

If one specifically wants to modulate only the contact signal, one could then imagine placing these clusters in a perfusion bioreactor, such that factors produced by the cells are swept away downstream (Figure 2.1b). However, some fraction of factors will diffuse through the extracellular matrix (ECM), and the flow may not penetrate into the ECM, so it is plausible that some diffusible signaling will persist (unpublished data from our lab).

A second way to modulate contact signaling would be to change the shape of cells (Figure 2.1c). Cuboidal cells could be made to have a larger surface area in contact with another cell as compared to spherical cells, which could result in increased contact interaction. However, changing the shape of cells also leads to changes in cytoskeletal tension[68], and it would be difficult to segregate the effects of altered cytoskeletal tension and contact interaction. As a result, we have taken the cluster-based approach, and used it to study and modulate both juxtacrine and diffusible cell interactions.

2.3 Technologies for making clusters of cells

Next, we must find a technology for making clusters of small number of cells. Several technologies are available, in principle. Perhaps the simplest option would be to make wells with a diameter of ~30-50 μm in a substrate, and trap cells in these wells. If the wells are seeded randomly, we would expect to obtain clusters containing different numbers of cells. Such an approach does, in fact, work (Figure 2.2a). However, when working with adherent cells, the cells in the resulting clusters have no room to attach (spread) and grow. A potential way to fix this would be to make larger wells, but now one cannot guarantee that cells will end up in contact with one other (Figure 2.2b-c), which is what we desire (above section).

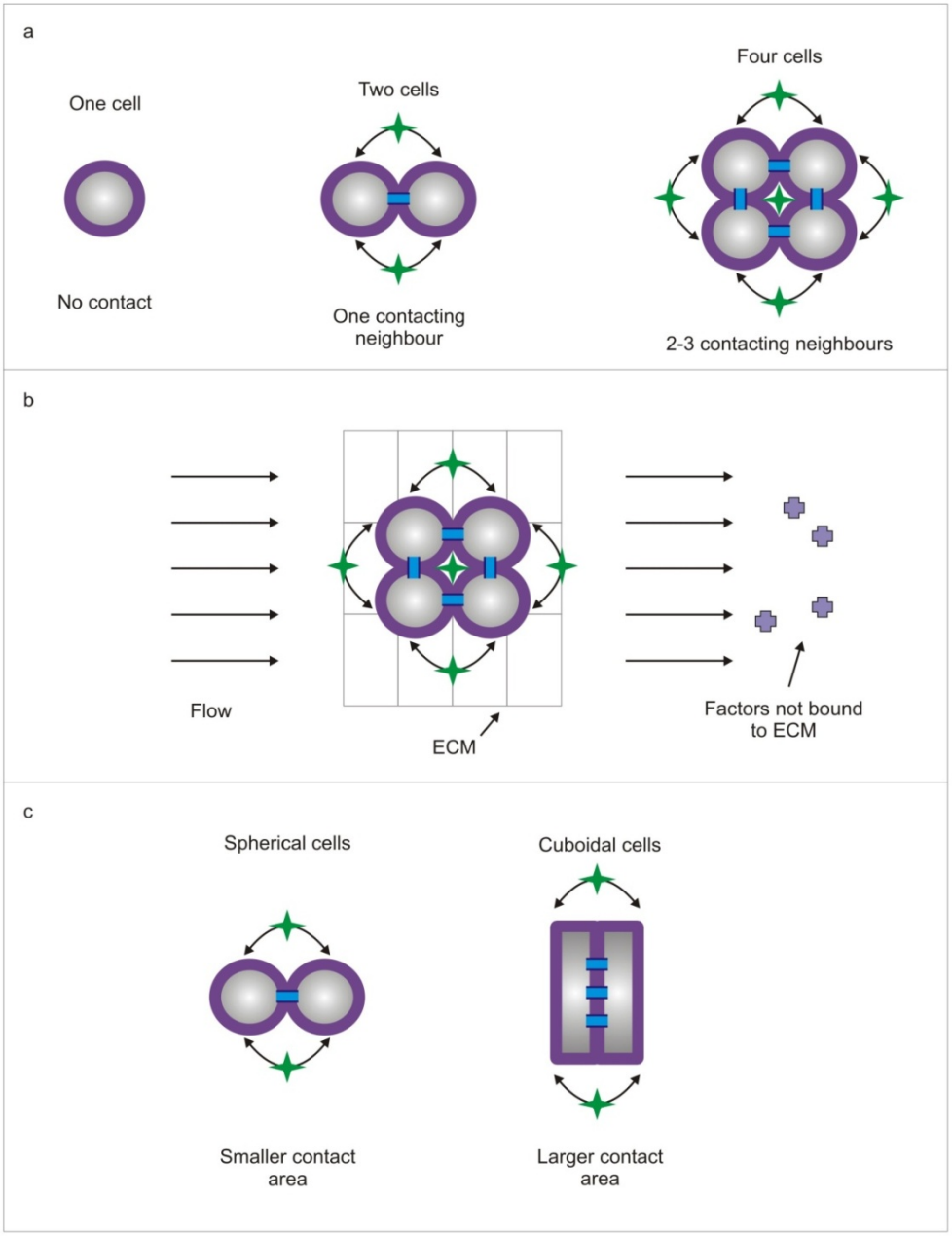

Figure 2.1 a. By making clusters of cells, one can modulate the amount of contact interaction experienced by a cell. A single cell does not experience any contact interaction. In a cluster of two cells, each cell has one neighbor; in a cluster of 4 cells, each cells is in contact with two neighboring cells. But the making of clusters also results in an increase in the local cell density, and a corresponding increase in the local concentration of diffusible factors. b. By placing the clusters under flow, it is possible to eliminate/reduce some types of diffusible interaction; the fluid flow will carry away factors unbound to the extracellular matrix (ECM) downstream. c. Another way to modulate the contact interaction between cells is to change the shape of cells such that they have varying amounts of their surface in contact with another cell.

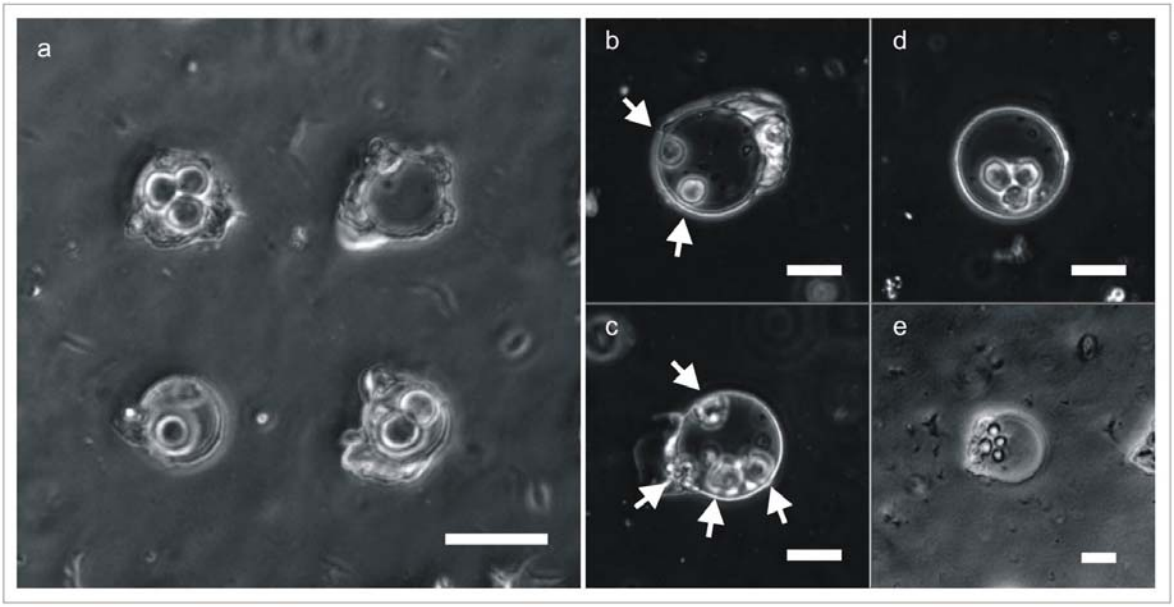

Figure 2.2 a. Clusters of small numbers of cells can be made by seeding cells onto a substrate containing wells with a diameter of 30 µm. b, c. When cells are seeded into 60 µm (diameter) wells, they sometimes do not form clusters. The white arrows indicate the location of cells. d, e. When mESCs are seeded into 60 µm wells however, most often they do form clusters. Scale bars represent 30 µm in all images.

In practice, for mESCs, which is the cell type we have investigated in detail, we later found that in >90% of cases clusters did form even in the larger wells (Figure 2.2d-e). We hypothesize that this is due to the random motion of cells within the well, combined with the fact that when these cells are brought into contact with one other, they stick to each other. Some evidence for the "stickiness" of mESCs is provided in chapter 3. However, we do not know whether such spontaneous clustering would occur on other cell types. Similar arguments apply for clusters that could be generated using surface patterning[69] instead of microwells.

To avoid the issues mentioned above we decided to use electrical traps to create clusters of cells. If the traps are ~30-50 µm wide, they would allow cluster creation as shown in Figure 2.2a. However, importantly, one can subsequently turn the fields (and traps) off, allowing cells to proliferate, as well as move around. Additionally, it is plausible that electric traps may be strong enough to "trap" clusters of cells, yet weak enough that they don't prevent the subsequent growth and motility of cells. Still, since one cannot claim that the mechanisms by which electric fields affect cells are completely understood, it is usually advisable to turn off the electric fields after the clusters have been created.

There are primarily three kinds of electrical traps used to pattern cells, they are traps based on electrophoresis, positive dielectrophoresis (pDEP), and negative dielectrophoresis (nDEP). Electrophoresis has been used to pattern cells inside physical structures[70, 71], but is generally considered to be unsuitable because it leads to the generation of radicals at the electrodes (due to the electrolysis of water), which can damage cells. While pDEP has been used by several groups to pattern cells[72], as well as create cell clusters[73, 74], it requires cells to be in a medium with low conductivity to guarantee that the cells are more polarizable than the media. In contrast, nDEP can be performed with cells

suspended in commonly used cell-culture media. This presents a significant advantage because it allows one to use the traditional media formulations optimized for cell culture. This avoids any gross viability issues associated with placing sensitive cells in artificial media[75]. The physics of DEP is described in greater detail in Appendix 1.

Adam Rosenthal from our lab had previously developed an nDEP trap that could be used to hold micron-sized *beads* at chosen locations on a substrate[67, 76]. Subsequently, he modified the design, so as to be able to pattern single *cells*[67, 75]. This required adding interdigitated electrodes to minimize non-specific cell adhesion (Figure 2.3) and determining operating parameters that minimized heating and electric field exposure. The resulting structures are termed nDEP microwells to reflect the fact that they present an electrical microwell to incoming cells, only allowing cell-substrate attachment inside the DEP trap. While the initial device was designed to trap only single cells, we believe that it would be straightforward to increase the well size, so as to be able to create and trap clusters of cells.

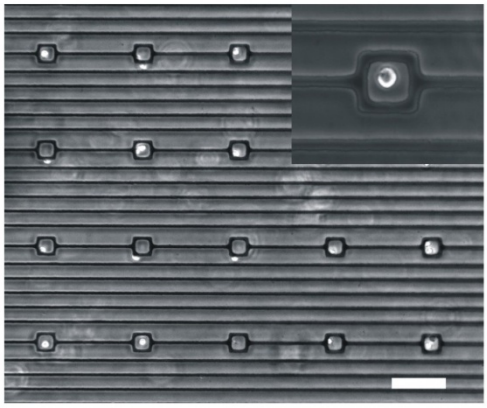

Figure 2.3 Image of an nDEP microwell array with HL60 cells trapped at most trap locations (white circles within the black rectangles). The inset shows an HL60 cell trapped inside a single nDEP microwell. Scale bar represents 100 μm.

I made two main contributions to the development of the nDEP microwell array:

i. I performed bio-compatibility testing of the system
ii. I developed an alternate loading protocol for loading the system with high efficiency

Both the above are described in greater detail below. The results of this work were published in Lab on a Chip[75].

2.4 Materials and Methods

Modeling

We extracted electric-field data from simulations using the commercial field solver Comsol Multiphysics (Comsol, Inc., Burlington, MA). Temperature modeling was also done using Comsol Multiphysics. After using the Electromagnetics module to determine the resistive heating in the flow chamber, we used the Heat Conduction module to determine the temperature at various locations on the device. We determined the transmembrane potential using the maximum value of

the electric field experienced by a trapped cell. For cell parameters, we used a membrane capacitance of 1.6 μF/cm^2, membrane conductivity of 0.22 S/cm^2, cytoplasmic conductivity of 0.75 S/m and cytoplasmic dielectric constant of 75. Medium conductivity is 1.5 S/m and dielectric constant is 80. These values are all taken from Huang *et al.*

Modeling temperature rises in microsystems is often inaccurate because the exterior boundary conditions (between the device and ambient) are not known or well controlled. In our case, we set the exterior of the device to a fixed temperature boundary condition of room temperature. To determine whether this would result in realistic temperature modeling, we experimentally verified the calculated temperatures. For this we used a slightly different device where we fabricated an on-chip resistor specifically for measuring temperature (using the temperature coefficient of resistivity of Au). These experiments were performed by Adam Rosenthal. As seen in Figure 2.4, the simulated and measured temperatures are comparable, validating our modeling approach. Thus, we believe that our thermal simulations are adequate design tools for avoiding thermal stresses.

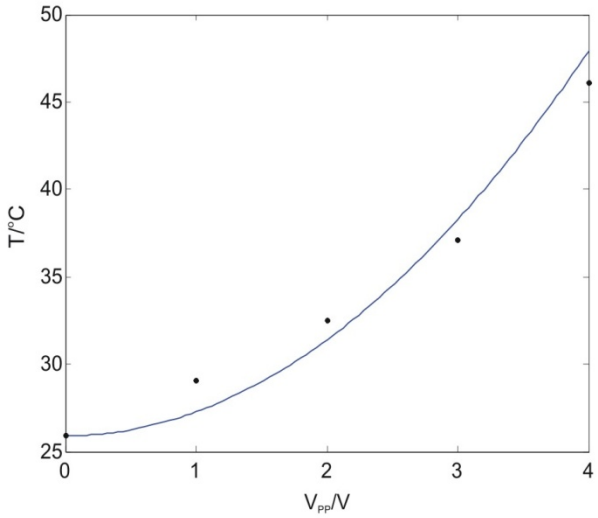

Figure 2.4 Validation of temperature modeling: Modeled temperatures (solid line) and measured temperatures (dots) versus voltage.

Electrode traps

We designed the DEP microwells as square electrodes with an inner square side length of 25 μm, and two other line electrodes spaced 10 μm away. All electrode widths were 10 μm. The microwells were in a 10 x 10 square array, with a trap-to-trap distance of 200 μm. In-between the DEP microwells we placed 3 other electrodes spaced by 30 μm each. These electrodes set up an interdigitated electrode array-like configuration (Figure 2.3).

We fabricated the electrodes by patterning gold onto Pyrex wafers. We cleaned wafers for 10 min in a Piranha solution (3:1 H2SO4:H2O2), blew them dry with N2, and then dehydrated them for 30 min at 225^{o}C. We then used the image-reversal photoresist Hoechst AZ-5214 (Celanese, Somerville, NJ)

and photolithography to define the electrode patterns. Finally, we evaporated 10 nm of titanium and 200 nm of gold onto the slides followed by resist dissolution and metal liftoff in acetone.

Flow chamber and packaging

We created the flow chambers using a silicone gasket (19 x 6 x 0.5 mm; Grace Bio-Labs, Inc., Bend, OR). A 4-5 mm thick sheet of baked PDMS (Sylgard 184, Dow Corning, Midland, MI) was used to form the roof of the chamber. We cored two holes in the PDMS sheet using syringe needles (0.065'' outer diameter; Hamilton, Reno, Nevada). We then inserted PEEK tubing (Upchurch Scientific, Oak Harbor, WA) through these holes to provide fluidic access to the chamber, and applied epoxy to hold it in place. Finally, we clamped the chamber top and gasket to the bottom electrode slide using two binder clips for easy assembling and disassembling. The chamber was clamped at an angle to the electrode array to allow for loading with a lower density of cells (Figure 2.7). Wires were electrically connected to the electrodes using conductive epoxy (Circuit Specialists, Mesa, AZ).

Fluidics

We connected the two inputs of a four-way valve (V-101D, Upchurch Scientific, Oak Harbor, WA) to a 3-mL syringe filled with cell suspension and a 5-mL syringe filled with media. The 5-mL syringe was controlled using a syringe pump (KD Scientific 210C, Holliston, MA). One output on the four-way valve was connected to the flow chamber using PET tubing (.03' I.D., 0.048' O.D.; Becton Dickinson and Co., Sparks, MD), and the other was connected to waste.

Cell culture

We cultured cells in 20 cm^2 dishes (Nunc, Rochester, NY). GFP-expressing HeLa cells (a generous gift from Dr. Sangeeta Bhatia) were maintained in Dulbecco's Modified Eagle Medium (DMEM; Gibco, Grand Island, NY) supplemented with 10% fetal calf serum, 100 µg mL^{-1} penicillin, and 100 µg mL^{-1} streptomycin and incubated in 7.5% CO_2 at 37 °C. We passaged them at preconfluency no more than 25 times. HL60 cells (ATCC, Manassas, VA) were cultured in RPMI medium with additions as above. Prior to patterning experiments, we released cells into suspension and concentrated them to 10^6 cells/ml. HL60 cells were fluorescently labeled with chloromethylfluorescein diacetate (CMFDA; Molecular Probes, Eugene, OR; 20 µM, 30 minutes) for identification at (ex/em) 492/517 nm wavelengths.

Imaging

Images were taken on a Zeiss Axiovert 200 microscope (Carl Zeiss MicroImaging, Inc., Thornwood, NY) using a Spot RT Color camera (Diagnostic Instruments, Inc., Sterling Heights, MI). For fluorescence imaging we used a X-Cite 120 illumination system (Exfo Life Sciences, Ontario).

Proliferation experiments

To demonstrate that cells patterned in our device are able to proliferate, we first patterned GFP-expressing HeLa cells in our device. After allowing the cells to attach for 30 minutes, we disconnected the patterning fluidics described above and attached a media containing syringe to

the fluidic input port of the device. Then we gently placed the device in a dish containing DMEM. The DMEM served to increase the local humidity in the dish and greatly reduce the rate of evaporation of media from the device. We subsequently fed the cells once a day using the attached media-containing syringe.

Electrical excitation

Sine wave excitation at 10 MHz was generated by an Agilent 33250A signal generator (Agilent, Palo Alto, CA). The signal was measured using a digital oscilloscope (Tektronix TDS 2024, Beaverton, OR).

2.5 Results and Discussion

2.5.1 Biocompatibility of the nDEP Microwell Array

Biocompatibility is one of the basic requirements of any device meant for use with cells. Three mechanisms have been described by which alternating electric fields can affect normal cell physiology[77], namely, (i) Joule heating of the cell suspension, (ii) induction of large transmembrane potentials ultimately leading to electro-poration of the plasma membrane[78] or the membranes of intracellular organelles[79], and finally, (iii) generation of reactive oxygen species[80, 81].

While detailed investigations of the stress response induced by DEP forces and electric fields have been performed by others in our lab[81], I have focused on the nDEP microwell architecture in particular, and on modeling, and aspects of gross physiology such as attachment and proliferation. We designed the nDEP microwell array to operate well beneath the damage thresholds associated with cell heating and membrane loading. We excluded any investigation of damage to intracellular structures since the fields responsible for these effects have been reported to be two orders of magnitude higher than the fields in our device[79].

To avoid any harmful effects due to Joule heating, we wanted to avoid temperature excursions above physiological levels (37^{o}C for mammalian cells). We simulated the temperatures experienced by cells at various voltages (Figure 2.5). Simulations included conductive heat transfer and neglected convection, which is typically minimal in these systems (Pe<1). We see that the temperature scales with the square of the applied voltage, as expected. Using a typical room temperature of 25 ^{o}C, we can avoid thermally stressing the cells by keeping the applied voltage to $\leq$ 2.5 V.

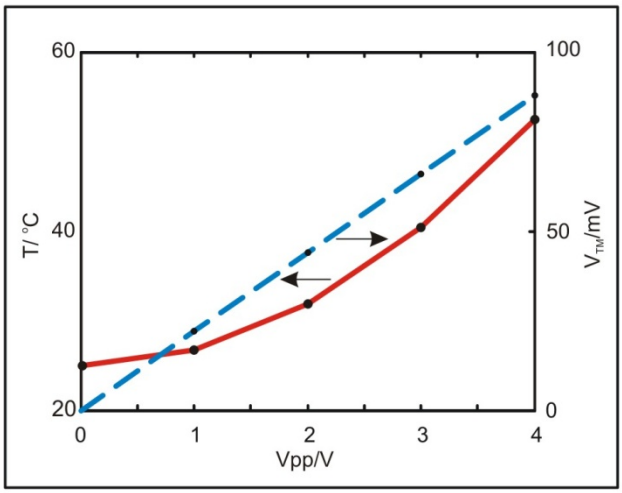

Figure 2.5 Simulated temperature in the center of the trap (solid red line) and transmembrane voltages (dashed blue line) on our chip for different peak voltages at 10 MHz. Similar values were obtained for cells levitated above the interdigitated electrodes.

Transmembrane potentials are the second way by which electric fields have been shown to affect cell physiology. When cells are placed in AC electric fields, an imposed AC voltage appears across the cell membrane. Since cells already maintain a constant (DC) transmembrane potential of ~60 mV across their membrane, adding an additional potential could alter cell physiology[77]. For a spherical cell in a uniform electric field, the maximum imposed transmembrane potential (V_{TM}) is given by[82],

$$V_{TM} = \frac{1.5\,ER}{\sqrt[2]{1+(\omega\tau)^2}}, \tau = \frac{RC_m(\sigma_{cyto} + 1/2\,\sigma_{med})}{1 + RG_m(\sigma_{cyto} + 1/2\,\sigma_{med})}$$

where E is the maximum electric field, R is the cell radius (we used 5 µm), ω is the frequency of the applied voltage, C_m is the capacitance of the cell membrane, σ_{cyto} is the cytoplasmic conductivity, σ_{med} is the conductivity of the medium, and G_m is the membrane conductivity for the cell. We see that the imposed transmembrane potential scales linearly with applied electric field and inversely with frequency above the critical frequency $1/\tau$. Thus, minimizing electric field intensity and increasing field frequency minimize V_{TM}.

We used our field modeling tools and the expression above to simulate the transmembrane potential experienced by cells due to the applied electric fields (Figure 2.5). As expected, the simulated transmembrane potential scales linearly with the applied voltage.

To use these simulations as a design tool, we must know the maximum potential that does not adversely affect cell health. Unfortunately, this value is not known, since the mechanism by which a rapidly oscillating potential affects cell physiology is not well understood. In addition, electric fields in DEP microsystems are necessarily non-uniform, which limits the accuracy of the simple V_{tm} expression above. Nonetheless, previous studies indicate that transmembrane voltages under 200

mV do not adversely affect cell physiology[77, 78], and this was the value used to obtain operating conditions for our array. As can be seen from (Figure 2.5), for our operating conditions (<2.5 $V_{pp,}$ 10 MHz), the transmembrane potential does not exceed 50 mV.

Finally, while we designed the nDEP microwell array to operate well beneath the damage thresholds associated with cell heating and membrane loading, an experimental demonstration of its biocompatibility must nevertheless be performed. In Figure 2.6 we show results of patterning HeLa cells, an adherent human tumor cell line. First, note again the high patterning fidelity (Figure 2.6 a, Day 0). More importantly, under these trapping conditions, we found that cells patterned on our array proliferated over 4 days (Figure 2.6 a) and showed normal morphology (Figure 2.6 b). This demonstrates that our nDEP microwells can successfully be used to pattern multiple single cells in physiological media without grossly affecting cell health.

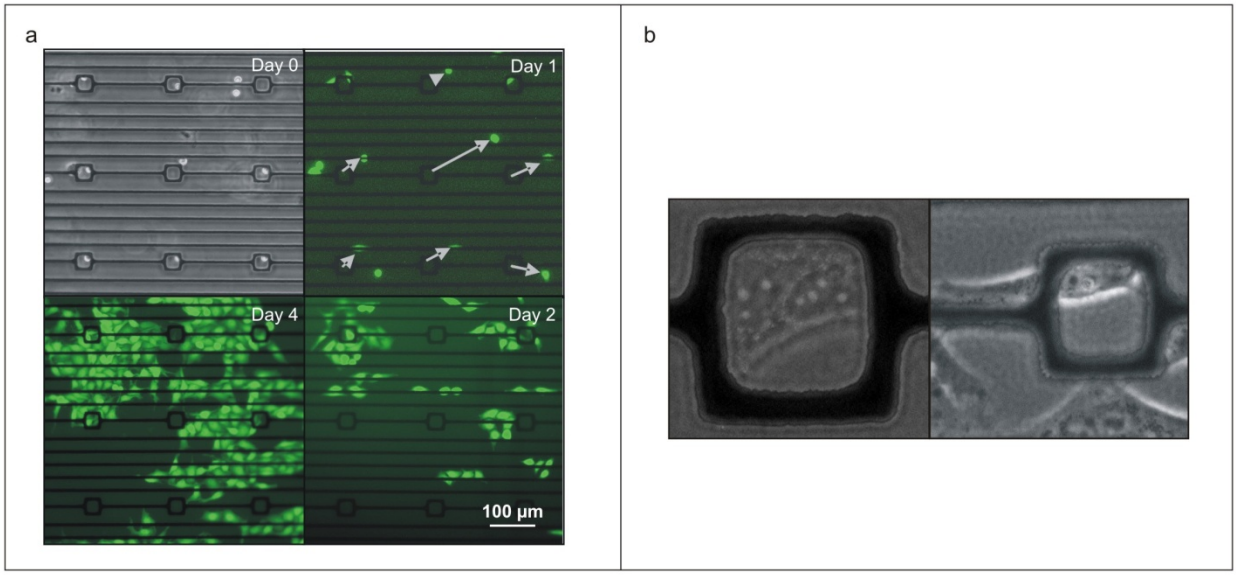

Figure 2.6 a. Phase and fluorescent images of GFP-expressing HeLa cells trapped in a nDEP microwell array, showing that they exhibit normal morphology and proliferation over 4 days after being trapped at 1 V_{pp} and 10 MHz. Arrows in the Day 1 figure (top, right) show the displacement of cells that moved out of the trap. The scale bar represents 100 µm. b. Phase images of single HeLa cells trapped in the nDEP microwells, showing that they exhibit normal morphology. The traps in b are 25 µm in width and height.

2.5.2 An Alternate Loading Protocol for the nDEP Microwell Array

Ideally one would like to fill all the traps in the array so as to be able to obtain the maximum amount of data from any experiment. In the first version of the operation protocol[67], the array was loaded using pressure-driven flow alone. Using this approach, an array of ~50 wells could be filled in approximately 15 minutes. I found that 64±6% of microwells are populated (3 experiments), and there is no control over which wells get filled. The loading efficiency for each experiment was calculated over the 25-trap region with the best loading.

I came up with two improvements to the above loading protocol. The first improvement was a simple adjustment to the loading protocol: it is natural to think of loading cells into the traps by applying pressure-driven flow along the line of traps, which leads to a relatively small loading zone (Figure 2.7). I.e. a cell must land in the region indicated by the top white rectangle to fill the trap directly in front of it. However, flowing at an angle allowed us to increase the loading zone by a factor of ~4 (Figure 2.7, lower white parallelepiped), and correspondingly, to use a lower cell density. This mitigated the clumping of cells, and would also be useful when working with primary cells, sometimes available only in small numbers.

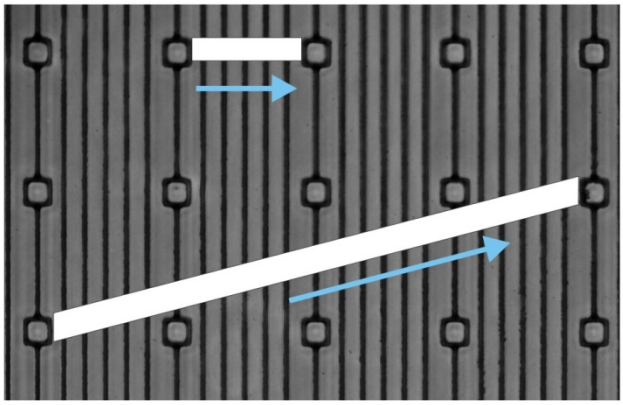

Figure 2.7 Flowing cells at an angle to the array increases the size of the loading zone (lower white parallelogram versus upper white rectangle) for each trap. The blue arrows indicate the direction of flow, while the white regions indicate the corresponding loading zone associated with a trap.

Additionally, I developed an alternate protocol for loading the array (Figure 2.9) where we take advantage of the global electrohydrodynamic (EHD) flows to obtain transverse flow in our device. There are several ways that AC electric fields can produce fluid flow, most notably buoyancy-driven flows, electrothermal flows, and AC electroosmosis[83]. Buoyancy-driven flow occurs when Joule heating causes a gradient in density that sets up a convective flow. Electrothermal flows occur when Joule heating causes gradients in electrical properties that are then acted upon by electric fields, while AC electroosmosis describes coupling between double-layer charge and a transverse electric field. We believe that buoyancy-driven flow is the cause for the flows seen in our systems. AC electroosmosis is negligible at the high conductivities (1 S/m) and high frequencies (10 MHz) that we are using. The relative contributions of buoyancy (F_b) versus electrothermal flows (F_{et}) can be estimated using equation (51) in Castellanos *et al*[83]

$$\frac{F_b}{F_{et}} = \frac{\left(\frac{\partial \rho_m}{\partial T}\right)(\pi r)^3 g}{\frac{1}{\sigma}\frac{\partial \sigma}{\partial T}\varepsilon V^2}$$

where $\frac{\partial \rho_m}{\partial T}$ is the rate of change of density with temperature (for the medium), r is the characteristic length scale, g is the acceleration due to gravity, σ is the conductivity of the medium, $\frac{\partial \sigma}{\partial T}$ is the temperature coefficient of conductivity, ε is the permittivity of the medium, and V is the applied voltage.

For our system, at 1 V_{RMS}, the ratio of the buoyancy force to the electrothermal force F_b/F_{et} is almost 1000. So the flow is dominantly buoyancy-driven. This flow pulled cells towards the center of the array (Figure 2.8). In principle, cells in the central region of the array could also be lifted by this flow. However, cells will not get lifted by the flow unless the viscous drag force due to the EHD flow is greater than the gravitational force on the cell. In our experiments we did not observe this to happen. Additionally, upon decreasing the array voltage back to 1 V_{pp} the EHD flow stopped almost instantaneously. Thus, we have a way to move cells over the array that is independent of the pressure-driven flow generated using a syringe pump i.e. we have 2-dimensional control over the cell velocity (Figure 2.9). Using a combination of these two independent flows, we were able to move cells into selected DEP microwells (Figure 2.9).

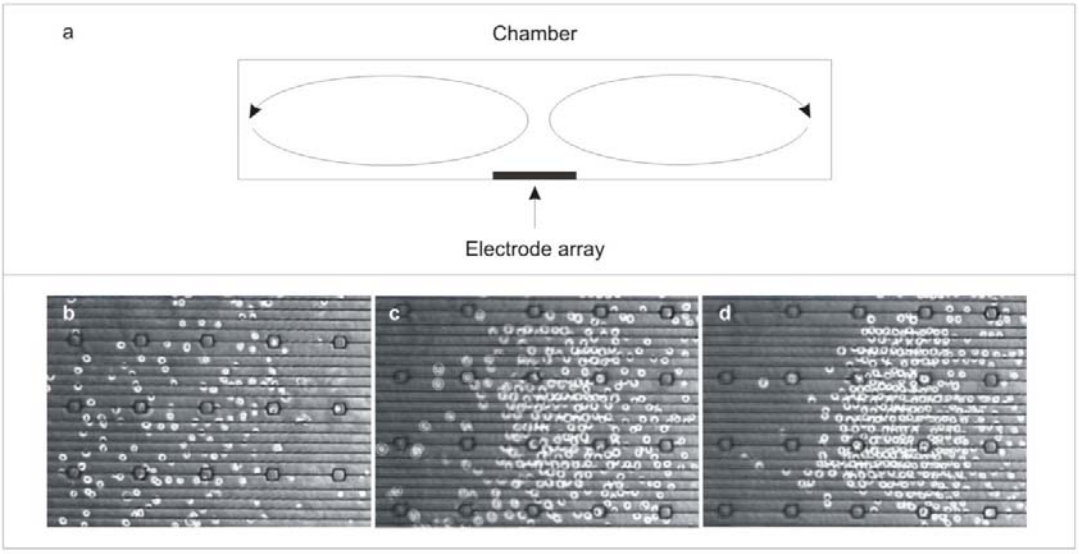

Figure 2.8 a. Schematic of convective flow in our device due to heating of the fluid by our electrode array. b → d. The convective fluid flow above the electrode array leads to the concentration of cells in the center of the array, demonstrating that the flow points radially inward at the bottom of the chamber.

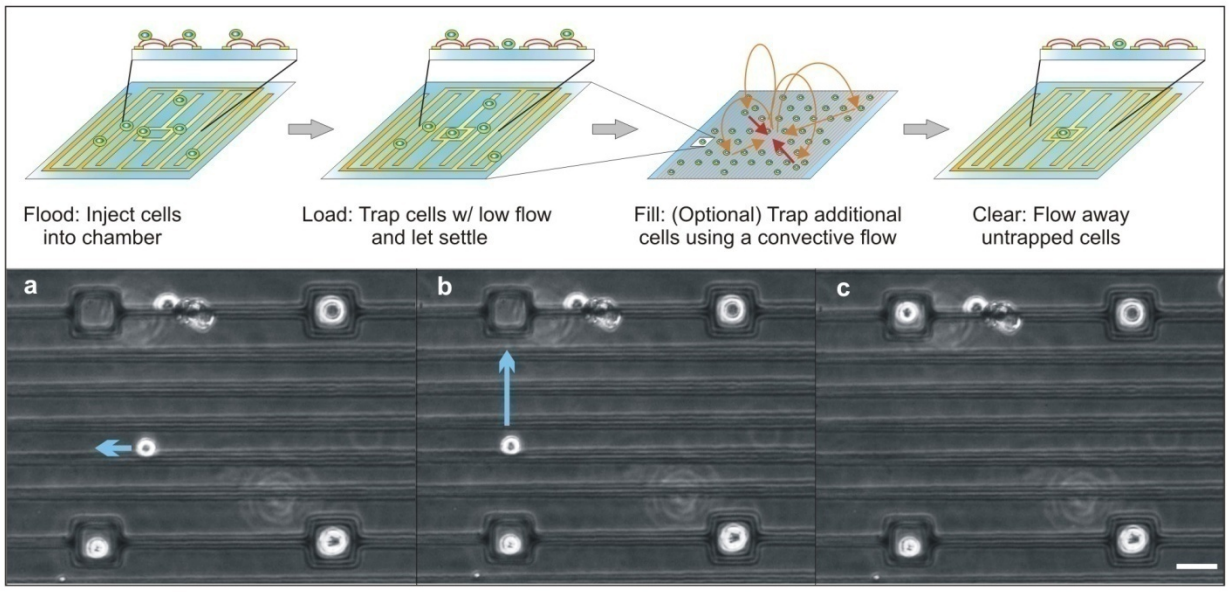

Figure 2.9 Top: Schematic of operating procedure. We first inject cells into the chamber, with the electrodes on, at relatively high velocities of hundreds of microns per second. We then load cells into traps by flowing at very low speeds of around 1 μm/s. If required, we can then fill additional traps using EHD flows. In the 'Fill' step, orange lines show the motion of the fluid while red lines show the motion of (two) untrapped cells. The flow must be kept slow enough (< 5 μm/s) so that cells do not get lifted with the flow. Finally, all untrapped cells are cleared from the array. Bottom: Use of convective flow to pattern cells. a → b: Convective flow pushes untrapped cells towards the center of the electrode array (not shown at this scale) when electrodes are driven at 2.5 V_{pp}. Blue arrows show the movement of cells between frames. This flow is used to align cells with the trap. b → c: Transition is made to pressure-driven flow using a syringe pump. All untrapped cells move in the same direction, along the array. The pressure-driven flow is used to push aligned cells into the traps. The scale bar represents 25 μm.

In principle, 2-d control should allow for 100% loading efficiency. Practically, using a combination of the two improvements listed above, we obtained a loading efficiency of 90±3% (again over the best 25-site region of the array, 2 experiments, Figure 2.3 and Figure 2.10). Note that since empty sites must be filled individually (as in the "Fill" step described in Figure 2.9) the time to load the array now scales with the size of the array. The additional gain of ~25% in loading efficiency obtained by using the EHD flow came at a time cost of approximately 15 additional minutes for a 25 site array. Thus, the time to load the array was approximately twice as much as without the EHD-based site-filling step.

Finally, in our current devices, cells often settle outside of the traps, in the region between the trap electrode and the adjacent electrode (Figure 2.10). We believe that this is because the gap between these two electrodes, in the region between traps, is larger than the gap between electrodes in all other parts of the array. As a result, the electric fields in this region will be weaker than the fields elsewhere on the array. We believe that this problem can be easily fixed by adding additional electrode elements in these regions.

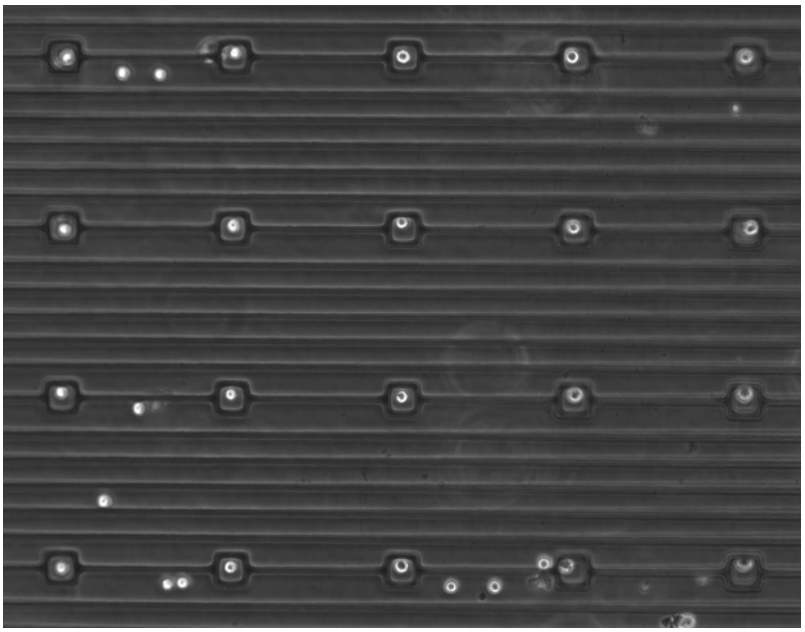

Figure 2.10 20 site region of an nDEP microwell array with 100% loading (HeLa cells). (Note: Loading efficiency was calculated over 25-site regions.)

2.6 Summary

In this chapter, I outlined a technique developed in our lab for screening for intercellular interactions via the creation of cell microarrays containing clusters with varying numbers of cells. Further, I presented my contributions to the first generation device built in our lab for achieving this objective – the nDEP microwell array. We have demonstrated that our device allows for the subsequent unrestricted spreading, movement, and proliferation of cells, enabling the study of these vital aspects of gross cell physiology. Finally, we have presented a new manipulation method that uses convective flows in combination with pressure-driven flows to achieve the two-dimensional positioning of cells. Besides improving loading efficiency in our device, we believe that this approach would be useful when the filling of adjacent sites in order to have a fixed intercellular distance is critical to a study, for example in studies of diffusible signaling and chemotactic responses. More generally, this technique can be applied to manipulate micron-sized objects in two-dimensions.

In the next chapter I will discuss the second generation cell-clustering device – the Bio Flip Chip and our investigation of mESC intercellular signaling using this device.

Chapter 3: Studying mESC Self-renewal using the Bio Flip Chip

In the previous chapter I have described a new technique for studying the effects of cell-cell interactions – via the creation of clusters of varying numbers of cells. I also described our first implementation of this technique – the nDEP microwell array. In this chapter I will describe the second implementation of a cell-clustering technology - the Bio Flip Chip (BFC). Further, I will describe the experiments we subsequently performed, where we used the BFC to modulate cell-cell signaling between mESCs, and studied the resulting effects on their self-renewal.

3.1 Introduction

While the nDEP microwell array demonstrated potential as a tool for making clusters of cells, our lab subsequently developed an alternate method for making cell clusters using the Bio Flip Chip[67]. This device is considerably easier to work with as compared to the nDEP microwell array and as such, we used this device to investigate cell-cell signaling in mESC cultures.

There is also a second advantage associated with using the BFC over nDEP microwells or physical microwells (Figure 2.2), which has to do with the substrate for cell culture. Tissue culture of especially adherent cell types (such as mESCs) is commonly done on treated polystyrene and the BFC enables the "printing" of cell clusters onto any substrate of choice. In particular, this allowed us to perform our assays on tissue culture polystyrene.

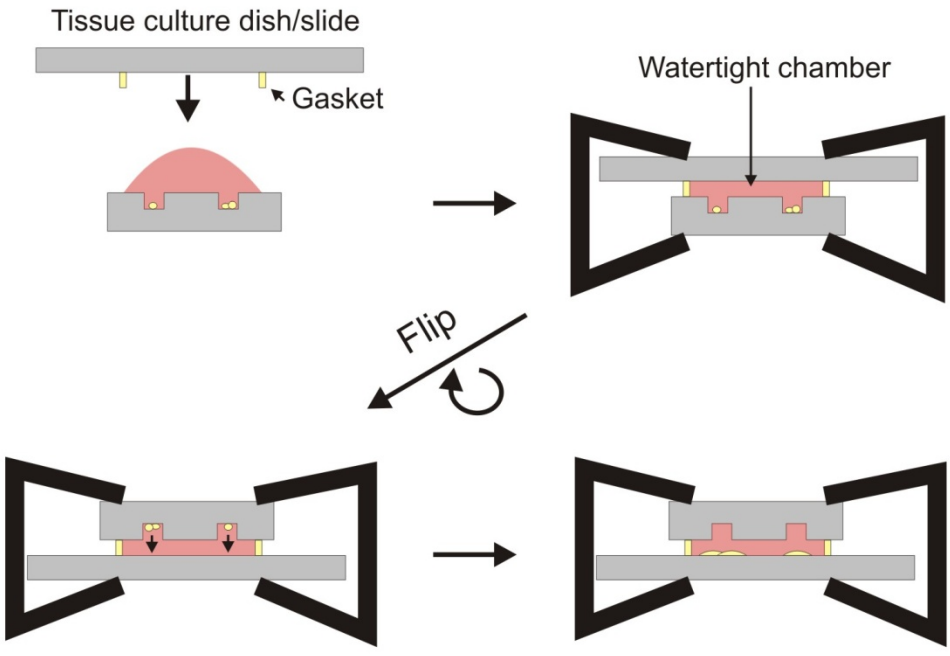

Figure 3.1 Schematic of the main steps in the operation of the BFC. After forming cell clusters within microwells in a PDMS substrate, a watertight chamber is formed by clamping the substrate to a tissue culture dish with a gasket. The system is then flipped over, allowing the cell clusters to fall under the influence of gravity. The cells can subsequently attach to the tissue culture dish.

3.2 Materials and Methods

Preparation of BFCs

Videos of the process for making Si master wafers, molding PDMS, as well as for the use of the BFC are available at the JOVE (Journal of Visualized Experiments) website (www.jove.com, only the last one was made by us). Below I provide a text description of the process, along with some suggestions (in parentheses) for a reader who may want to use BFCs.

We made the BFCs by molding polydimethylsiloxane (PDMS) onto a 4" Si master wafer. For preparation of the master wafer, we started by dehydrating Si wafers for 30 min at 130 ^{o}C. Then SU8-50 (Microchem) was patterned using the manufacturer's protocol, reproduced here for the convenience of the reader. We poured 2 ml SU8-2050 onto the wafer, ramped the spin speed at 300 rpm/s to 3000 rpm, and spun for 30 s to yield feature heights of ~40µm. After spinning, we baked the wafer at 65^{o} C for 5 minutes (pre-bake), and then at 95^{o} C for 15 min (soft-bake). We exposed the wafers to a UV dose of 200 mJ/cm^{2} on a contact aligner (Karl Suss, MJB-3 Mask Aligner) using a dark-field mask printed at 20,000 dpi (CAD/Art Services). We baked the wafer (post-bake) at 65^{o}C for 1 minute, then at 95^{o}C for 4 min, and then again at 65^{o} C for 1 min. We rinsed the wafers with PM acetate (Doe and Ingalls) while we spun them at 500 rpm for 3 min. We rinsed the wafer with isopropanol, and dried it. We then silanized the wafers for 30 min to prevent the PDMS from adhering to the Si master wafer (using T2492-KG, UCT Specialties, PA).

We mixed PDMS (Dow Corning, Sylgard 184) in a 10:1 ratio, poured it over the master Si wafer (~10 g per wafer), and let it cure overnight at room temperature. The reason for doing this versus the more traditional curing at 60^{o} - 80^{o} C which usually only takes about 2 hours was that we found that the longer curing time resulted in a more uniform thickness across the chip, which made the patterning as well as subsequent imaging easier. The cured PDMS was then slowly peeled off the Si wafer and each chip was cut out using a razor blade and bonded to a 1"× 1" cut microscope slide to make the handling easier, and to distribute the pressure resulting from clamping the chip to the gasket and substrate (a subsequent step).

We soaked the BFC overnight in PBS to hydrate it and thereby reduce absorption of media into the PDMS during the experiment, which otherwise led to the formation of bubbles in the chamber. We coated the BFC surface with 200 µL of 7.5% Bovine Serum Albumin (BSA) (Invitrogen) and scraped it gently with a pipette tip to disperse the BSA and remove any bubbles from the wells. (Scraping it too hard will result in tearing of the microwells. Some practice may be required to achieve the correct pressure level.) The BSA helped to prevent cells from sticking to the PDMS. We left the BSA on the BFC surface for ~30 min. We made gaskets out of a 0.5 mm thick silicone sheet (Invitrogen). This spacer gasket is required in order to provide the cells with enough media to prevent nutrient depletion (see Discussion for a more detailed discussion of this issue).

We sterilized the gasket, BSA-coated chip, and 2 binder clips under UV light, in a Class II biosafety cabinet, for 1 minute. We then applied the gasket to a sterile tissue-culture polystyrene (PS) slide (Nunc Delta surface, Thermo Fischer Scientific). We then added ~200 µL of 0.1% gelatin solution (Chemicon

International) into the gasket, spread it over the surface of the slide contained within the gasket, and let it sit for ~20 min.

Operation of BFCs

We rinsed the BFC twice with 200 µL PBS. After aspirating the PBS, we applied 175 µL of cell solution (~3×10^5 cells/mL) to the BFC surface, and let the cells settle for 5-10 min. We placed the BFC in a closed dish and imaged it to check that most wells were loaded. (If necessary one can add more cell solution to improve the percent wells loaded.) If required, we also tapped the microscope gently to push settled cells along the surface of the chip and into wells.

To clear away the cells outside the microwells, we tilted the BFC towards one corner at a ~15^o angle and slowly pipetted the cell solution off with a 200 µL pipette. Next, we placed the BFC flat and added 100 µL of media to the opposite BFC corner. Upon tilting the BFC again, this media collected in the lower corner, and we again pipetted it off. We observed the BFC under the microscope to make sure cells were still loaded in the wells and rinsed the BFC an additional 2-4 times if necessary, to ensure that there were very few cells (<20 in the lowest corner) outside of the wells. These washes also ensure that the BSA and PBS used in the preparation of the BSA are reduced to trace levels on-chip.

We aspirated the gelatin from the PS slide, rinsed it once with medium, and added ~100 µL of medium to keep the surface wet. Then we inverted the slide (+ gasket), and applied it to the surface of the BFC, starting from one side, and gradually lowering the opposite side. We applied some pressure to the resulting chamber to seal it. While continuing to apply pressure to the chamber using the thumb and middle finger of one hand, we applied binder clips to two opposite sides of the chamber to hold it shut. (During this step, it is very easy to introduce bubbles into the chamber. Some practice may be required to determine the correct amount of pressure that must be applied to the chamber while the binder clips are put on, so as to avoid bubble formation.) We removed the upper prongs of the binder clips so as to increase the stability of the chip once it was flipped over and resting on the clips. Finally, we flipped the setup over onto the shelf of an incubator. After imaging the BFCs to determine the number of cells at each spot in the array, we placed each BFC in a 10 cm dish within the incubator. Inside each 10 cm dish we placed a small vessel (usually the cap of a 15ml Falcon tube) containing sterile PBS. This maintained the humidity around the chip at a high level, which was crucial to avoid the formation of bubbles due to evaporation from the sides of the chip. Biocompatibility of the device was assessed by measuring the single cell colony-forming efficiency in the device (Appendix 2).

Cell culture

We cultured ABJ1 and CCE mESCs without feeders in mESC media: DMEM (Invitrogen) supplemented with 15% ES-qualified fetal bovine serum (Invitrogen), 4 mM L-glutamine (Invitrogen), 1 mM non-essential amino acids (Invitrogen), 50 U/mL penicillin, 50 µg/mL streptomycin (Invitrogen), 100 µM β-mercaptoethanol (Sigma-Aldrich), and 500 pM leukemia inhibitory factor (Chemicon, ESGRO). The ABJ1 cell-line was developed by the Page Lab at MIT and kindly provided to us by George Daley's lab (Harvard Medical School) and expresses green fluorescent protein under control of the Oct-4 promoter[84]. We cultured cells directly on TCPS dishes (Nunc, Delta surface) in a 37^oC humidified environment with 7.5%

CO_2. For maintenance of mESCs, we fed cells daily and passaged every other day using 0.25% trypsin-EDTA (Invitrogen), no more than 25 times. Cells were replated at 10,000 cells/cm^2.

BFC experiments and Imaging

After making clusters of mESCs on a substrate, we counted the number of cells in each cluster by imaging them on a microscope (Zeiss Axiovert 200), using a 10X objective (Zeiss, phase contrast). We then returned them to a dish placed in the incubator. After two days, we removed the BFCs from the incubator, and again imaged them as described above, to determine the colony-forming efficiency. Colony-forming efficiency measurements were made in collaboration with Stephanie Flavin, an undergraduate researcher in our laboratory. Very rarely we saw colonies with a combination of necrotic and live cells; such colonies were still scored as live when determining the colony-forming efficiency. To determine the self-renewal potential (see Results), we imaged colonies using the same objective, but using the fluorescence channel. For fluorescence imaging we used an X-Cite 120 illumination system (Exfo Life Sciences, Ontario) and a Spot RT Color camera (Diagnostic Instruments, Inc., Sterling Heights, MI). We quantified the fluorescence and areas of colonies using Metamorph (Molecular Devices). To measure the background fluorescence, we drew circles on 4 sides of the colonies and measured the average fluorescence across the circles. We used the same circles for all images from a given experiment. The circles had a radius of approximately 50 μm. For the colony-forming efficiency data, the averages from 10 experiments are presented. Two chips were typically used for each experiment (each chip had 200 wells). We only report the colony-forming efficiency for a particular number of cells if there were at least 10 clusters containing that number of cells across the two chips.

The Self-Renewal potential (SRP) data (section 3.3.3) was obtained from 4 experiments with two chips per experiment. It was found that the colonies in the center of the chip had higher SRP than colonies towards the edges (see Appendix 2 for details). Thus only colonies within a radius of 4 mm from the center were included in the analysis (chip size was 1 inch). The number of colonies eligible for analysis were 13, 18, 20, 39, 27, 49 & 27 respectively, for initial numbers of cells in the cluster going from 1 to 7.

For varying the seeding density we fabricated a new device with smaller wells (diameter of 25 μm), and with two regions, each having a different well spacing (Appendix 2). On one side of the chip we had a well spacing of 150 μm, while on the other side we had a spacing of 50 μm. With this device we were able to seed cells at 2 different densities on the same slide. The two regions were separated into two chambers with a gasket so as to not allow factors from one side to diffuse to the other side. Two experiments were performed for each cell-line (ABJ1 and CCE mESCs), and 1-2 chips were used in each experiment. Plated cells were imaged immediately after seeding, and the resulting colonies were imaged on day 1 as well as day 2.

Data analysis

Fitting was performed using the Curve-fitting toolbox in Matlab (Mathworks). Curves shown are the best fit to the set of all mean values. Fluorescence data from different experiments were normalized by using the following procedure: we plotted the area versus fluorescence for all colonies imaged on a given chip; we then fit this using a linear function and determined the average fluorescence for an object with a size

of 340 square pixels (corresponding to an object with a radius of 7.5 µm, i.e. one cell). We normalized all fluorescence values for that experiment by this value.

For the seeding density experiments, we counted the number of cells by using Metamorph's auto-thresholding function on phase contrast images. This function selects for the bright border of cells in phase contrast images. The number of thresholded objects can then be counted by using the Integrated Morphometry Analysis tool. These numbers were confirmed manually, and ghost cells (see Results) were excluded. For determining colony areas, after thresholding images we binarized them, and then dilated them using a circular filter (10 pixel diameter). This last step was required to include portions of the border that were sometimes excluded by the auto-thresholding function.

3.3 Results

In chapter 2 I described the principle behind a new method for modulating and studying cell-cell interactions – via the creation of cell clusters. Further, I described a first implementation of a device for creating clusters of cells – the nDEP microwell array. Subsequently, our lab developed a second device for making cell clusters – the BFC[67]. Below I describe results related to the use of the BFC for creating clusters of mESCs, and for studying the effects of cell-clustering on mESC survival.

3.3.1 Patterning clusters of cells using the BFC

Using the BFC, we were able to create clusters of 1-7 cells (Figure 3.2 a, b; Appendix 2). Sometimes clusters contained dark "cells" when imaged using phase contrast (Figure 3.2 c). These objects are most likely lysed cells i.e. the plasma membrane of cells, without a nucleus or cytoplasm[85, 86], and were not included as a contributing cell to the cluster. Interestingly, cells in a cluster were occasionally not all in the same plane – see, for e.g., the cluster to the top and right in Figure 3.2b. There are 2 cells in focus (top left), and 3 that are somewhat out of focus (bottom right). However, perhaps this is not surprising since the weight of a cell is only about 0.5 pN, while we have found that non-specific adhesion between a cell and pyrex, for e.g., is O(10 pN)[75]. In addition, the attachment force between a cell and a protein-coated substrate can be of the order of nN[87]. So it is conceivable that the adhesion forces between neighboring cells are sufficient to balance their weight. Occasionally (<5% of all clusters) this led to difficulties in the determination of the number of cells in such cluster, and such clusters were excluded from the analysis. This is also why determination of the cell number in clusters of more than 7-8 cells was not possible using phase microscopy. However, it may be possible to study clusters with more than 8 cells by using confocal imaging.

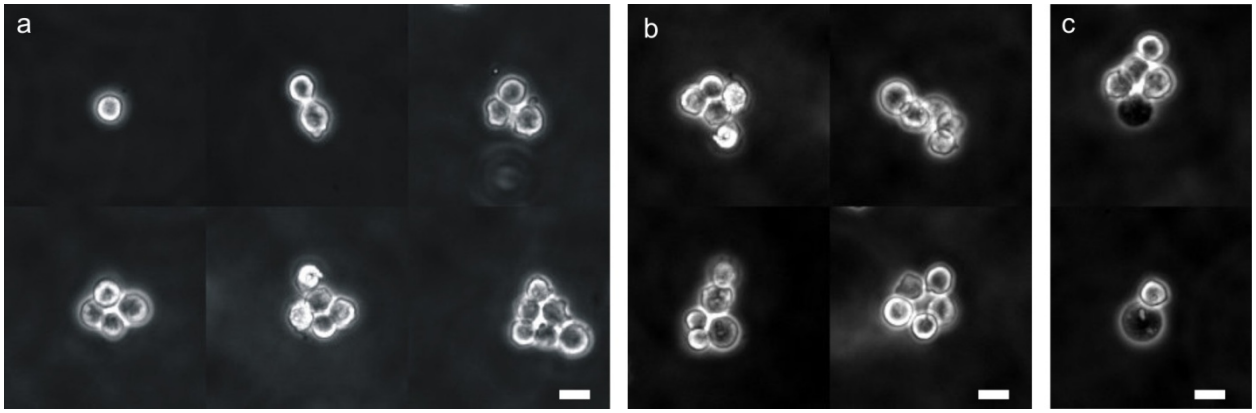

Figure 3.2 Making clusters of mESCs using BFCs. a. Clusters of 1-6 cells can be easily deposited and counted using the BFC (stitched image). b. Clusters were not always symmetric. For e.g., clusters of 5 cells were deposited in several different configurations. c. Clusters sometimes contained darker cells, which most likely do not contain a nucleus, and were excluded from the count. Scale: ABJ1 mESCs have a mean diameter of ~15 µm. Scale bars represent 20 µm.

We found that the deposited clusters re-organized over a timescale of 2-3 hours (Figure 3.3). To avoid errors in the counting of cells due to this re-organization, we restricted the length of time during which we counted cells to one hour.

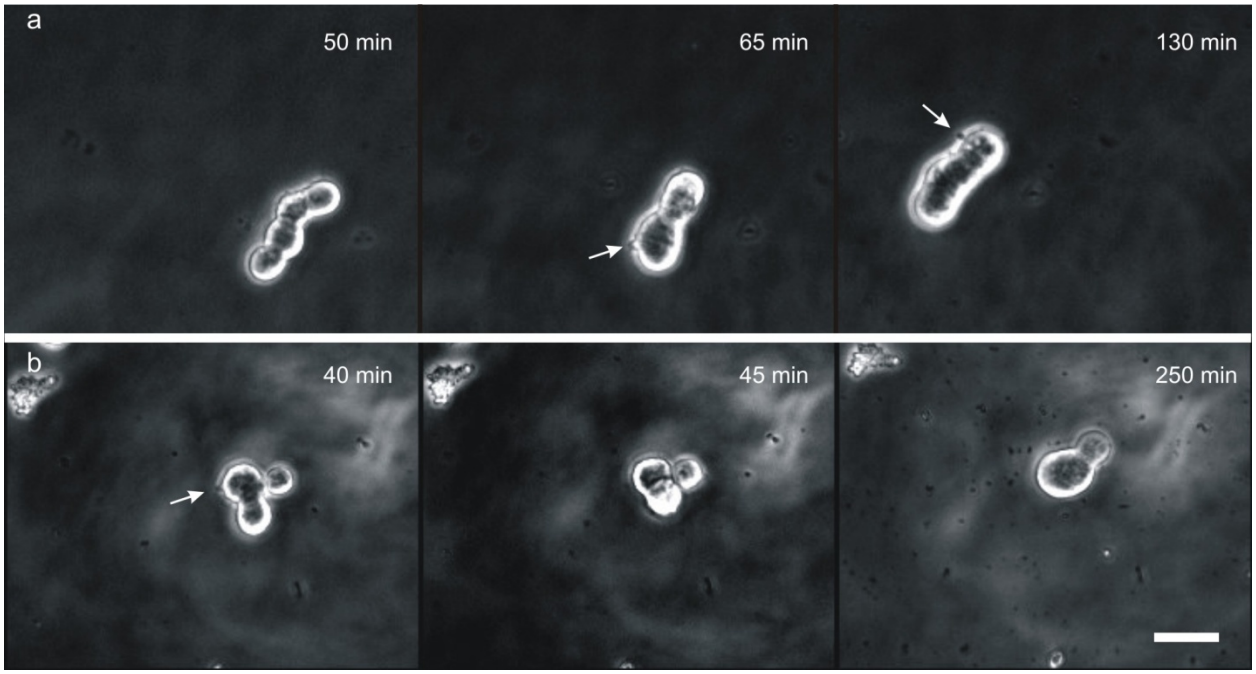

Figure 3.3 Two examples of clusters re-organizing after they were deposited onto a gelatin-coated slide. The locations of uropod-like structures are indicated by white arrows. Scale bar represents 30 µm.

The movement of cells was likely facilitated by uropod-like structures visible using phase microscopy (Figure 3.3, Figure 3.4, white arrows). Some structures were thin and string-like akin to filipodia[88] (Figure 3.4a), while others were considerably wider (akin to uropodia[88], Figure 3.4b). These structures were highly dynamic and appeared to re-organize on the timescale of minutes (Figure 3.4c), similar to what

has been observed in other cell types[89]. Finally, biocompatibility of the device was assessed by measuring the single cell colony-forming efficiency in the device (Appendix 2).

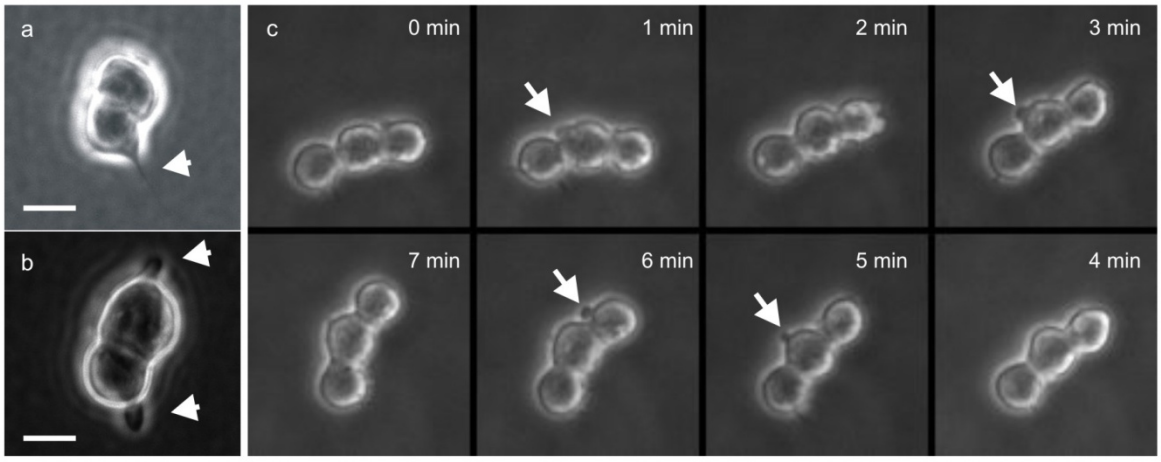

Figure 3.4 a & b. Magnified images of cell pairs showing filipod-like (a) and uropod-like (b) structures (white arrows). Scale bars represent 20 µm. c. Timelapse images of a cluster of 3 ABJ1 cells. Uropods showed dynamic behavior, re-organizing over a timescale of the order of minutes. Scale: ABJ1 mESCs have a mean diameter of ~15 µm.

3.3.2 Variation of colony-forming efficiency with the number of cells in a cluster

We are interested in investigating the role of intercellular signaling in the growth of mESCs. In the BFC, the readout is microscopy based. However, for mESCs visual determination of the number of cells in a colony is challenging for two reasons (i) mESC colonies are often 3-dimensional, though this is cell line-dependent (ii) boundaries between cells are indistinct even under phase microscopy. For example, Figure 3.5 shows a magnified phase contrast image of a typical mESC colony. The colony shown below has several tens of cells, based on average measurements of the number of cells in colonies at this stage of growth. However, none of the individual cells can be distinguished.

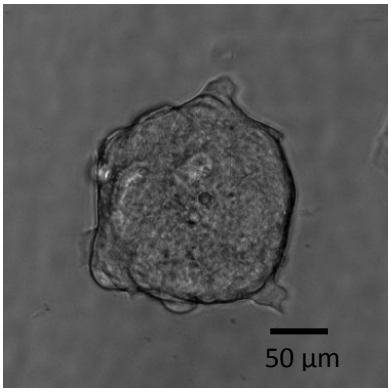

Figure 3.5 Phase contrast image of a typical mESC colony.

As a result, growth rate measurements could not be made in our laboratory. We instead decided to measure the survival probability of cell clusters, which is usually referred to, especially in the biology literature, as the colony-forming efficiency (CFE). These two quantities are the same when the length of

the experiment is much longer than the doubling time i.e. if the cell survives for a time much longer than the doubling time, it must also divide (a few times) in this period, resulting in the formation of a colony. Since our experiments were run for 48 hours while the mESC doubling time is ~12 hours, it is reasonable to use these terms interchangeably (see also Discussion).

Growth encompasses cell proliferation and cell death, therefore measuring survival/death provides information on one aspect of growth. In fact, we will see later in this thesis that diffusible interactions in mESC culture only modulate cell survival and not the division rate. The CFE is straightforward to determine since cells that die disintegrate. So on day 2 (48 hours after plating) one either sees a colony at the location that the cluster was initially present, or an unpopulated region. Occasionally we saw clusters of necrotic cells that were similar in appearance to the dark cells in Figure 3.2c, and such "colonies" were scored as dead. Larger initial clusters typically led to larger colonies (Appendix 2), indicating that the colonies observed on day 2 did correspond to the initial cluster of cells patterned on day 0, and had not migrated to a new location over two days. Additionally, we tracked several colonies over 24 hours and found that the migration speed was less than 100 µm/day (measurements made by Somponnat Sampatavanich). The distance between clusters on our chip was 750 µm. Thus colonies can be assigned with confidence to the clusters they arose from.

As shown in Figure 3.6, the colony-forming efficiency increases monotonically with the number of cells in the initial cluster. We then checked if this data indicated that the cells interacted with one another in a manner that affected the CFE. For this, we determine the expected form of the increase in CFE with the initial number of cells in a cluster for non-interacting cells. Let $\boldsymbol{p_d}$ be the probability that a cell in the initial cluster does not produce any cells (daughters etc.) that survive till day 2. If the cells are non-interacting, the probability of forming a colony, or more accurately, the probability that at least one cell produces cells that survive to day 2 is given by $\mathbf{CFE_{NI} = 1 - p_d^n}$, where $\boldsymbol{n}$ is the initial number of cells in the cluster. We fit this function to our data (see methods for details). As can be seen in Figure 3.6a, the measured CFE increases faster than $\mathbf{CFE_{NI}}$, indicating that the cells do interact with each other (statistics are described below). Also, the measured CFE is higher than $\mathbf{CFE_{NI}}$ (for n=5), indicating that the interaction improves survival.

To quantify the improvement in survival we then determined the average probability for a cell in the cluster to give rise to cells that survive till day 2. If $\boldsymbol{p_{d,av}}$ is the average probability that the above does not happen, then the relation between the measured CFE (CFE_{meas}) and $\boldsymbol{p_{d,av}}$ is given by $\mathbf{CFE_{meas} = 1 - p_{d,av}^n}$. Here again, $\boldsymbol{n}$ is the initial number of cells in a cluster. Then the average single cell CFE/progeny survival probability is given by

$$\text{Average single cell CFE} = 1 - \boldsymbol{p_{d,av}} = 1 - (1 - CFE_{meas})^{\mathbf{1/n}}.$$

Figure 3.6b shows that the average single cell CFE for a cell in a cluster increases by about 6% for every cell added to the cluster (p(ANOVA)=0.004).

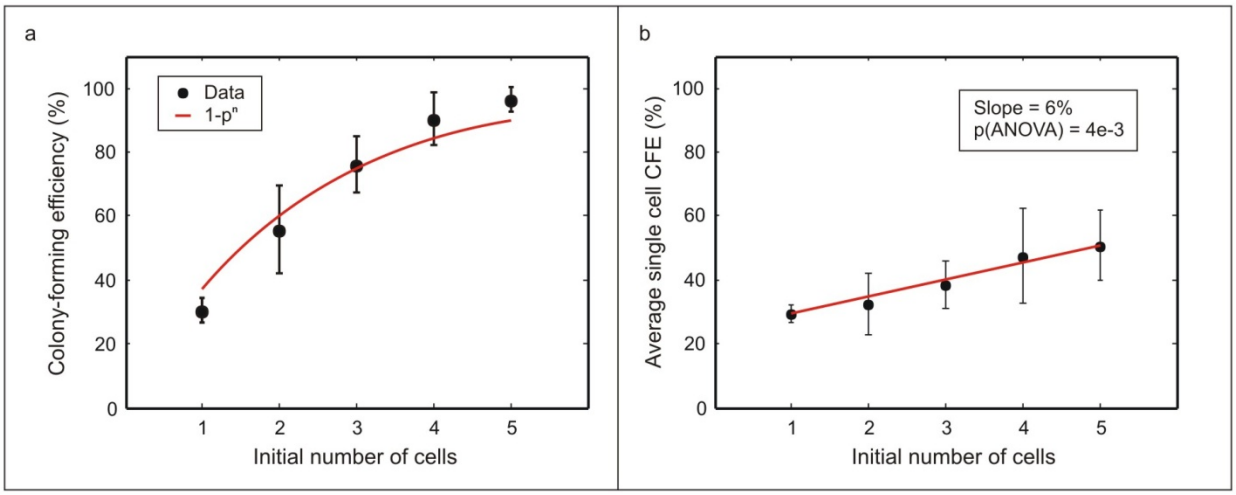

Figure 3.6 a. Measured (dots) and calculated (solid line) colony forming efficiency for CCE mESCs versus the initial number of cells in the cluster. b. The average CFE for a single cell within the cluster versus the initial number of cells in the cluster (dots). The solid line is a linear fit to the data.

3.3.3 Self-renewal potential and its variation with the number of cells in a cluster

We next decided to investigate a more comprehensive measure of self-renewal. To do this we first need to define a quantitative measure of self-renewal. Since the process of self-renewal consists of cell division while maintaining the pluripotency of cells, we wished to determine the growth rate as well as the level of pluripotency of cells (defined as the percentage of pluripotent cells in a colony) in the colony resulting from a cluster of cells. Pluripotency can be assessed via a number of assays. The least stringent functional assay for the developmental potential of a cultured cell is *in vitro* differentiation followed, with increasing stringency, by the generation of teratomas (germ cell tumors), chimera formation, and germ line contribution[90]. The most rigorous test for developmental potency is the injection of cells into 4n host blastocysts[91, 92], which results in animals composed only of the injected donor cells ("all ES" embryos or animals) rather than a chimeric composite of injected and host-derived cells. However, these approaches are challenging to perform with single cells, and when one is interested in assaying large numbers of cells. A commonly used alternative is to measure the expression level of certain proteins that are referred to as pluripotency markers[157, 158]. These proteins are highly expressed in ES cells, but not in differentiated cell types. Three proteins that are widely accepted as pluripotency markers for mESCs are the transcription factors Oct-4, Sox-2, and Nanog[23]. Ideally one would like to separately measure the growth rate and marker expression of cells. However, as mentioned before, measuring the growth rate for ESCs is challenging in a system such as ours where the readout is microscopy based. Therefore we decided to instead measure the total Oct-4 expression of the *colony* formed from a cluster of cells, i.e., the product of the Oct-4 expression level per cell and the number of cells in the colony. We call this quantity the self-renewal potential (SRP) of a cluster of cells. Since the SRP depends on the Oct-4 expression level as well as the number of cells in the resulting colony, it encompasses both features of self-renewal. Our choice of Oct-4 over Sox-2 or Nanog was determined by the availability of a cell-line expressing green fluorescent protein (GFP) under the control of the Oct-4 promoter (ABJ1 cell-line[84]), which allowed for an easy, microscopy-based determination of the SRP.

As seen in Figure 3.7a, the SRP increases with the initial number of cells in the cluster (***n***). For ***n*** = 6 and 7, the SRP is higher than expected from an extrapolation from n = 1 to 5. In Figure 3.7b, we plot the SRP per (initial) cell for ***n*** = 1 - 5 and ***n*** = 6 – 7, which are significantly different (p = 0.05).

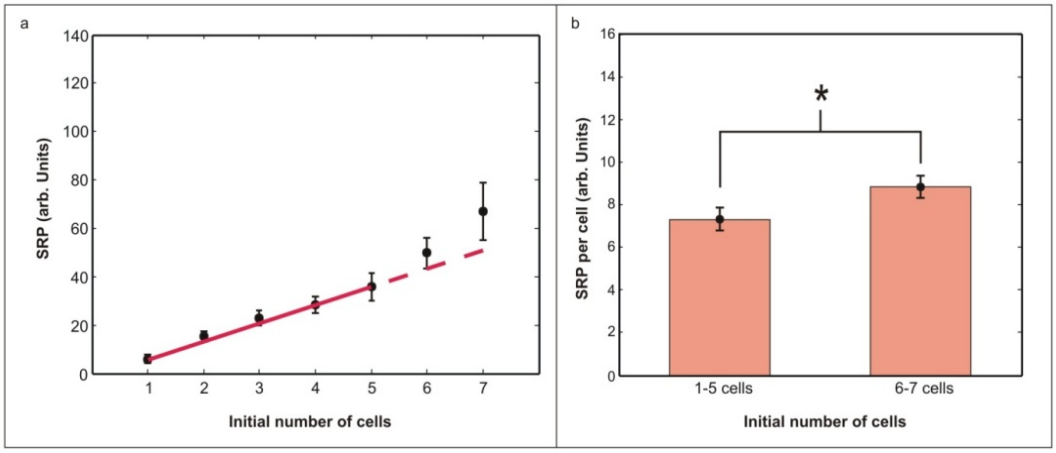

Figure 3.7 a. The Self-renewal potential (SRP) of clusters of cells versus the initial number of cells in the cluster. Error bars show standard error b. The SRP per cell for n = 6 - 7 is significantly higher than for n = 1 – 5 (p=0.05). Error bars show standard error.

Further evidence of intercellular interaction can be found by examining the standard deviation of the SRP. Figure 3.8a shows the standard deviation of the SRP versus initial number of cells. The total variance in the self-renewal potential (v_t) has contributions from measurement error (v_m) and the true biological variance (v_b). Since the measurement error and biological variance come from independent processes, $v_b = v_t - v_m$. The standard deviation is the square root of the variance. Then,

$$\sqrt{v_t} - \sqrt{v_m} \leq \sqrt{v_b} \leq \sqrt{v_t} + \sqrt{v_m}\,.$$

By repeatedly making measurements of the fluorescence level of the same colony, we estimate that our measurement error $\sqrt{v_m}$ is less than 5%. Therefore in Figure 3.8b we plot $\sqrt{v_b}$ as $\sqrt{v_t}$, with error bars of $\sqrt{v_m} = 5\%$ (of the mean values from Figure 3.7a). We fit this data to a polynomial funtion and found that the best-fit exponent was 0.97. For a non-interacting system of cells, we would expect standard deviation to increase much slower – with an exponent of only 0.5. The best-fit with an exponent of 0.5 is also shown in Figure 3.8b (orange line). Note that more stringently, since $\sqrt{v_b} = \sqrt{v_t - v_m} \leq \sqrt{v_t}$, we can actually use one-sided error bars. However, this would not change our conclusions. The above two results (Figure 3.7 and Figure 3.8) indicate that mESCs within a cluster do interact with one another, and that the interaction also improves their self-renewal (in addition to the CFE).

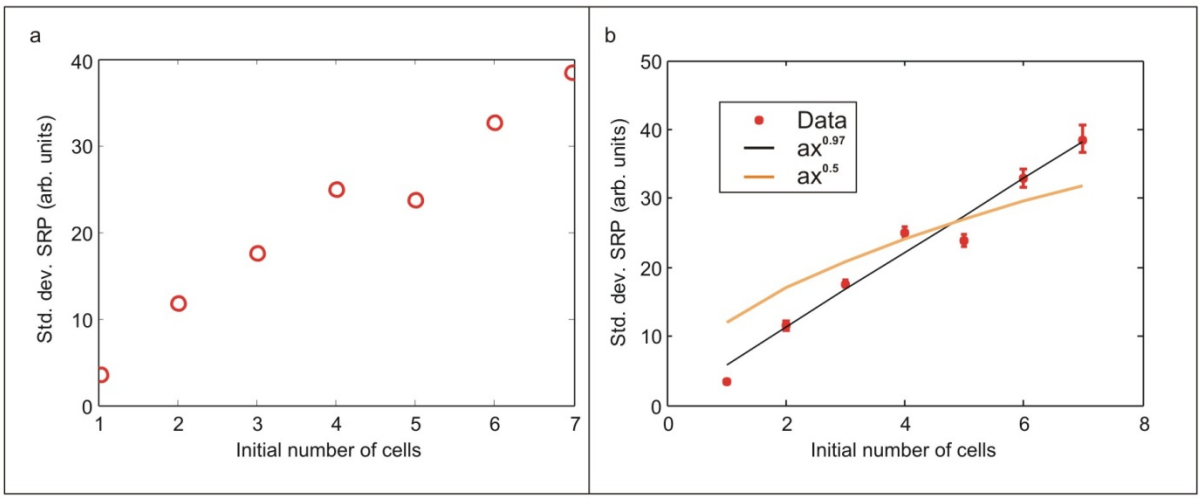

Figure 3.8 a. The standard deviation of SRP versus the initial number of cells in a cluster. b. The standard deviation of the SRP increases almost linearly with the initial number of cells suggesting that the cells must be interacting with one other. For non-interacting cells the standard deviation would increase as the square root of the initial cell number (orange line).

3.3.4 Variation of colony-forming efficiency and colony area with plating density

Finally, we wished to determine whether diffusible signaling may play a role in the effects mentioned above. To do this we investigated the effect of plating density on the CFE; by varying the plating density we vary the amount of diffusible signal that cells can exchange. Measuring colony-forming efficiency (CFE) as a function of density is typically challenging because colonies may merge, especially at higher densities. We used the BFC to mitigate this problem. We fabricated new devices, where each chip had two regions with well-to-well spacings of 300 µm and 100 µm. We can typically load ~50% of these wells and so most cells start out at least 200 µm apart (see Appendix 2). Additionally, as will be shown below, only ~50% of these cells form colonies, so colonies on Day 2 are typically 400 µm apart. Since most Day 2 colonies have a diameter of less than 150 µm, they do not merge. This is in contrast to traditional assays that vary density in dishes, without patterning. In that case the colonies may merge (especially at higher plating densities) because there is no enforcement of a minimum colony-colony distance. I.e. although one can plate cells such that on average they are 200 µm apart, there is a large variation in the cell-cell spacing. Especially when experiments are performed in multiwell plates, we have observed that cells tend to preferentially attach towards the edge of the well, leading to an increased local density in that area and exacerbating the tendency of colonies to merge. The BFC, by enforcing a minimum inter-colony spacing, allows investigation of higher global densities than is possible without patterning.

The new BFCs also had smaller wells (diameter of 25 µm) to increase the fraction of sites that contained single cells. By starting with primarily single cells at both densities, we set the initial amount of contact interaction to zero. Using this device, we observed that for ABJ1 cells plated at ~300 cells/cm^2, the CFE was ~45%, while for cells plated at ~3000 cells/cm^2, the CFE was ~60% (Figure 3.9a, Appendix 2). This difference was statistically significant (p=0.004). Additionally, the value of the CFE at the higher density represents a lower bound estimate of the actual CFE, since some of the "colonies" on day 1 did seem like they had merged by day 2 due to a combination of growth and migration. Figure 3.9b shows that for

ABJ1 mESCs, the colony area is also greater for cells plated at the higher density (p=0.001, colonies that seemed like they have merged were excluded from the t-test). For CCE mESCs, there was a significant difference in the CFE at low densities relative to high densities (Figure 3.9c, p=0.01), but not for the colony areas (Figure 3.9d, p=0.36). The increase in CFE at the higher density for both cell lines indicates that the variation in CFE seen in our previous experiments (Figure 3.6) is at least partly due to the effects of diffusible signaling.

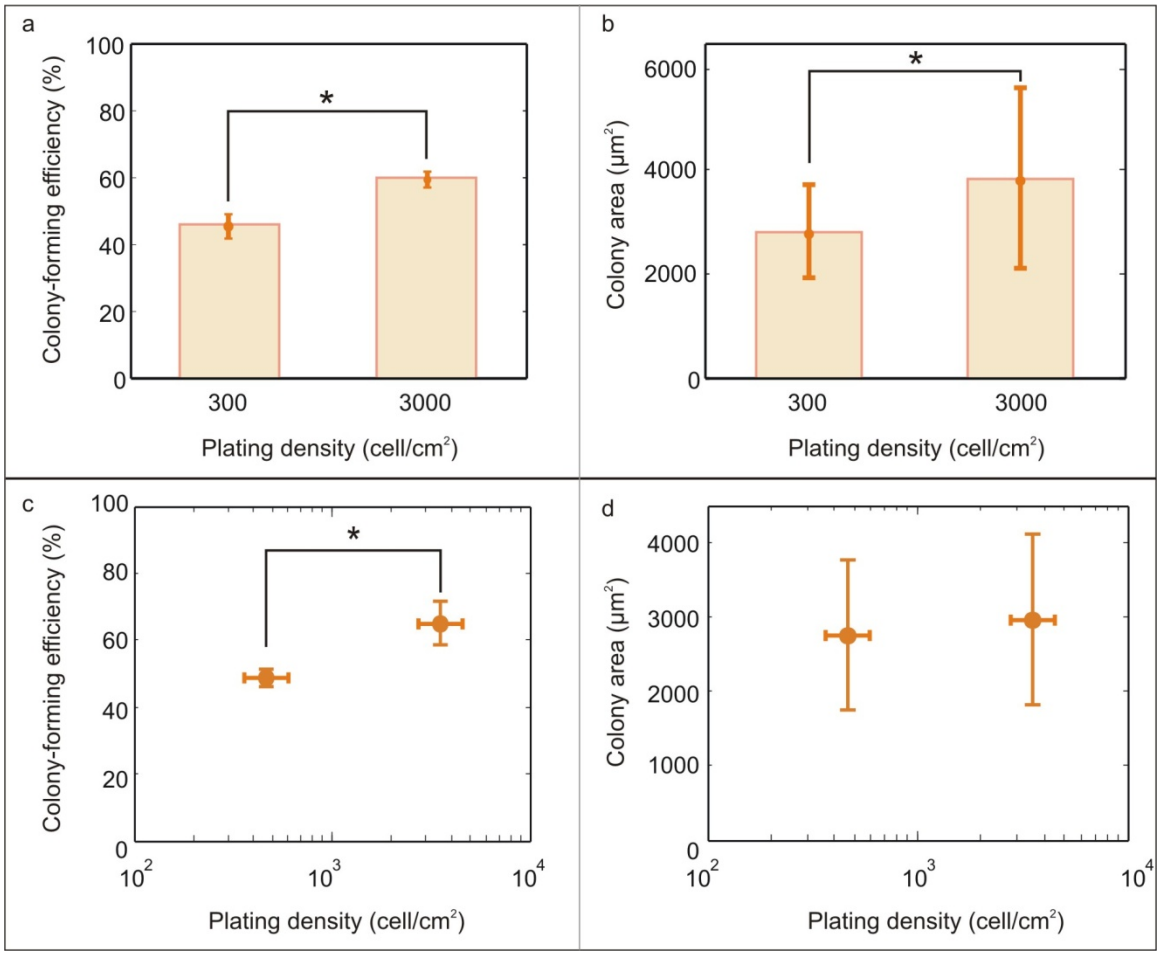

Figure 3.9 The colony-forming efficiency for mESCs plated at ~300 cells/cm^2 and ~3000 cells/cm^2 (a & c, for ABJ1 and CCE mESCs respectively). The colony area for mESCs plated at ~300 cells/cm^2 and ~3000 cells/cm^2 (b & d, for ABJ1 and CCE mESCs respectively).

3.4 Discussion

In this chapter we presented results from 3 different experiments performed using BFCs that all suggest that mESCs interact with one another in a manner that affects their colony-forming efficiency and self-renewal potential. In the first two experiments we used the BFC as a screening tool to create clusters of different numbers of cells, thereby varying the level of diffusible and contact signaling between cells. In these experiments we found that the CFE and SRP of cells increase with the initial number of cells in a cluster. Interestingly, while the CFE appears to increase linearly with the initial number of cells, for the SRP it appears as if there is a threshold value of 6 cells per cluster below which there is no effect of the

altered signaling level on the mean SRP. The fact that these trends are different is perhaps not surprising given that pathways that govern survival and growth and pluripotency could be distinct.

With regard to the equivalence of CFE and survival efficiency, one caveat is worth mentioning. Biologists will often differentiate between survival during the initial stage of culturing when adherent cells are in the process of attaching to the substrate, and subsequent survival of cells. In our BFC experiments with mESCs we have not made this distinction, because it does not appear to be possible to make a visual assessment of attachment for mESCs – for example, the cells in Figure 3.3a or Figure 3.4c have the ability to move and re-organize, and show the presence of uropods, suggesting that they have made attachments with the substrate, but the cells still exhibit a round morphology. In contrast, for other cell types such as fibroblasts or endothelial cells, attachment is associated with distinct morphological changes (spreading). For such cells it should be fairly straightforward to separately measure survival during and after attachment. At the end of the attachment period, survival could be assessed by whether or not a cell has attached, and cell death could perhaps be reconfirmed when measuring the CFE to determine post-attachment survival.

With regard to the plating density experiments, we have observed in other experiments that over a 48 h period, nutrient depletion becomes an issue when mESCs are plated at a density of greater than 10,000 cells/cm^2. In those experiments the height of the medium was ~2.5mm. In the BFC, the height of the medium layer is only 0.5mm, so we may expect nutrient depletion to become an issue at plating densities of greater than 2000 cells/cm^2. So if one were to control for nutrient depletion, it is conceivable that one may see an even greater difference in the CFE at low versus high densities.

It is interesting to compare our technique with one developed by Christopher Chen's lab[156]. Their technique is analogous to that shown in Figure 2.2, where they trap cells in agarose wells to create clusters (Figure 3.10). In their analysis of their data they have ignored the effects of altered diffusible signaling within cell clusters. Our data suggest that such an assumption may not be justified. Additionally as mentioned in chapter 2, because the cells are constrained by the wells and do not appear to be able to divide, they are constrained to performing assays over short periods of time. In their assays they have assessed growth by measuring the amount of incorporation of 5-bromo-2′-deoxyuridine (BrdU) into cells, which is a measure of the DNA synthesis rate. One advantage of constraining cells using their method is that it prevents the movement of cells. Thus they can easily measure growth separately for each of the cells in the cluster. The cell in the center has 2-3 neighbors (clusters with 3 and 4 cells respectively) while the cells at the corners contact only one cell. Thus good internal controls are obtained. In future it may be interesting to track individual cells within clusters in the BFC, though as mentioned earlier, for mESCs this may not be feasible. Another advantage of their design is that the length of the contact boundary between cells is constrained to be fairly constant. On the other hand, it is not clear as to how constraining cells in this manner affects their physiology. The BFC provides a complementary approach for studying cell signaling. In the BFC cells are able to move and grow. This necessitates the use of timelapse imaging for tracking the fate of *individual* cells. For example, in Figure 3.10G all cells within the 3 cell cluster have two contacting neighbors, while in Figure 3.10E only the central cell contacts two other cells. In principle cells within 3 cell clusters could switch between such configurations. Additionally, the length of the contact boundary between cells is variable, though it is

not known whether this parameter is physiologically meaningful. On the other hand, cells within clusters in the BFC are very likely in a physiological state that is much closer to that of cells studied via more traditional assay methods.

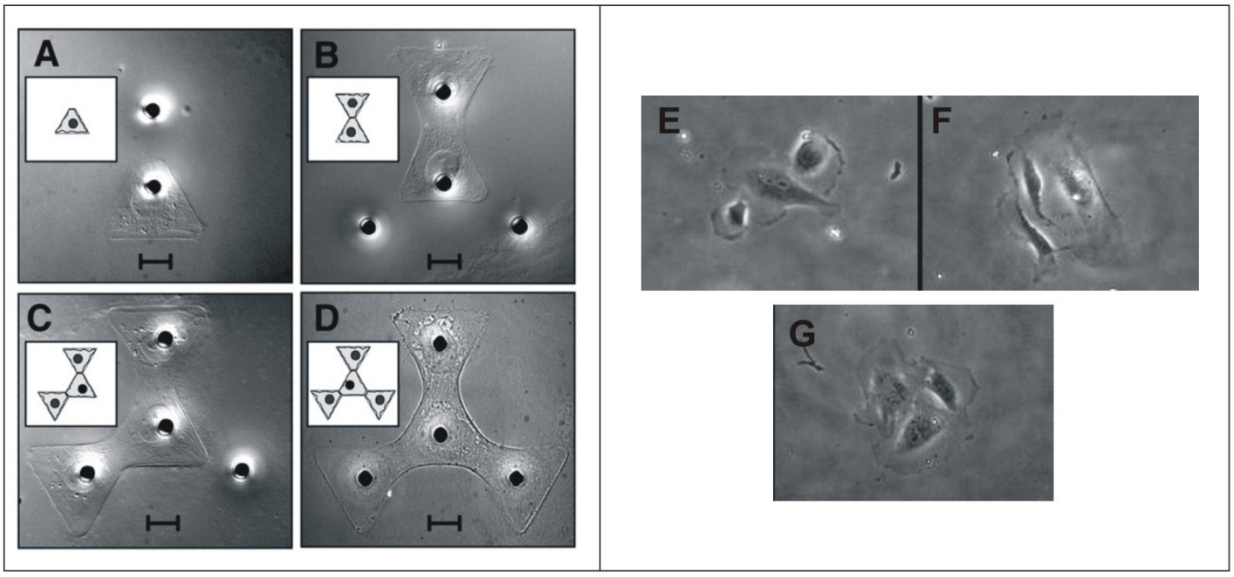

Figure 3.10 A-D. Clusters of cells generated via a technique developed by Christopher Chen's laboratory wherein cells are trapped within wells in a layer of agarose. Clusters of 1-4 cells are shown. Scale bars are 10 µm. Image reproduced from Gray *et al.*, Experimental Cell Research 314 (2008) 2846-2854. E-G. Images of 3-cell clusters within a BFC; these images illustrate that the length of the contact boundary between cells is variable.

Finally, we discuss the various possible implications of the increase in the self-renewal potential (SRP). An increase in the SRP could be the result of increases in growth rate, or increase in Oct-4 expression, or both. We will show in the next chapter that the growth rate for mESCs is dependent on the plating density. Thus it is certainly plausible that the growth rate could increase with the number of cells in the cluster. The other possibility is that signaling (also) leads to an increase in the expression of Oct-4. Results from Davey and Zandstra[94] suggest that mESCs also secrete factors that increase the expression of Oct-4 and Nanog, though it is worth noting that in their experiments the substrate was coated with fibronectin, which is atypical when culturing mESCs. One caveat associated with the use of Oct-4 as a pluripotency indicator is that overexpression of Oct-4 has also been shown to lead to differentiation[152]. However, Oct-4 is still widely used as a pluripotency marker[23], suggesting that without the use of transgenes it is perhaps unlikely that Oct-4 will be overexpressed by mESCs. Finally, it is worth noting that Oct-4 appears to be downregulated rapidly in cells undergoing differentiation because the distribution of single cell Oct-4 levels has been shown to be bimodal. Thus, changes in the Oct-4 expression at the colony-scale, or a culture as a whole must be due to changes in the %Oct-4+ cells and not due to incremental changes in Oct-4 expression[95].

3.5 Summary

In this chapter we presented results from 3 different experiments performed using BFCs that all suggest that mESCs interact with one another in a manner that improves their colony-forming efficiency and self-renewal potential. In the first two experiments we used the BFC as a screening tool to create clusters of different numbers of cells, thereby varying the level of diffusible and contact signaling between cells. In these experiments we found that the CFE and SRP of cells increase with the initial number of cells in a cluster. For the SRP it appears as if there is a threshold value of 6 cells per cluster below which there is no effect of the altered signaling level on the mean SRP. We also found that the variance of the SRP increased much faster than would be expected for a non-interacting system of cells.

In the final set of experiments we plated cells as single cells, but at different densities, and found that the CFE is proportional to the plating density. This suggests that the increase in CFE seen in the first experiment is at least partially due to a diffusible signal.

In the next chapter I will describe experiments we performed that support results obtained using the BFC, thereby validating the technology.

Chapter 4: mESC cultures contain an autocrine survival factor

In the previous chapter I described several experiments we performed, with the aid of the BFC, which indicated that mESCs may interact with one other. In particular, the final experiment where we found that variations in the plating density affect the colony-forming efficiency of mESCs suggested that mESCs may communicate with one other via a diffusible growth/survival factor. In this chapter I describe further experiments we performed to corroborate this result.

4.1 Materials and methods

Cell culture and staining

We cultured cells directly on TCPS dishes (Nunc, 172958) in a 37^{o}C humidified environment with 7.5% CO_2. For maintenance of mESCs, we fed cells daily and passaged every other day. Cells were replated at 10,000 cells/cm^2. More information on our cell lines is provided in Appendix 5.

Serum-containing medium: For some experiments (see Results) we cultured ABJ1 and CCE mESCs without feeders in serum-containing mESC media: DMEM (Invitrogen, 11960-044) supplemented with 15% ES-qualified fetal bovine serum (Invitrogen, 16141-079), 4 mM L-glutamine (Invitrogen, 25030-081), 1 mM non-essential amino acids (Invitrogen, 11140-050), 50 U/mL penicillin, 50 µg/mL streptomycin (Invitrogen, 15140-122), 100 µM β-mercaptoethanol (Sigma-Aldrich, M7522), and 500 pM leukemia inhibitory factor (Chemicon, ESGRO ESG1107).

Serum-free medium: The second set of experiments described in this chapter were performed in a serum-free medium formulation developed for mESCs by Austin Smith's group[159]. They refer to this medium as N2B27, supplemented with LIF and BMP-4. N2B27 is a 1:1 mixture of N2 medium and B27 medium, where the N2 formulation is slightly modified from the original. The N2 medium was developed for growing of neuroblastoma cells[96]. The original N2 formulation consists of 5 µg/ml insulin, 100 µg/ml transferrin, 20 nM or 6 ng/ml progesterone, 20nM sodium selenite, and 100 µM, or 16 µg/ml putrescine added to DMEM/F12. The modifications to the formulation for mESCs include additional insulin and the addition of BSA. The final concentration of insulin and BSA in the modified N2 are 25 µg/ml and 50 µg/ml respectively. The B27 supplement was developed for growing embryonic hippocampal neurons[97]. It is a proprietary formulation by GIBCO, and is added to Neurobasal medium. N2B27 is supplemented with 500 pM LIF and 10 ng/ml BMP-4. For growth in this serum-free formulation, plates must be coated with gelatin. Plates were incubated with 0.1% gelatin (Millipore) for 15 minutes at room temperature and then washed once with PBS prior to plating cells. Additionally, cells were dissociated from the surface with TryplE Select (GIBCO) instead of using 0.25% trypsin-EDTA. Finally, after dissociation and addition of some medium, the suspension was spun down, supernatant was aspirated, the (cell) pellet was washed once with medium, and then finally re-suspended for plating. Cells were adapted in this medium for 15 passages prior to performing experiments. Experiments were performed between 3-8 passages after thawing adapted cells.

Staining with YO-PRO-1 Iodide (Invitrogen) was performed for 15 minutes at 37^{o}C, at 2 μM final concentration. TUNEL assay reagents were purchased from Roche and staining was performed according to manufacturer's protocols.

Growth versus density experiments

Growth versus density experiments were performed in 12-well plates (Nunc, Delta surface). In smaller wells we found that the meniscus effects were strong and led to the accumulation of cells in the center of the well, which meant that the local density in the center of the well was much higher than the desired average density. To avoid possible complications due to this effect we always performed these experiments in 12-well plates. Cells were counted using a coulter counter (Beckman Z2). A background subtraction was performed by using equivalent amounts trypsin and media not containing cells.

For experiments where we measured the fold growth at two different time points, we created two copies of the experiment and counted each at one time point. Data for the growth of ABJ1 cells in serum-containing medium are from 2 separate experiments, with two wells corresponding to each density. Data shown for CCE mESCs shown is from a single experiment done in triplicate. This experiment was repeated for confirmation, and the same trend was observed though values differed numerically from the same experiment. The experiments in serum-containing medium were done ~5 passages after thawing cells, when the growth curves were relatively independent of passage number.

Conditioned medium

To prepare conditioned medium, after collecting the medium from a cell-culture dish, we filtered it (and the control) through a 0.25 μm filter (with a syringe) to remove floating cellular debris. The control was also incubated for the same length of time in a similar dish as the cell culture. This is to address the issue of evaporation which otherwise concentrates the proteins only in the cell culture and leads to erroneous results (data not shown). Since cells also take up nutrients from the medium, we wished to replenish all nutrients before performing further growth assays. To do this, since all the nutrient molecules are <1 kDa, we dialyzed the conditioned and control medium using a 3 kDa centrifugal filter unit (Millipore). Then we replenished the > 3 kDa portion with fresh < 3 kDa nutrient components. We also added LIF, or LIF and BMP4 in the case of the serum-free medium, to ensure that cells grown in these media would be in a self-renewing state. For Day 0-1 growth assessment, CM was collected at 24 hours from cells plated at 1-1.5e4 cm^{-2}. For Day 1-2 growth assessment, CM was collected over Day 1-2 from cells that were plated at 3e4 cm^{-2}, and then fed at 24 hours with fresh medium. The CM was typically applied to cells plated at 2e3 cm^{-2}. For CCE mESCs in serum-containing medium (Figure 4.3), 3 experiments were performed, each in triplicate. For ABJ1 mESCs in serum-free medium (Figure 4.4), 2 experiments were done, in triplicate. Data from different days were normalized using the control data.

Statistical analyses of growth data

For Day 0-1 a single-factor ANOVA test was applied to the data. For Day 1-2, we divided all Day 2 cell counts by all Day 1 cell counts (for a given density) and performed a single-factor ANOVA test on the resulting dataset.

Attachment rate measurements

Cells were plated in 12-well plates with one plate for each time point. 3 wells were plated for each density. At each time point each well was gently washed once in its own medium and this medium, along with unattached cells, was collected for counting. We then washed each well with PBS, detached the attached cells using TryplE (Invitrogen), and counted the number of attached cells. Finally we computed the percentage of unattached cells for each well and averaged over the triplicates. Data shown is from a single such experiment. In a second experiment, similar trends were obtained though actual values differed slightly.

Catalase titration experiment

Different concentrations of catalase were added to mESCs grown in N2 medium (+ LIF and BMP-4) and the number of cells at the end of day 2 was determined using a Coulter counter. B-27 was not added to the above medium since it already contains catalase.

4.2 Results

4.2.1 Variation of growth rate with plating density

In the last chapter (3.3.4) we showed that the colony-forming efficiency for mESCs is proportional to the plating density. We then decided to check whether the growth rate is also dependent on the plating density. As mentioned in section 3.3.2, determination of the growth rate using the BFC is challenging (for mESCs) since the readout has to be visual. Thus we decided to resort to more traditional dish-based assays for the second portion of this thesis. Since these assays are much simpler to perform, it also allowed us to extend the range and resolution of the densities studied. Finally, by performing these assays in a more traditional and widely accepted well-plate format, and comparing the results to those obtained with the BFC, we can further assess the biocompatibility of the BFC, and also evaluate its use as a tool for studying intercellular signaling.

In Figure 4.1 we show the variation of fold growth (over two days) with plating density for ABJ1 and CCE mESCs. For ABJ1 cells, the fold growth increases logarithmically with plating density for densities from 250 to 5000 cells/cm^2, then levels off, and finally starts to decrease. The increase in fold growth in the range of 250 to 5000 cells/cm^2 is in agreement with the results of section 3.3.4 where the colony-forming efficiency was higher for cells plated at 3000 cm^{-2} versus those plated at 300 cm^{-2}. The decrease in fold growth at higher densities is likely due to the combined effect of nutrient depletion and metabolite accumulation. CCE mESCs which grew a little slower relative to ABJ1 cells also showed an increase in fold growth with density, but did not show a decrease in fold growth at higher densities. For the increasing portion of the curve for ABJ1 cells (Figure 4.1a) the p value from an ANOVA test is 9.6e-7, while for the CCE data, the p_{ANOVA} is 3.8e-6.

4.2.2 Post-attachment post-lag growth of mESCs

Next, we decided to investigate the time dependence of the fold growth in further detail. The commencement of growth in cell cultures (including mammalian cell cultures) is preceded by a lag phase[98, 99]. Additionally, when adherent cells are re-plated, for reasons that are not understood, not all

cells will attach. One might hypothesize that this is due to injury of cells during the trypsinization/trituration process. We wanted to separate the contributions of density–dependent differences in lag phase and attachment (if any) from density-dependent differences in proliferation and survival (if any) towards the overall growth over two days.

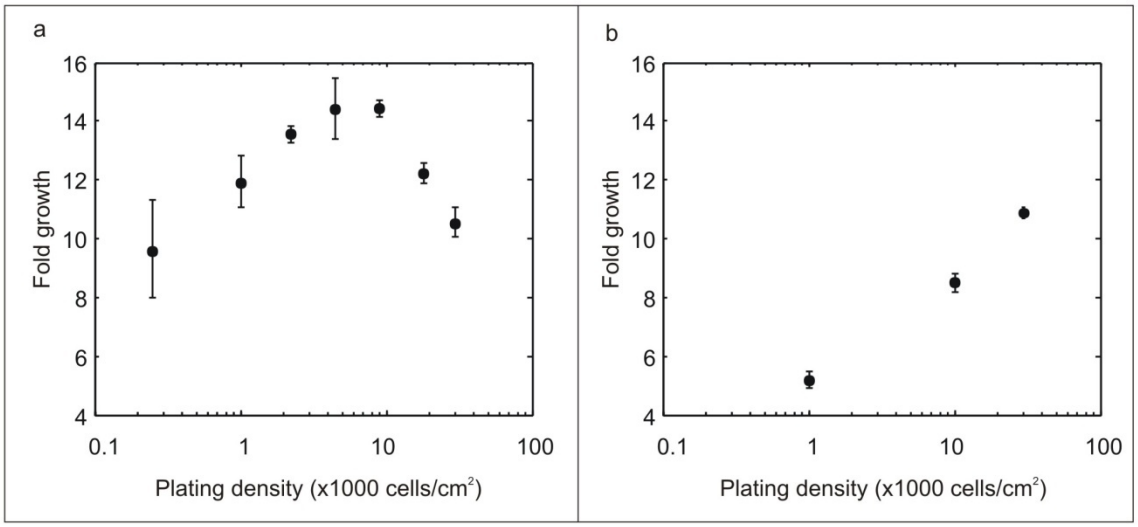

Figure 4.1 Variation of fold growth with plating density for ABJ1 mESCs (a) and CCE mESCs (b). Error bars correspond to one standard deviation in all figures.

Note again that attachment and survival are related in that a healthy adherent cell is expected attach to its substrate. However, biologists will often distinguish between attachment (and/or survival during attachment) and post-attachment survival (personal communications). We hypothesize that survival during the attachment phase may include different mechanisms as compared to post-attachment survival, such as the ability to recover from re-plating associated insults. Regardless, since the attachment phase is typically much shorter than the length of the entire culture process, it is interesting and useful to distinguish between survival during attachment and post-attachment survival.

Modulation of the lag phase is a second early mechanism by which the overall growth rate of a culture is affected. The molecular circuitry associated with the lag phase is just starting to be explored[99, 100], primarily using yeast as a model. A widely accepted hypothesis is that the lag in growth in yeast is at least partly caused by the transition of cells from a slow-growing post-log phase phenotype associated with a nutrient-poor environment to a rapidly-growing log-phase phenotype associated with a nutrient-rich environment[99]. Brejning *et al.* have shown that when yeast are inoculated into fresh medium, ~5% of genes are more than 5-fold induced and ~2.5% are more than 5-fold repressed[100]. Their study and work by others[99] suggests that differences in glucose concentration may be primarily responsible for these changes in transcription.

Perhaps the most interesting aspect of growth is post-attachment, post-lag-phase growth, because it reflects a *more* normal, *in vivo*-like state of a cell, free of artifacts associated with having to re-attach to a substrate, and having to re-adapt to fresh medium. Initially, based on our observations of mESC cultures via microscopy, we estimated that attachment is complete within 24 hours after re-plating of

cells. Additionally, studies in other mammalian cells have shown that the lag phase is typically less than 24 hours[101, 102]. Later in this chapter I will present our measurements of these quantities for mESCs, but in a different (serum-free) medium formulation. To assess post-attachment post-lag growth in the serum-containing medium used in all our assays thus far, we measured the fold growth at 24 and 48 hours after plating. Figure 4.2 shows that a density-dependent increase in fold growth is observed on Day 1-2[c] as well (for some range of densities). These trends are statistically significant - for ABJ1 cells (Figure 4.2a), for Day 0-1, p(ANOVA) is 5.7e-6. For Day 1-2, since we are particularly interested in knowing whether the *increasing* trend is statistically significant, we applied the ANOVA analysis only to the range 500-2500 cells/cm^2 (see Methods for details); this yielded a p-value of 2.6e-3. Thus the density-dependent growth is not caused by differences in attachment or length of lag phase alone. CCE mESCs show similar growth trends (Figure 4.2b) and similar analyses yielded p values of 1.4e-4 for Day 0-1, and 1.1e-11 for Day 1-2. Additionally, we found that the cells grew much faster on Day 1-2 as compared to Day 0-1; this is likely due to a combination of the effects of the lag phase and the fact that the attachment efficiency is <100%. Since density-dependent increases in growth rate are one of the hallmarks of systems with autocrine signaling via growth factors[43], these results again suggest that mESCs produce one or more diffusible growth factors.

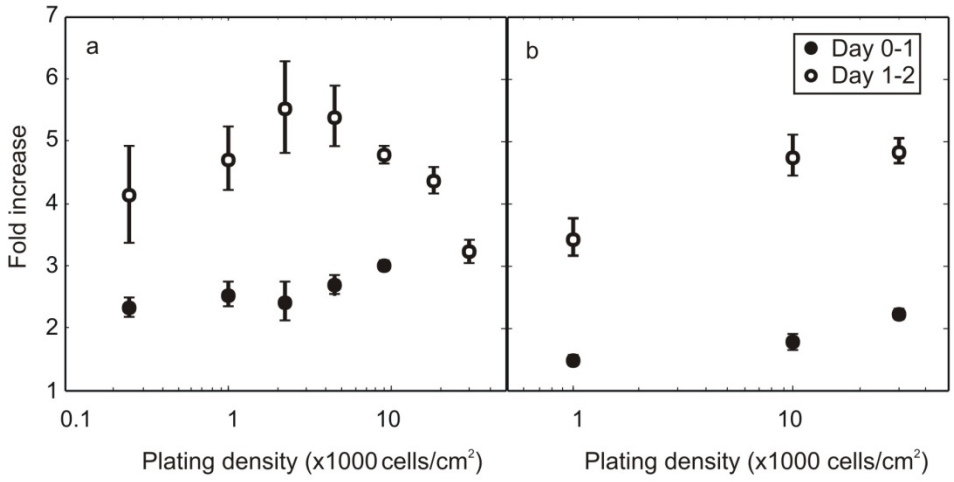

Figure 4.2 (a) Variation of fold growth with plating density for ABJ1 mESCs for Day 0-1 (solid) and Day 1-2. (b) Similar data for CCE mESCs.

4.2.3 Conditioned Medium improves mESC growth

To further confirm whether the increase of fold growth with plating density is due to a diffusible signal we compared the growth of cells in conditioned medium (CM) versus control, unconditioned medium. We found that CM collected at 24 hours did increase the fold growth of cells from Day 0-1 by 9% (p=0.03), and CM collected over 24 to 48 hours after seeding (i.e. Day 1-2), increased the fold growth of cells from Day 1-2 by 18% (Figure 4.3, p=2e-6).

[c] I use the following notation: Day 1-2 refers to the period 24-48 hours after the commencement of culture, and Day 0-1 refers to the period 0-24 hours after the commencement of culture.

4.2.4 Interpreting and improving upon growth data

The above results seem to prove that mESCs produce one or more growth factors. However, in reality, by varying the plating density, one actually varies two rates: the rate of secretion of factors into the medium, and the rate of uptake of factors from the medium. Similarly, while the CM contains cell-secreted factors, some of the proteins present in the original medium may have been depleted to a greater extent than in the control medium. (Note that even in the control medium one would expect some depletion of proteins to occur via adsorption to the tissue culture surface.) Therefore, the effects that we observe could also be produced by the depletion of a growth-inhibiting protein from the culture medium. Since the contents of serum are not completely known, it is not possible to rule out the existence of a growth-inhibiting molecule as one of its constituents.

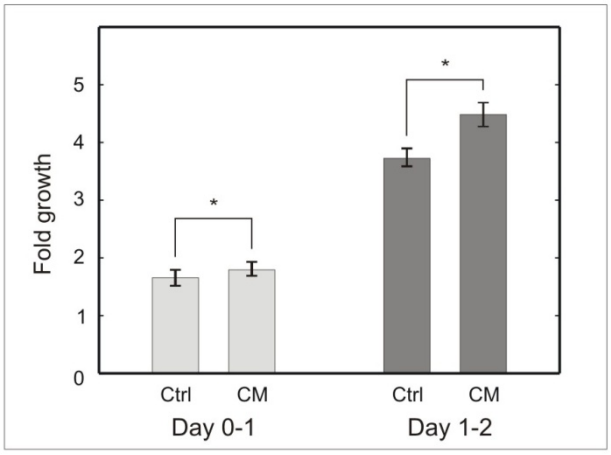

Figure 4.3 Comparison of growth of CCE mESCs in conditioned medium versus control medium (serum-containing media). From Day 0-1 cells were grown in CM collected on Day 1, or control. Similarly from Day 1-2, cells were grown in CM collected on Day 2, from cells fed on Day 1; or control.

There are a few approaches that could be used to distinguish between the above two mechanisms that can both account for a positive effect of CM on growth. One approach would be to equalize the levels of all the *original* proteins in the CM and control. A second approach is to find a medium that does not contain growth-inhibiting proteins, and do experiments in this medium. Finally, a third approach would be to compare (numerically) the benefit provided by CM with the effects of depleting growth inhibitors. It is clear that for any approach, it will be necessary to work with a defined medium, i.e. one in which specific proteins are added to the culture medium and the protein composition is therefore "defined" i.e. known.

The first approach mentioned above is challenging, because, after conditioning the medium, one must determine the levels of all the proteins (typically ~10) prior to equalization. This is not only time-consuming and expensive, but since there will be ranges associated with each measurement, it is not clear that such an approach would work, in practice. The second approach i.e. finding/developing a medium without growth inhibitors appears challenging, except that it is likely that defined media developed by other laboratories in the past are unlikely to contain growth inhibitors, given that the

usual objective of a medium is to provide conditions for expansion of cultures. While this is the approach we used ultimately, a caveat related to the above statement must be noted: for stem cell media, in addition to facilitating the expansion of cultures, since one is usually seeking to propagate the cells as *stem cells*, it is important that the medium be able to maintain the cells in a self-renewing state. It is conceivable that proteins added to the culture for this latter, self-renewal maintenance purpose may not also be growth supportive. Finally, the third approach suffers from the same drawbacks as the first.

4.2.5 mESC Cultures contain an Autocrine Growth-supportive Large Molecule

As a first step towards determining whether the growth-supportive effect of CM were due to enhancer production or inhibitor depletion, we grew cells in a serum-free medium formulation (N2B27) developed by Ying *et al*.[159] specifically for expanding mESCs while maintaining them in a pluripotent state. We created conditioned media from this culture, dialyzed it against fresh media using a 3 kDa membrane, and compared growth of cells in dialyzed CM against control medium that was treated identically except that it was never in contact with cells. We observed that the large-molecule fraction of CM (> 3 kDa) prepared using this medium was growth supportive on Day 0-1 and Day 1-2, resulting in a ~15% increase in growth (relative to control) on Day 0-1, and a ~25% increase in growth on Day 1-2 (Figure 4.4a).

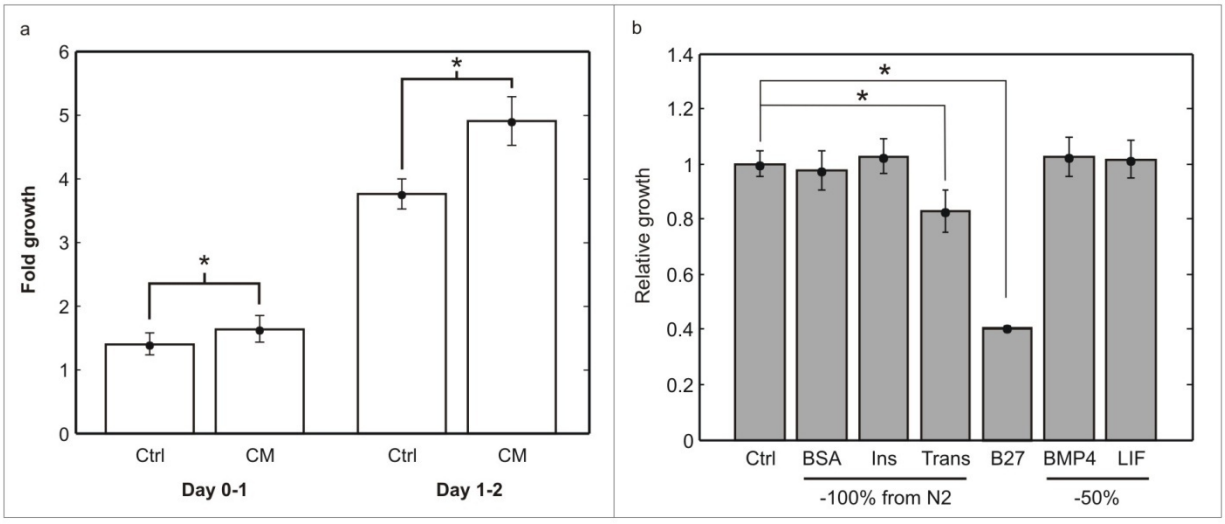

Figure 4.4 Effects of secreted proteins and medium proteins on mESC growth in a serum-free medium. a. Fold growth over Day 0-1 and Day 1-2 for ABJ1 mESCs grown in conditioned medium versus control. CM increased proliferation by ~15% on Day 0-1 (p=.02) and ~25% on Day 1-2 (p=5e-4). b. Fold growth over Day 1-2, relative to control, in media where different components were removed. Removal of BSA or insulin (Ins) from N2 resulted in no significant decrease in proliferation. Removal of transferrin from N2 (Trans), or of the high MW components of B-27 entirely, caused significant growth reduction (p=7e-4 and 1e-3 respectively). Reduction of LIF or BMP-4 concentrations by 50% resulted in no change in fold growth.

The serum-free medium (N2B27) actually consists of a 1:1 mix of N2 medium and Neurobasal/B-27 medium, to which LIF and BMP-4 are added to prevent the differentiation of the mESCs. There are a total of 7 large molecules in the final medium – bovine serum albumin (BSA), transferrin, insulin, superoxide dismutase-1 (SOD), catalase, LIF, and BMP-4[159]. Most of these molecules have been shown to

be growth supportive for several other cell types[103, 104, 160]. A nice review of the growth supportive effects of insulin, transferrin and BSA can be found in Keenan *et al.*[160] To summarize:

- Insulin typically exerts a mitogenic influence through the IGF-1 receptor.
- Transferrin is a vital iron transporter
- The growth-supportive action of BSA is usually due to fatty acids that BSA binds.

Additionally, SOD (Superoxide dismutase) and Catalase are extracellular antioxidant enzymes that prevent cell damage due to reactive oxygen species[103, 104].

Although the above molecules have been shown to be growth supportive for several other cell types we examined whether they might be growth inhibitory for mESCs. Because B-27 is a proprietary formulation (Invitrogen), we were unable to remove the protein components on an individual basis. Instead we removed the protein components of N2 (BSA, transferrin, and insulin) and then removed the high MW components of the B-27 formulation entirely. When we removed the BSA or insulin from N2, we observed no significant change in the growth of mESCs over two days (in N2B27 + LIF + BMP-4, Figure 4.4b), indicating that unless there is a substantial decrease in the concentration of these proteins, they are neither growth supportive nor inhibitory (these proteins are present in B-27 as well). When we removed transferrin from N2 we found that the growth rate of mESCs decreased by ~15% (p=7e-4), demonstrating that transferrin is growth supportive for mESCs. When we removed the high MW components of B-27 altogether, there was a sharp decrease in mESC growth indicating that B-27, which consists of BSA, transferrin, insulin, SOD, and catalase, is strongly growth supportive, perhaps due to the synergistic action of some of these proteins. Separately, we also examined the impact of catalase supplementation on growth of mESCs in N2, and observed a growth-supportive effect (Figure 4.5). Finally, although complete removal of LIF and BMP-4 from the medium would induce differentiation, we assayed whether reduction of LIF or BMP-4 concentrations by 50% would affect growth, which it did not. Other studies have shown that near-complete depletion of LIF[161] or BMP-4[105] does lead to a reduction in mESC survival, indicating that they are growth-supportive as well. These results demonstrate that the large molecules present in N2B27 + LIF + BMP-4 have either no effect or a supportive effect on growth, and thus are not growth inhibitory.

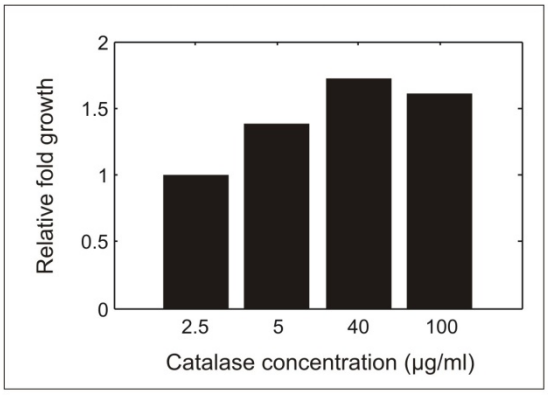

Figure 4.5 Fold growth versus catalase concentration for mESCs (relative to growth in 2.5 µg/ml catalase).

To summarize, we have shown that the large-molecule fraction of CM is growth supportive *and* that there are no large growth-inhibitory molecules in the original medium. Thus, the growth supportive effect of the CM must be due to the production of a large growth-supportive factor by the cells used to condition the medium. This further implies that the density-dependent growth observed in Figure 4.2 is at least partially due to the presence of a >3 kDa growth-supportive autocrine molecule. Finally, cells showed density-dependent growth in this medium (N2B27 + LIF + BMP-4) as well (Figure 4.6).

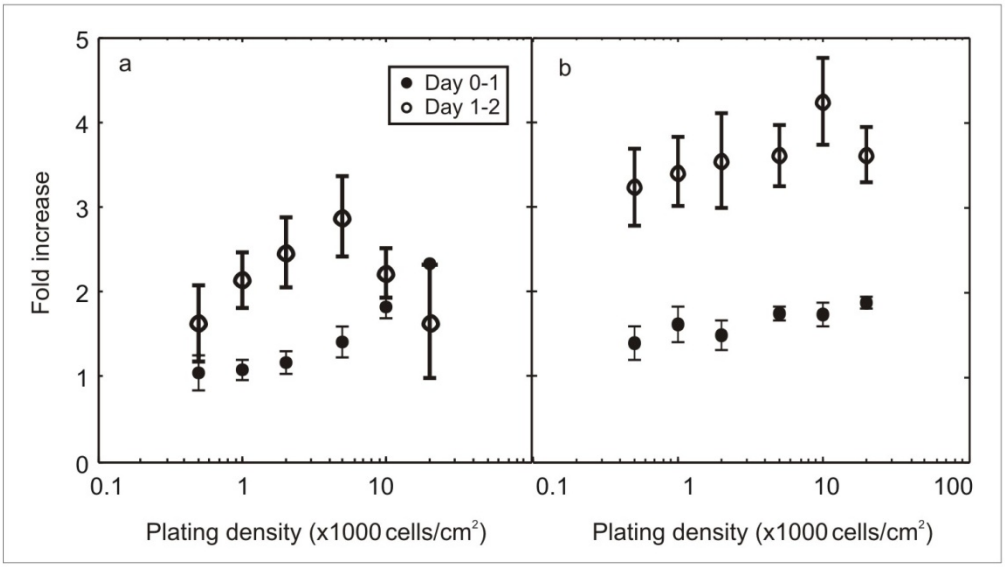

Figure 4.6 Density-dependent growth in a serum-free medium (N2B27 + LIF + BMP-4). (a) Fold growth for day 1 and day 2 for ABJ1 mESCs plated at various densities. day 1 p_{ANOVA} = 1e-11, day 2 p_{ANOVA} = 1e-6 for the increasing part of the curve. (b) Fold growth at the end of day 1 and day 2 for D3 mESCs plated at different densities. day 1 p_{ANOVA} = 0.06, day 2 p_{ANOVA} = 0.008 for the increasing part of the curve.

4.2.6 Length of attachment period and lag phase

In the above experiments, to interpret Day 1-2 growth as post-attachment, post-lag growth, we made the assumption that attachment and the lag phase are complete on Day 0-1. To validate this assumption, we measured the attachment rate and the length of the lag phase for mESCs in N2B27+LIF+BMP-4. In Figure 4.7a we show the percentage of unattached ABJ1 cells as a function of time for two plating densities. The cells plated at the higher density attach at a faster initial rate (p=1e-3), but for both densities, maximal attachment is complete within 6-8 hours. Additionally, the attachment efficiency is ~7% higher at the higher density (p=3e-3). In Figure 4.7b we show the percentage of ABJ1 cells in the S-phase as a function of time for cells plated at two densities. Similar strategies have been used by others to estimate the length of the lag phase[102, 106]. We observe that cells initially accumulate in the S-phase. The return of the percentage S-phase cells to its baseline level represents the end of lag phase. The lag phase for cells plated at 10,000 cells/cm^2 lies between 3 and 6 hours, while the lag phase for cells plated at 2500 cells/cm^2 lies between 6 and 9 hours. We used cell counting to confirm that the lag phase is indeed in the 6-12 hour range (Figure 4.7c). Thus attachment and lag phase are indeed complete within 24 hours after the commencement of culture. Additionally, density-dependent

differences in attachment rate, attachment efficiency, and length of the lag phase contribute to the observed differences in fold growth on Day 0-1.

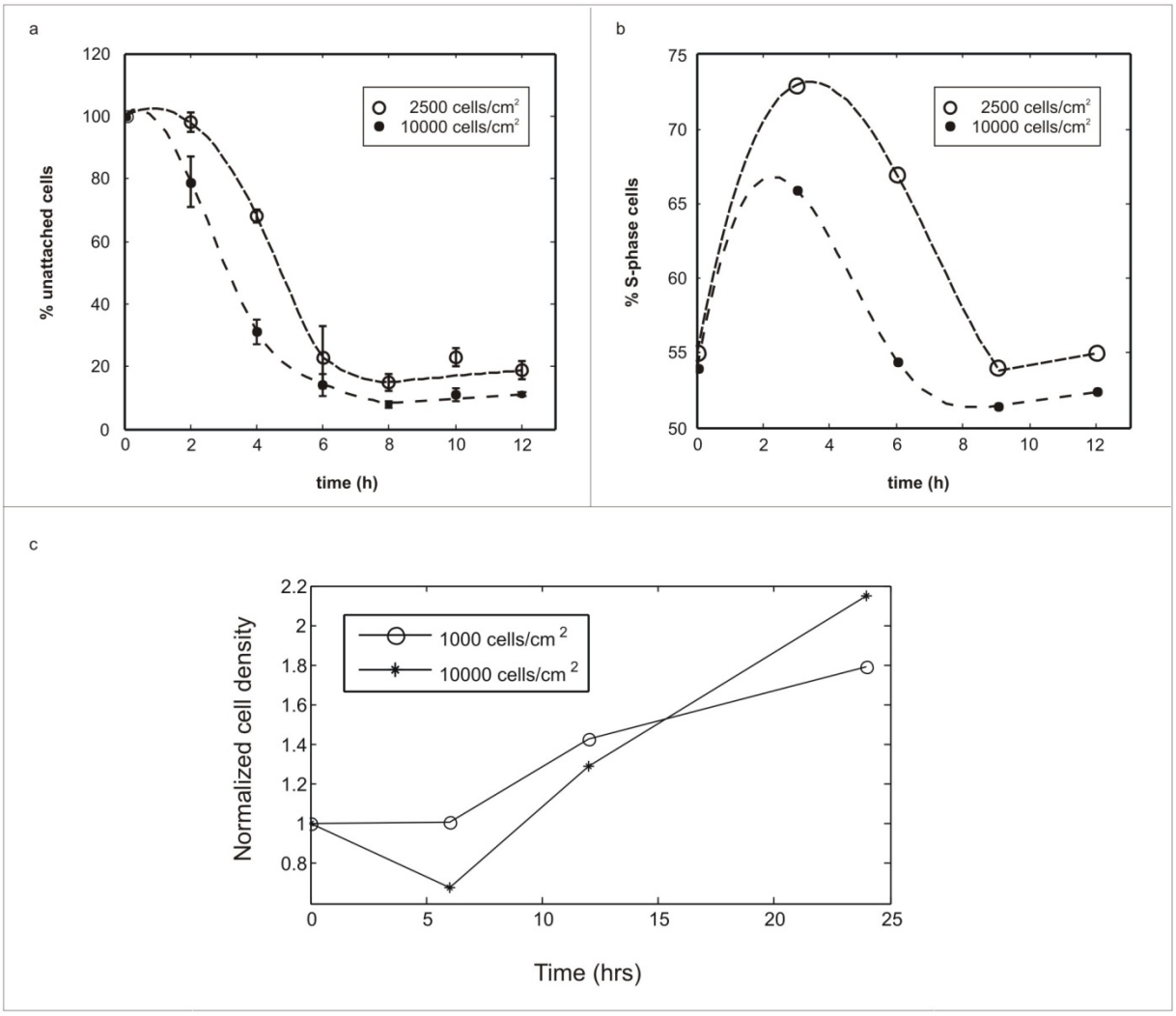

Figure 4.7 Measured percentage unattached cells at various time points for two plating densities. The lines are splines fitted to the data. Measured % S-phase cells at various time points for two plating densities. c. Normalized cell density versus time for ABJ1 cells plated at two densities.

4.2.7 The autocrine growth factor(s) in mESC cultures is (are) not mitogenic, but improve(s) survival

The growth rate of a culture can be increased via two mechanisms – a reduction in the length of the cell cycle ("mitogenic activity", i.e., increased proliferation rate), or a reduction in the rate of cell death. We wanted to determine whether the enhanced growth of mESCs at particular densities was due to increased mitogenic activity and/or improved survival. If a mitogenic factor was being produced by the cells, one would expect that the G1 phase would be shorter (because S and G2/M are typically fixed), and hence the proportion of cells in G1 would decrease. Using flow cytometry, we measured the proportion of cells in different phases of the cell cycle at two densities at 24 hours. The cell-cycle

distribution has the expected trend, with a high number of cells in S-phase[36]. We observed no difference in the proportion of cells in different phases of the cell cycle for cells cultured at two different densities (Figure 4.8a). Addition of CM also did not affect the cell-cycle distribution (Figure 4.8b). This indicates that the growth enhancement at higher densities is not due to increased mitogenic activity but is instead likely due to a decrease in the rate of cell death. The lack of mitogenic activity is perhaps not surprising, given that ES cells appear to lack the mitogen-dependent early G1 phase[35].

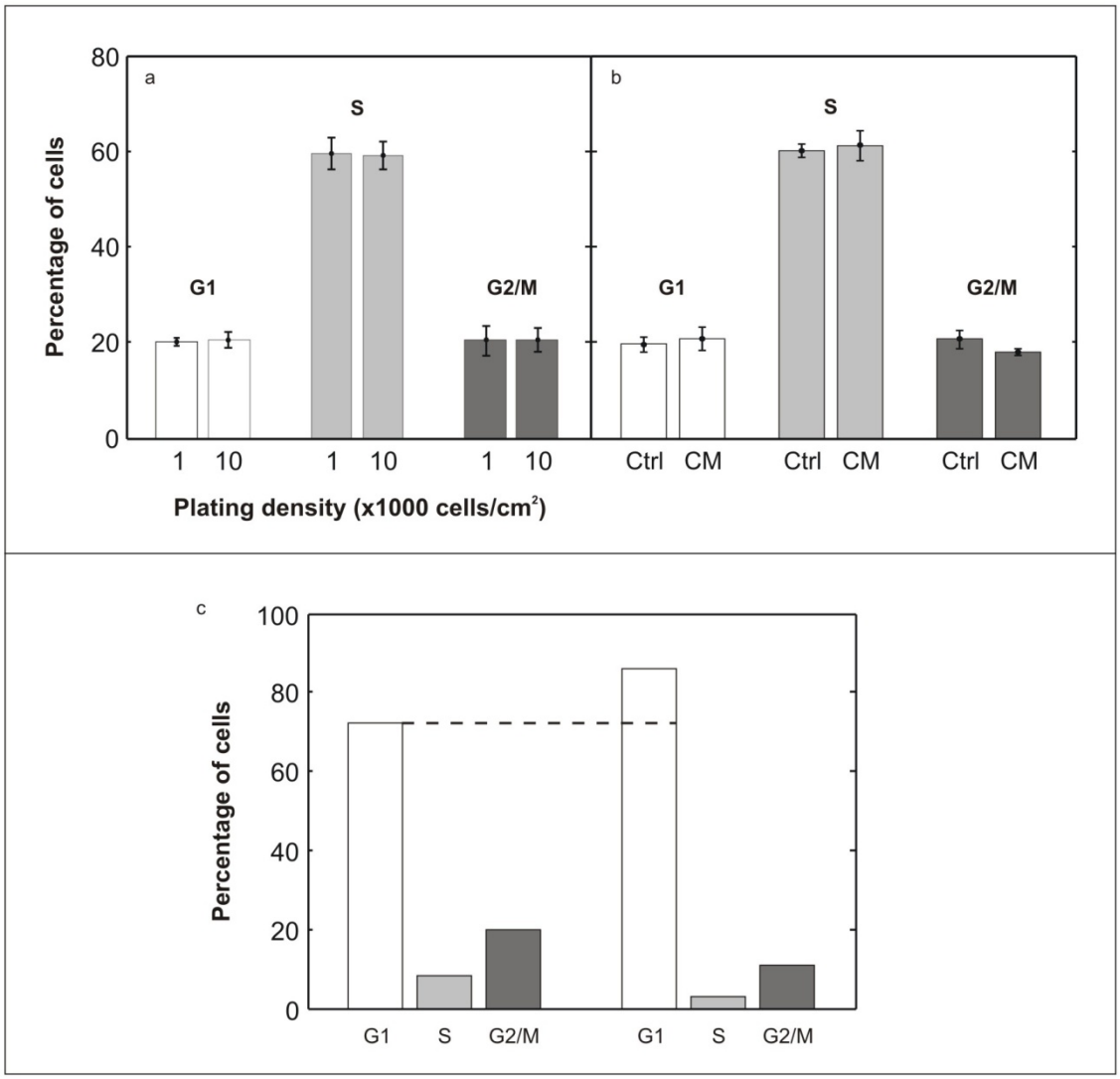

Figure 4.8 a. Cell cycle distribution for ABJ1 cells plated at 1000 cells/cm^2 and 10,000 cells/cm^2. b. Cell cycle distribution for ABJ1 cells plated in conditioned medium (CM) and control medium (Ctrl). c. (left) Cell cycle distribution for 3T3 fibroblast cells and (right) 3T3 fibroblast cells that were serum-starved for 24 hours.

To demonstrate that our protocol can indeed detect changes in cell cycle demonstration we additionally measured the cell cycle distribution for 3T3 fibroblast cells. As expected, unlike mESCs, these cells have a high percentage of cells in the G0/G1 phase[36] (Figure 4.8c). Additionally, serum-starvation for 24 hours in 0.1% bovine calf serum (versus 3% serum for the control) led to a detectable accumulation of cells in the G0/G1 phase (Figure 4.8c).

Since the colony-forming efficiency improves with increasing density (Chapter 3), this suggests that there is indeed improved survival at the higher densities. To confirm this further, we measured the fraction of dead cells in the culture at the end of Day 1-2 (48 h). We focused on Day 1-2, because the difference in the death rate on Day 0-1 could also be due to differences in the attachment efficiency. We added either CM or control medium to cells at 24 hours; at 48 hours we stained cells using YO-PRO-1 Iodide which selectively stains dead cells. We observed that when grown in CM, the fraction of stained cells was only 62 ± 10% of the corresponding fraction for cells grown in control medium (Figure 4.9a). This result confirms that mESC secreted factors promote survival in an autocrine manner.

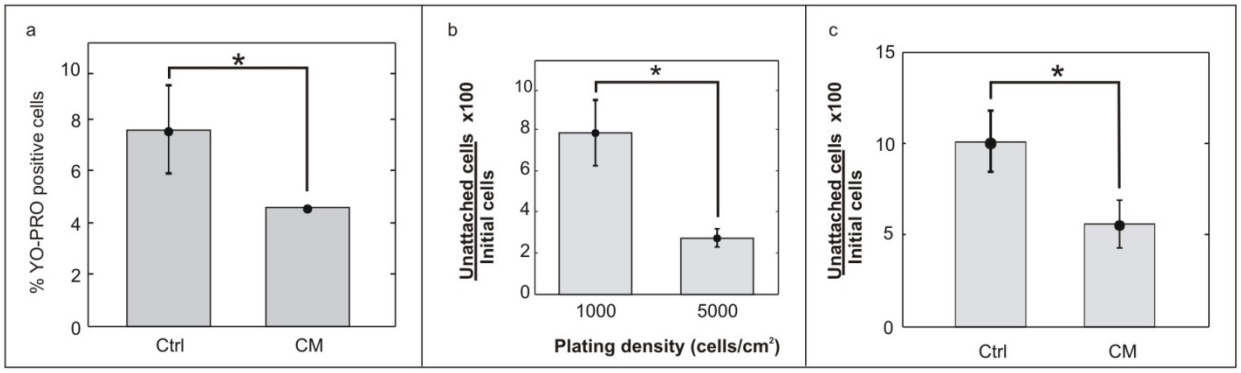

Figure 4.9 a. The percentage of YO-PRO-1 positive (dead) cells in the culture at the end of Day 1-2 for cells grown in conditioned medium (CM) versus control (p=0.01). b. The fraction of cells that detached on Day 1-2, for two plating densities (p=0.01) c. The fraction of unattached cells at the end of Day 1-2 for cells grown in conditioned medium (CM) versus control (p=2e-5).

Interestingly, we observed that most cells that stained positively for YO-PRO-1 exhibited an unattached, rounded morphology (142/143 cells or 99%, Figure 4.10), and conversely 95% (142/149) of unattached cells stained positively for YO-PRO-1 iodide, indicating a compromised membrane. Similarly, 97% of unattached cells showed the presence of DNA nicks (Figure 4.10d). Thus death and loss of attachment seem to occur almost simultaneously in mESC cultures. This observation enables an alternate method for measuring the rate of cell death in these cultures – via counting of the fraction of unattached cells in the culture. We counted the fraction of cells that were detached at 24 hours and 48 hours, at 1000 cells/cm^2 and 5000 cells/cm^2, the latter being the density that shows the highest growth on Day 1-2 in serum-free conditions (Figure 4.6a). From this, we calculated the fraction of cells that detached on Day 1-2, and indeed found a density-dependent decrease in the fraction of these cells (Figure 4.9b). Additionally, cells grown in CM on Day 1-2 showed a ~50% reduction in the percentage of unattached cells (Figure 4.9c), again confirming that the autocrine factor(s) decrease the rate of cell death in mESC cultures.

4.3 Discussion

In this chapter I have shown results of fold growth measurements for mESCs in culture. The fold growth is indeed density-dependent, with a single maximum, consistent with our hypothesis that competition between the positive feedback provided by autocrine growth/survival factors and negative feedback provided by nutrient depletion etc. could, in the simplest case, lead to such a trend (chapter 1). The

growth measurements are also consistent with CFE measurements made with the BFC (chapter 3), validating the use of the BFC for screening for intercellular signaling.

An interesting feature of growth related to the existence of a lag phase is that lag phase leads to partial synchronization of the culture (Abu-Absi *et al*.[106], Figure 4.7b). A consequence of this is that the growth curve (at least for mammalian cells) does not have a purely exponential trend (Abu-Absi *et al*.[106], Figure 4.11). Given that the attachment period and lag phase lengths are very similar (Figure 4.7), we also hypothesize that they may be causally related in our cultures i.e. that perhaps mESCs are unable to progress into G2/M without first attaching to the substrate.

Interestingly, ICM (inner cell mass) cells have also been found to undergo apoptosis *in vivo*; ~10-20% of cells in the mouse and human ICM are undergoing apoptosis on Day 5 post-fertilization[107]. Again, the percent of dead cells has been shown to be inversely correlated with the total number of cells in the blastocyst[107], suggesting that anti-apoptotic factors play a role in modulating this process.

4.4 Summary

In this chapter I have shown results of fold growth measurements for mESCs in culture. The fold growth is indeed density-dependent, with a single maximum. Further, we have measured the attachment rate and lag phase length and shown that these increase and decrease respectively at higher densities. Importantly, we demonstrated that post-attachment, post-lag growth is also density-dependent, and improves with the addition of conditioned medium. By switching to a defined medium we demonstrated that these effects are at least in part due to the secretion of one or more high MW (>3 kDa) factors by the cells. Finally, we explored the mechanism of action of these factors and showed that the net effect of these factors is to improve the survival of mESCs. In the next chapter I will describe our use of biochemical techniques to establish the identity of these factors.

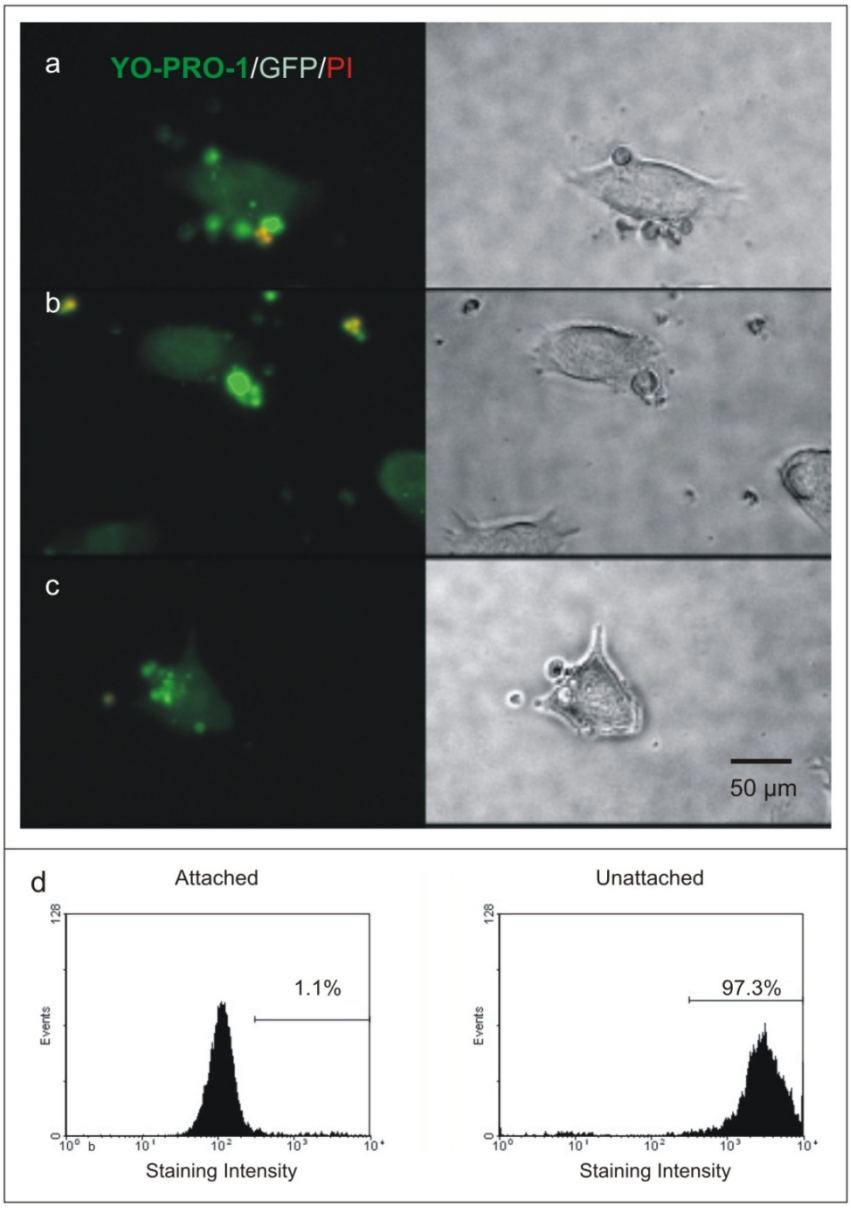

Figure 4.10 a-c (Left) Fluorescence images of Oct4-GFP mESCs labeled with YO-PRO-1 Iodide (bright green) and PI (red). The bright green cells labeled with YO-PRO are cells in the early stages of apoptosis. In some cases, fragmentation of the nucleus can be seen (see especially c). The dim green signal is the Oct4-GFP signal. The orange cells which are labeled with PI and YO-PRO are likely late stage apoptotic (or alternately necrotic) cells. (Right) Phase contrast images of the corresponding colonies shown in the left panel, showing that the apoptotic cells are rounded and likely loosely attached to other cells in the colony. d. 97% of unattached cells in mESC cultures (at 24 h) stain positively in the TUNEL assay, indicating that they have fragmented DNA.

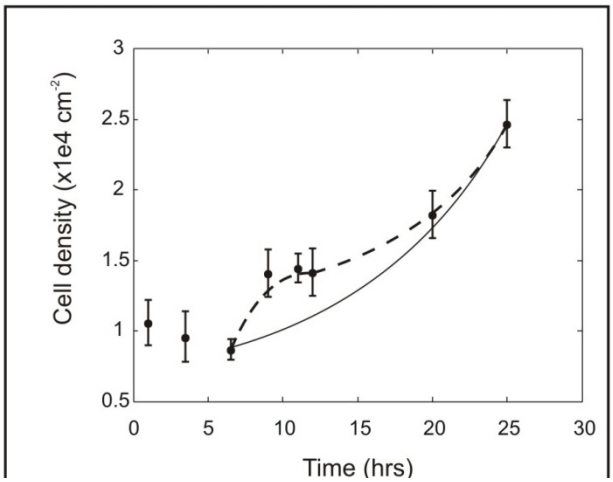

Figure 4.11 Cell density versus time for ABJ1 mESCs plated at 10,000 cells/cm^2. The solid line represents exponential growth; the dashed line is a guide to the eye.

Chapter 5: Cyclophilin A is an autocrine survival factor in mESC cultures

In the previous chapter we demonstrated that there is indeed an optimal density for (2-day) culture of mouse embryonic stem cells. We were interested in verifying the mechanisms that determine the existence and value of this optimal density. A likely candidate mechanism for the initial increase in fold growth with plating density is the production of autocrine growth/survival factors[43]. We demonstrated in chapter 4 that mESC cultures do indeed contain one or more such factors. In order to obtain a quantitatively accurate description of the role of these factors in growth it is necessary to obtain the production rate of these factors as well as the variation of growth rate with factor concentration. To do this we must first discover the identity of these factors. In this chapter I will describe our efforts to discover the identity of autocrine survival factors in mESC cultures.

5.1 Materials and Methods

5.1.1 Numerical modeling

Numerical modeling of autocrine/paracrine signaling was performed using the Diffusion (time-dependent) module in COMSOL Multiphysics. The geometry we used is shown in Figure 5.1. The effect of plating density (σ) is included in the model by varying the parameter L (Figure 5.1). The height of the liquid layer was 2.5 mm, which corresponds to the liquid height in our experiments, which is fairly typical. The cell was modeled as a hemisphere with a radius of 7 μm.

The diffusion constant of the factor in the medium was taken to be 10^{-6} cm^2/s which is typical for proteins in the 5-40 kDa range[108]; most diffusible proteins are in this mass range. No-flux boundary conditions were applied on all surfaces, except the hemisphere corresponding to the cell. For this surface we set the normal flux of the protein to $r - k_{on}Rc_s$, where r is the secretion rate, k_{on} is the binding constant, R is the number of receptors per cell, and c_s is the concentration of factor at the cell surface (c_s is solved for within the simulation). Values of the other parameters above are described in the results section. We assume that the number of free receptors is constant. Previous work by Lauffenburger and colleagues[109] has shown that the receptor number reaches a steady state within 2 hours after the commencement of culture. Therefore this assumption is justified. We have also briefly investigated a model that included unbinding events and receptor dynamics (Appendix 3).

The geometry was meshed using the default mesh parameters to generate a triangular mesh with 1696 points. For one set of parameter values we checked that increasing the number of mesh points by a factor of 10 led to a 0.07% change in the highest factor concentration and a 0.08% change in the lowest factor concentration. Thus the original number of mesh points (1696) is adequate for computing factor concentrations. We also used the default solver which is GMRES with an algebraic preconditioner, and default timesteps, with a maximum timestep of one hour.

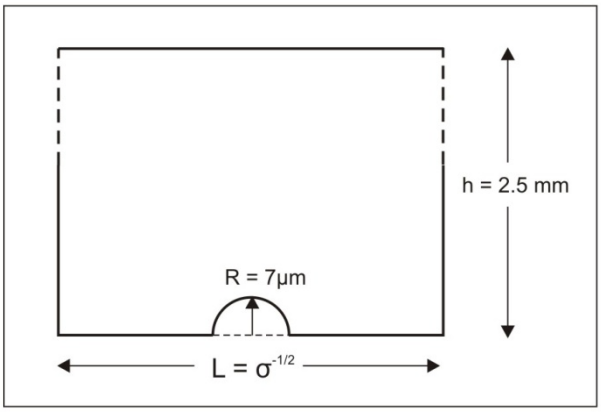

Figure 5.1 Side view of the geometry used for modeling in COMSOL Multiphysics.

5.1.2 Cell culture

Cell culture was performed in serum-free medium with adapted cell lines, as described in chapter 4. Recombinant mouse (rm) Cystatin C, rmTIMP-1, rmOsteopontin and rmClusterin, recombinant human (rh) FGF-4, and rhCyclophilin A were purchased from R&D Systems. Human CypA shares a 96% sequence similarity with mouse CypA, while human FGF-4 shares an 80% sequence similarity with mouse FGF-4.

5.1.3 SDS-PAGE and mass spectrometric analyses

Cells were plated at 30,000 cells/cm^2, fed at 24 hours, and CM was collected at 48 hours. Control medium (RM) was similarly incubated, but without cells. 4 ml CM and RM were concentrated to approximately 100 µl using a 3 kDa centrifugal filter unit (Millipore). CM and RM were mixed 1:1 with Laemmli buffer (Bio-Rad), heated at 95^{o}C for 5 minutes, and run on 12% or 18% polyacrylamide gels (Bio-Rad) at 15 mA. Gels were stained using a silver stain (SilverQuest, Invitrogen) for visualization. For mass spectrometric analyses, 15 ml CM and RM were concentrated using a 3 kDa centrifugal filter unit (Millipore) first, followed by drying in a SpeedVac to approximately 15 µl. Following SDS-PAGE, gels were stained using Coomassie Blue (SimplyBlue, Invitrogen). Appropriate bands were analyzed using LC/MS-MS at the Biopolymers Laboratory at the Koch Institute for Integrative Cancer Research (MIT).

5.2 Results

To determine candidate autocrine factors that might be responsible for the observed growth supportive effects, we examined literature as well as the CM itself. Several proteins have been shown to be secreted by mESCs, but when testing for the effects of potential autocrine ligands, it is important to test the response of cells to these ligands *in the concentration ranges found in cultures*. Using ELISA it is easy to determine the concentration of a particular ligand in the conditioned medium i.e. the average concentration in the culture. We wondered whether there may be a large concentration gradient across the height of the culture with a high concentration of ligand near the source i.e. the bottom of the dish where the cells attach, and a low concentration at the surface of the medium layer. To obtain a relation

between the average ligand concentration and the concentration at the cell surface, we used numerical modeling.

5.2.1 Determining protein concentrations in cell cultures using numerical modeling

To estimate the concentration at the bottom of the dish (at the location of the cells) we set up a simple model using commercially available software (COMSOL Multiphysics, see methods). The model simulates cells producing a factor which can further bind back to receptors on the cell. We assume that the transport of the ligand is purely diffusive, i.e. that there is no convection in the dish. The presence of convection will reduce the concentration gradients. Thus, by making this assumption we will obtain an upper bound on the concentration gradient.

The model has three parameters: the factor secretion rate (r), the binding constant (k_{on}), and the number of receptors per cell (R). These parameter values were taken from Shvartsman *et al.*[109] (see Figure 4 in that paper): secretion rate (r): 1-1000 molecules/cell/second; binding constant (k_{on}): 10^8 M^{-1} min^{-1} (we tested 10^7 - 10^9 M^{-1} min^{-1}); number of receptors per cell (R): 10^5 (we tested 10^4 – 10^6). Finally, the model has one geometric parameter – the area of the bottom surface, which is the inverse of the plating density.

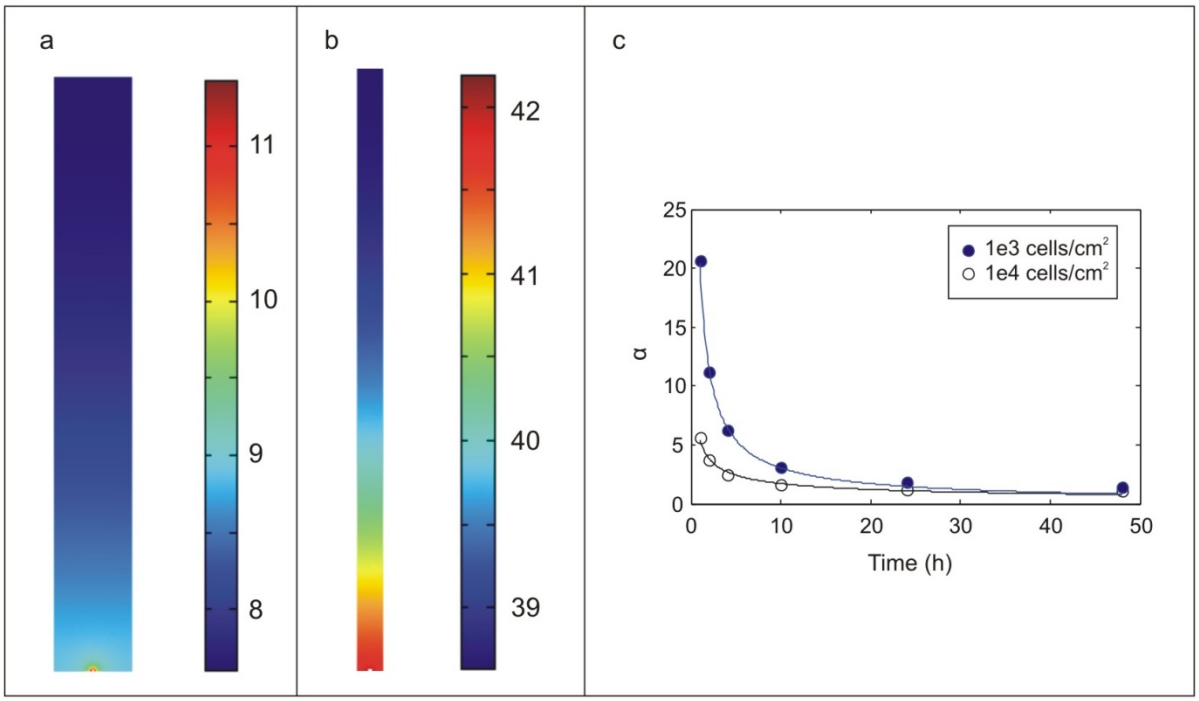

Figure 5.2 Concentration profiles above single cells from our simulations, for cells plated at 1000 cells/cm^2 (a) and 10,000 cells/cm^2 (b) at t = 48 h. Concentration is shown in units of picomolar (pM). (c) Graph of α versus time. Circles are obtained from the simulation. The lines shows the best-fit power function and are only meant as a guide to the eye. For these simulations, r = 5e-13 moles/m^2/s, k_{on} = 1e8 1/(M.min), R = 1e5 receptors/cell.

In Figure 5.2 we show some typical concentration profiles above single cells, for cells plated at 1000 cells/cm^2 (a) and 10,000 cells/cm^2 (b) at t = 48h. Using the model we then computed the ratio of the factor concentration at the cell surface to the average factor concentration in the whole culture (α).

In Figure 5.2c we show the time-dependence of α as calculated from our model. The rapid decay of α is perhaps not surprising given that the time required to diffuse across 1 mm is approximately 3 hours (167 minutes) assuming that the diffusion constant is 1e-10 m^2/s.

We focus on the value of α - 48 hours after the start of culture (α_{48}). We report results at 48 hours because in the ELISA experiments that will be described in the next section, Singla *et al*.[110] collected conditioned medium from cells after 48 hours. Let us first consider the dependence of α on the plating density. One would expect α to be inversely correlated with density; for example, the concentration from a point source drops off as a^{-3}, where a is the distance from the source; but if there are "several" point sources arranged to form a line source, then the concentration only drops off as -log(a). We calculated α for two plating densities: 1000 cells/cm^2, and 10,000 cells/cm^2 and found that α was indeed higher at the lower plating density (Table 5.1). In ELISA experiments described in the next section, Singla *et al*.[110] plated cells at 9000 cells/cm^2, but collected CM from Day 1 through Day 3. As we have seen in chapter 4, fold growth from Day 0-1 is in the range of 1.1-2. Therefore the effective plating density at the beginning of their CM collection (i.e. Day 1) must have been in the range of 10000-18000 cells/cm^2. We will use 10000 cells/cm^2 for further discussion, and as shown above, this will provide an upper bound on the values of α.

Table 5.1 Values of α_{48} for two plating densities and a range of k_{on} values.

R = 1e5 receptors/cell, secretion rate = 100 molecules/cell/s

k_{on} ($M^{-1}min^{-1}$)	Plating density (cm^{-2})	
	1000	10000
1e7	1.46	1.13
1e8	1.42	1.06
1e9	1.26	1.01

Not surprisingly, while changes in the secretion rate (*r*) lead to a change in the actual concentration, the ratio α is independent of *r*. Finally, let us look at the effects of varying k_{on} and the receptor number (*R*). Both these parameters affect the flux in a similar manner, since the net flux is $r - k_{on}Rc$ (see methods).

Table 5.2 Values of α_{48} for a range of k_{on} and *R* values, for σ = 10000 cells/cm^2 and *r* = 100 molecules/cell/s.

k_{on} ($M^{-1}min^{-1}$)	*R* (No. of receptors per cell)		
	1e4	1e5	1e6
1e7	1.15	1.13	1.06
1e8	1.13	1.06	1.01
1e9	1.06	1.01	1.003

We found that α_{48} was relatively constant across a wide range of parameter values (Table 5.2), varying from 1.003 to 1.15 for our range of parameter values. By the end of day 2, cells will have divided into colonies and we wondered whether the existence of a group of cells versus a single cell may significantly

alter the gradient. For one case (k_{on} = 1e8 $M^{-1}min^{-1}$, R = 1e5 per cell) we simulated the concentration profile above a hemisphere of radius 14 μm, corresponding to a group of 4 cells (approximately). For this case we determined that α_{48} is 1.003. Thus the presence of a larger number of cells does not appear to significantly alter the value of α at this plating density.

Finally, we have briefly investigated a model that includes receptor dynamics (Appendix 3), which gave similar results (α_{48} = 1.03). Based on these results, we tested our factors at the concentration found in the CM, as well as twice the concentration found in the CM.

5.2.2 Previously known mESC secreted proteins are not growth-supportive for mESC

Cystatin C, TIMP-1, Osteopontin, and Clusterin have been identified (via multiplexed ELISA) as proteins secreted from mESCs grown without LIF for two days[110], while TIMP-1 has also been found in the CM of mESCs grown with LIF[161]. Additionally, transcripts for Osteopontin and Clusterin have been detected in mESCs grown in medium containing LIF[19]. FGF-4 has been separately identified as being secreted by mESCs, but does not affect the survival or cycling rate of mESCs[111]. We examined the effect on mESC growth of supplementing the media with recombinant versions of each of these proteins at levels likely to be present in the culture.

In Figure 5.3 we show the effects of adding these proteins to mESC cultures at the concentrations measured by Singla *et al*. to be present in the conditioned medium (CM), and/or twice those concentrations. For Cystatin C and Clusterin we found that there was no effect on growth at the concentration measured in CM, but a reduction in growth at twice that concentration. For Osteopontin and TIMP-1, we found that there was no significant change in mESC growth relative to the control. Finally, the concentration of FGF-4 in mESC CM was not measured in the above study, but other studies have shown that 2 ng/ml FGF-4 can increase the number of neural precursor cells obtained by differentiating mESCs[162]. We found that FGF-4 at 2-4 ng/ml did not affect the growth rate of ABJ1 mESCs, in agreement with the observations of Wilder *et al*.[111]

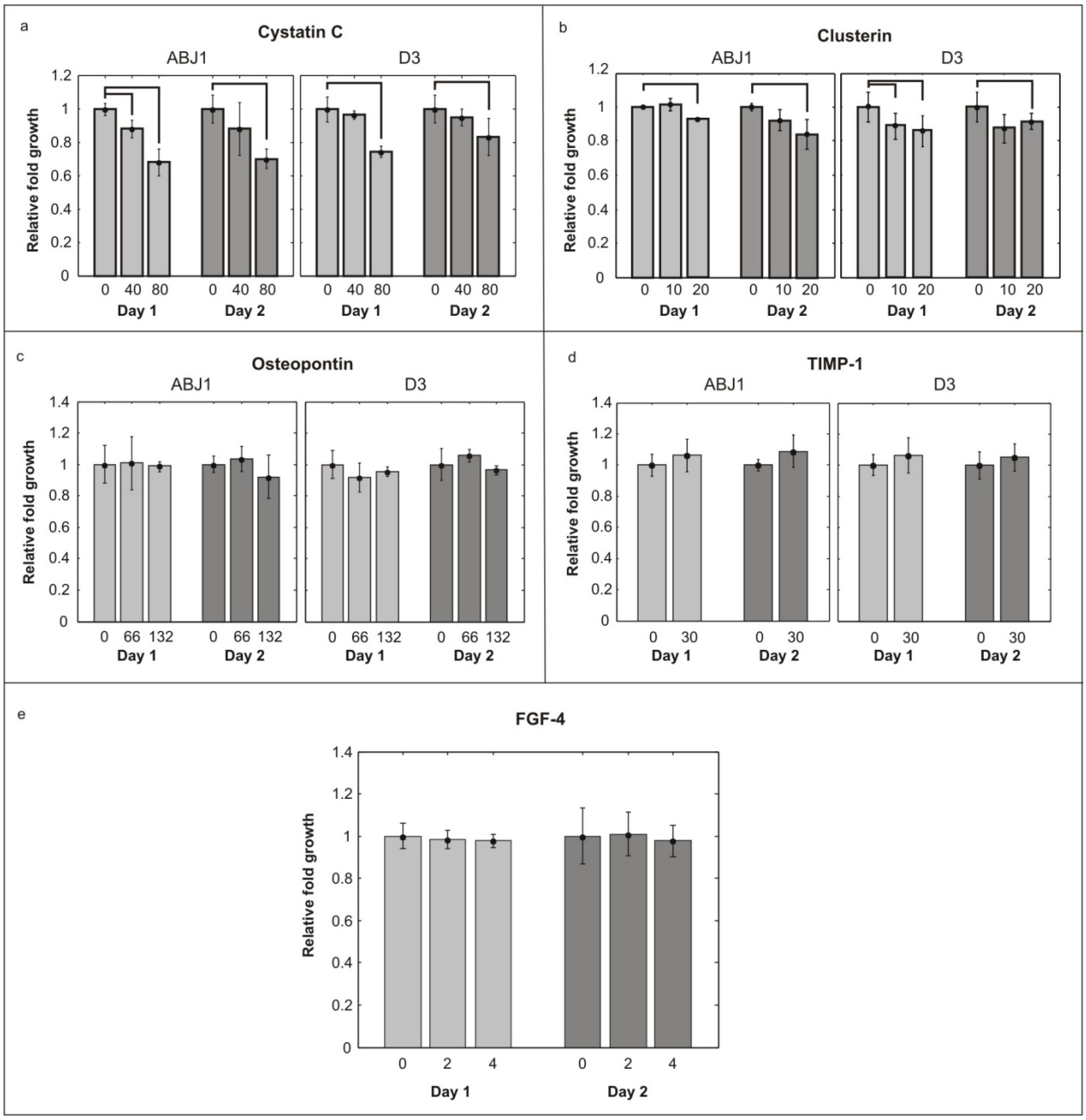

Figure 5.3 a. Relative growth of ABJ1 (left) and D3 (right) mESCs upon addition of 40 ng/ml and 80 ng/ml rmCystatin C. For all graphs the values on the x-axis are factor concentrations in ng/ml. b. Relative growth of ABJ1 (left) and D3 (right) mESCs upon addition of 10 ng/ml and 20 ng/ml rmClusterin. c. Relative growth of ABJ1 (left) and D3 (right) mESCs upon addition of 66 ng/ml and 132 ng/ml rmOsteopontin. d. Relative growth of ABJ1 (left) and D3 (right) mESCs upon addition of 30 ng/ml TIMP-1. e. Relative growth of ABJ1 mESCs upon addition of 2 ng/ml and 4 ng/ml rmFGF-4.

5.2.3. Proteomic analysis of mESC conditioned medium

To determine what other proteins might be secreted by mESCs, we performed a gel analysis of mESC medium followed by LC/MS-MS. In the figure below, we show an SDS-PAGE gel on which we ran control medium (N2B27 + LIF + BMP-4), as well as conditioned medium from ABJ1 and D3 mESCs. The most likely constituents of bands in the control medium are mentioned in parentheses, based on the molecular weights of the corresponding proteins. The other bands are "contaminating" proteins, coming from the BSA and transferrin. Thus, even this defined medium is not completely defined. We also tried to use recombinant BSA, but found that this had several additional proteins as well. However, when testing for the effects of different proteins on mESC growth (Figure 4.4), we used the same BSA as we add to the medium; therefore the effects of these contaminating proteins are assayed as well.

We detected two bands in the CM lane of the gel that were not present in the control (labeled 1 & 2). The darkness of the bands that are present in the control lane is either the same, or more than that of the corresponding bands in the CM lanes, indicating that the loading is even and that perhaps some of the original proteins have been bound by the cells or the culture surface. Also, for reasons that we don't understand, the LIF we add to the medium (ESGRO from Millipore) does not appear in the stained gel, perhaps because it does not stain with the silver stain kit we used.

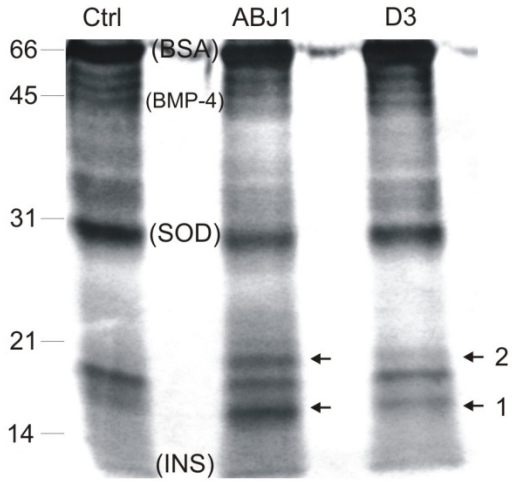

Figure 5.4 Image of a portion of a silver-stained gel resulting from SDS-PAGE of medium conditioned by ABJ1 cells, D3 cells, and from control (serum-free) medium. The arrows indicate the location of two additional bands observed in the CM media. The most likely constituents of bands in the control medium are mentioned in parentheses, based on the molecular weights of the corresponding proteins.

In our gel analysis we were primarily interested in the locating bands in the range of 15-35 kDa, since most cytokines are in this size range. As can be seen in the figure above, there is a dark, wide band at ~30 kDa in all three lanes, which most likely corresponds to SOD-1 (predicted MW is 32 kDa). We wondered if this band may be concealing the presence of other proteins in the CM. Since SOD-1 comes from the B-27 added to the medium, we also analyzed CM collected from mESCs grown in N2 medium alone (with LIF and BMP-4). Austin Smith's group has demonstrated that the proteins in B-27 are not required for self-renewal[159].

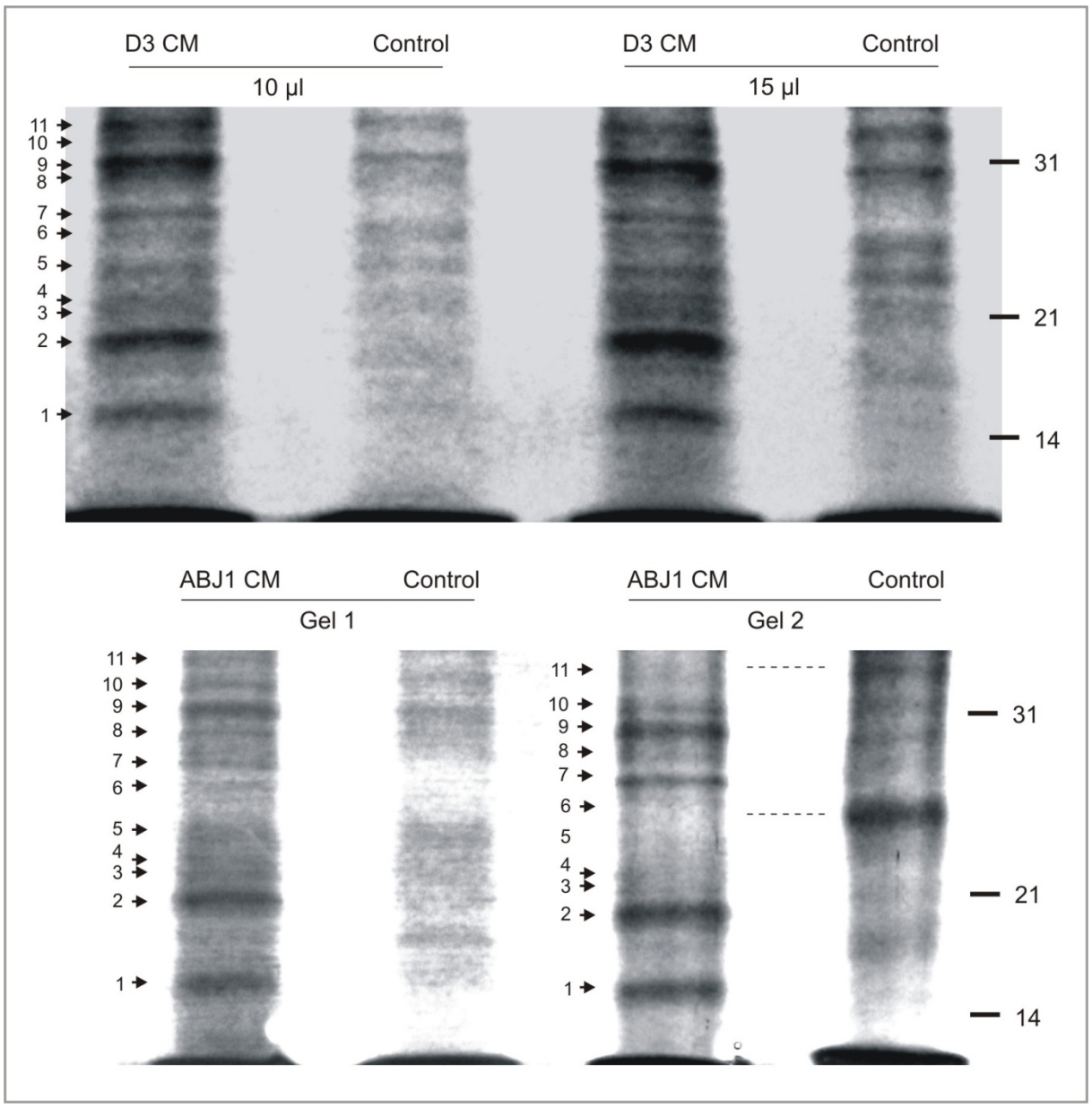

Figure 5.5 Image of a portion of a silver-stained gel resulting from SDS-PAGE of medium conditioned by D3 cells (top) and ABJ1 cells (bottom) along with corresponding controls, in media without B27. The arrows indicate the location of bands observed in the CM media.

Figure 5.5 shows some typical results from running these CM on a 12% SDS-PAGE gel. In the top figure we show results from CM obtained from D3 cells grown in N2 alone, loaded with different amounts of medium. In the lower figure we show results from 2 separate gels run with ABJ1 CM. We again clearly observe the two bands (1 & 2) that we saw in the previous figure. In the region where we formerly saw the band due to SOD (~30 kDa), a band is still present in the CM as well as control (band 9), but the band in the CM is now darker. In addition to band 9, we now see other bands in the CM that are either not present in the control (7), or darker than a corresponding band in the control (3, 4, 8 & 10). Finally,

bands 5, 6 and 11 are present in the control lanes as well, and are as dark as, or darker than, the corresponding bands in the CM lanes. Thus these cannot be ascribed to secreted proteins.

5.2.4 Mass spectrometric analysis of gel slices

Mass spectrometric analyses of bands 1 and 2 were performed. Additionally, a pooled analysis of bands 3, 4, 7-10 was performed. Band 1 was found to consist primarily of Profilin-1 (UniProt MW 15 kDa, 8-10 peptides), Cystatin C (UniProt MW 15.5 kDa, 4-5 peptides), and Thioredoxin (UniProt MW 12kDa, 2-3 peptides). The presence of Profilin-1 is somewhat unexpected as it is an intracellular protein, although a study of proteins secreted by neurospheres found Profilin-2, also an intracellular protein, in the CM[112]. The major component of band 2 was found to be Cyclophilin A (CypA), also known as peptidyl-prolyl isomerase A (Ppia). It was also the only detected protein in this band that is known to be present extracellularly.

As mentioned in the previous section, bands 3-11 were only evident when cell were cultured in N2 medium alone. A pooled LC/MS analysis of these bands was performed and several proteins were identified, but almost all of these proteins were intracellular (mostly cytoplasmic) proteins (Appendix 3). However this is not surprising, since in the N2 medium alone we observed that a lot of cells died, likely releasing (some of) their contents into the medium. Indeed, we showed earlier that growth in medium without the high molecular weight components of B-27 is very poor (Figure 4.4b). We did detect four extracellular proteins: TIMP-1 (predicted MW 22.6 kDa), Hepatoma-derived growth factor (HDGF, predicted MW 26.2 kDa), Kallikrein-8 (KLK-8, predicted MW 28.5 kDa), and Insulin-like growth factor binding protein-2 (IBP-2, predicted MW 32.7 kDa), in addition to LIF, BSA, and transferrin that we know are supplied in the medium. However, the apparent molecular weight (MW) of these proteins suggests that they do not correspond to any of the bands 3-11, except for TIMP-1 (see table below) and perhaps KLK-8. We have already assayed the effects of TIMP-1 and demonstrated that it does not affect growth in the concentration range present in the culture (Figure 5.2d).

Table 5.1 Apparent MW of extracellular proteins in bands 3-11

Protein	Apparent MW
TIMP-1	29[113]
IBP-2	35[114]
HDGF	38[115]
KLK-8	Unknown

It is possible that the HDGF, IBP-2 and KLK-8 are present in the original medium at relatively high concentrations and were therefore detected in our slices – it is common to find traces of highly abundant proteins across the whole gel (Dr. I. Papayannopoulos (Biopolymers Lab, MIT Cancer Center), personal communication). For e.g., we even detected peptides from transferrin (MW 80 kDa) and BSA (MW 66kDa) (which are supplied in the medium) in our MS analysis. IBP-2 (also known as IGFBP-2) at least, is present in human serum at high levels of ~700 ng/ml[116] and therefore may be present as a 'contaminating' protein in BSA at a relatively high level.

5.2.5 Assaying function of proteins detected via mass spectrometry

We next sought to determine whether supplementing media with any of the above factors would improve mESC growth. We were especially interested in the extracellular proteins detected in bands 1 and 2 since these were the bands visible when the CM was collected from cells incubated with the complete medium (N2B27+LIF+BMP-4, Figure 5.4). As mentioned above, we found that Cystatin C was not growth supportive for mESCs (Figure 5.3a). CypA secretion has been shown to be induced by oxidative stress[117, 118], and CypA has been shown to protect various types of cells against cell death induced by such stress[117, 119]. Additionally, CypA^{-}/$^{-}$ embryos show slightly reduced fertility[120] indicating that it may play a protective role in embryos, and Cypa protein is expressed in mouse ESCs[121]. Given the above, we decided to then investigate the effects of CypA on mESC growth. Based on the relative intensity of staining of the bands in the gel, we estimated the concentration of CypA in the CM at ~100 ng/ml (as of this writing, no ELISA kit for CypA is commercially available). When we added recombinant CypA to N2B27+LIF+BMP-4, we observed a 9% increase in growth at 100 ng/ml, and a significant 21% increase at 200 ng/ml for ABJ1 mESCs (Day 1-2, p=0.03, Figure 5.6a). This increased growth upon CypA addition was confirmed in an independently derived cell line (Figure 5.6b, p=0.03, D3 mESCs).

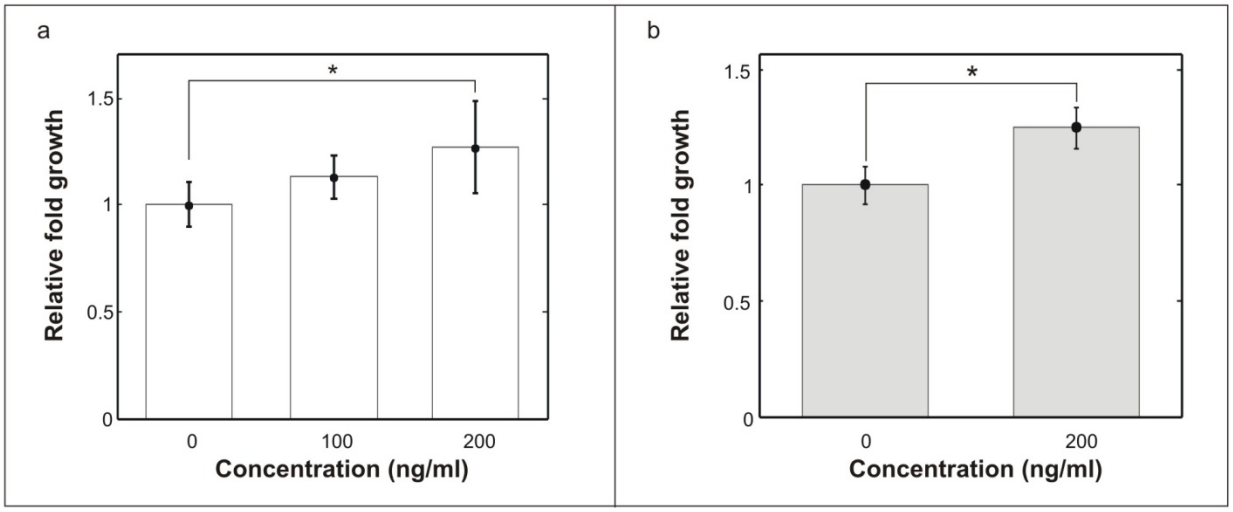

Figure 5.6 Relative fold growth (Day 1-2) versus concentration of Cyclophilin A for ABJ1 mESCs (a) and D3 mESCs (b).

We next sought to block the Cycophilin A receptor. Yurchenko *et al.* have identified CD147 (also known as Basigin and/or Emmprin) as a receptor for CypA[64]. In particular, they determined that the proline 180 and glycine 181 residues in the extracellular domain of CD147 are critical for signaling induced by extracellular CypA. mESCs have been found to express the Cyclophilin A receptor CD147[122], with expression decreasing as the cells differentiate. No monoclonal antibody against mouse CD147 appears to exist, that has been shown to specifically target only the CypA binding site on mouse CD147. However, when we added a polyclonal anti-CD147 antibody on day 2 to mESC cultures plated at 5000 cells/cm^2, we did observe a decrease in the growth rate of ABJ1 mESCs by ~20% relative to no antibody or normal goat IgG (Figure 5.7a, $p<0.05$ for both). The observed decrease in growth upon addition of the receptor antibody is comparable to the increase in growth produced by the action of mESC CM (Figure 4.4a). Similar results were obtained for D3 mESCs (Figure 5.7b, $p<0.05$ for both). However, the decrease

in growth was less (p=2e-3) than the corresponding decrease for ABJ1 mESCs, which consistent with lower production of CypA by D3 mESCs - observe in Figure 5.2 that band 2 for D3 CM is much fainter than band 2 for ABJ1 CM. Together, these results demonstrate that Cyclophilin A is an autocrine survival factor in mESC cultures.

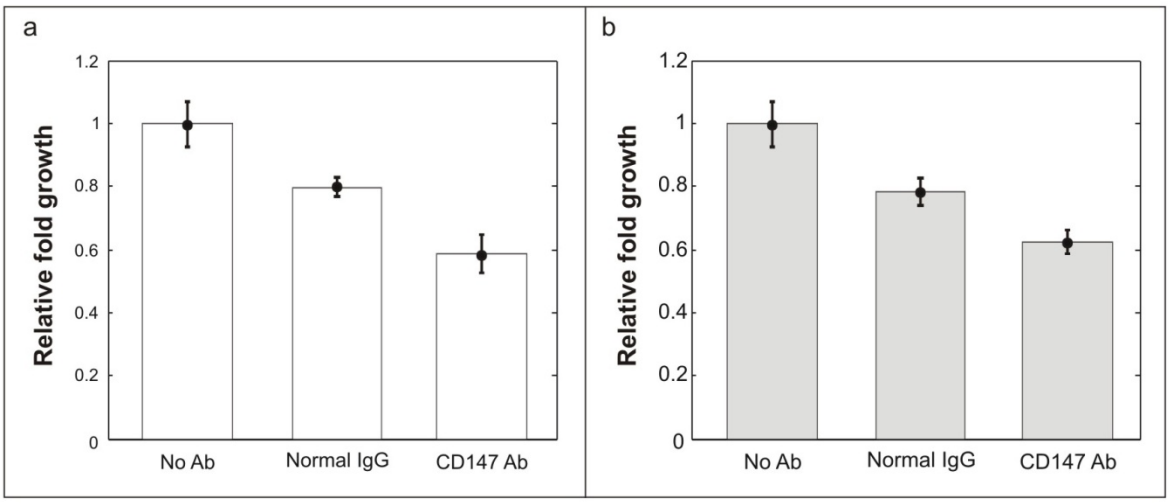

Figure 5.7 Addition of a polyclonal antibody to CD147 (2 μg/ml) significantly decreased the growth of ABJ1 mESCs (a) and D3 mESCs (b) as compared to normal goat IgG at the same concentration, or no antibody. All pair-wise comparisons are significant ($p<0.05$).

5.3 Discussion

In this chapter I have described our efforts at probing the mESC secretome and the effects of several secreted proteins on growth. Importantly, as far as we know, ours is the first study to address the issue of relevant protein ranges for assaying the effects of secreted factors. Let us highlight the importance of this analysis with a concrete example. Say that one assays the effect of an extracellular protein A on growth and finds that 100 ng/ml is the minimum concentration required to improve growth. Further one assays the conditioned medium collected from cells plated at a relatively high density (>1e4cm^{-2}) and finds that protein A is only present at 10 ng/ml. Our analysis indicates that the concentration at the cell surface is not likely to be more than 20 ng/ml. In such a scenario it is not likely that protein A acts as an autocrine growth factor in the culture because 20 ng/ml would not lead to improved growth in the culture. It is worth noting that our model does not preclude the existence of larger factor gradients at very low densities. In Figure 5. 8 we show α versus time for cells plated at 16 cells/cm^2. For this case α_{48} is ~30.

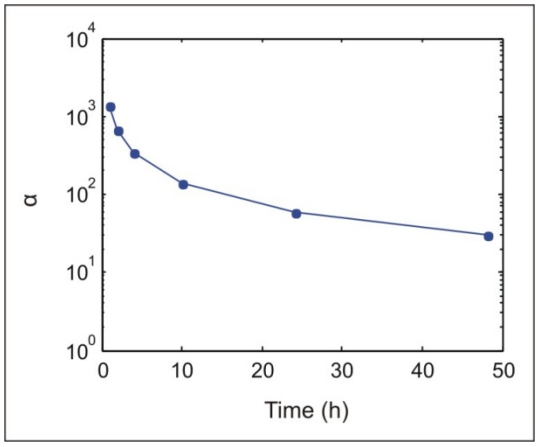

Figure 5. 8 α versus t for 16 cells/cm^2. The model is otherwise identical to that used for Figure 5.2.

It is also worth noting that response to exogenously added ligands may not be necessary for demonstrating the existence of an autocrine loop. Models developed by Lauffenburger and colleagues predict that a cell may bind as much as 65% of the ligand it secretes[109]. Thus it is conceivable that such a cell may already be in a saturation regime and may not respond to exogenously added ligands. Such "saturated autocrine loops" cannot contribute to density-dependent growth. Saturation could result from binding of all receptors, or saturation of activity within the internal pathway that processes ligand binding activity. For the EGF system numerical modeling indicates that receptor occupancy is typically less than 10%. Thus, if such saturation is achieved, it would be likely be due to the latter mechanism.

We have used a fairly simple one-dimensional size-based separation (SDS-PAGE) to compare mESC CM and the control medium. Such a comparison would certainly benefit from the use of a more advanced analysis method such as two-dimensional protein separation where an additional charge-based separation of proteins is performed. Using 2-d separation may clarify whether mESCs actually secrete some of the higher MW proteins we detected in our bands, namely HDGF, IBP-2, and perhaps KLK-8. Additionally, we did not assay the effects of Thioredoxin which was detected in band 1; this would be interesting to do in the future. Alternately, the SILAC method could be used to look for secreted proteins (Stable Isotope Labeling by Amino Acids in Cell Culture)[165]. In this method, cells are grown in media lacking a standard essential amino acid but supplemented with a non-radioactive, isotopically labeled form of that amino acid. This amino acid will be incorporated into proteins made by the cell, and thus proteins made by the cell can be distinguished from proteins originally added to the medium.

We have observed that D3 mESCs produce considerably less CypA as compared to ABJ1 mESCs – in Figure 5.4 band 2 is qualitatively fainter in the D3 CM lane as compared to the ABJ1 CM lane. This observation is consistent with the observation that for D3 mESCs the increase in growth with density is weak till a density of 5000 cells/cm^2 (slope =5e-5 cm^2/cell), while for ABJ1 mESCs the increasing trend is strong right from 500 cells/cm^2 (Figure 4.6, slope = 1e-3 cm^2/cell).

Caveats associated with the use of the polyclonal antibody to CD147 are that it has not been shown to block Cyclophilin A binding, or to suppress receptor activation. However, by the definition of polyclonal, it is likely that some fraction of the molecules will exhibit such effects.

Finally, over the last few years it has been found that CypA and CD147 are *over*expressed in several cancers[123, 124, 166, 167], suggesting that they may support growth in other cell types as well.

5.4 Summary

In this chapter I have described our efforts at probing the mESC secretome and the effects of several secreted proteins on growth. Initially, using numerical modeling we demonstrated that for cells plated at ~10,000 cells/cm^2 the concentration of secreted factors at the cell surface is quite similar to the average concentration in the bulk medium. Thus, to assay physiologically relevant protein concentrations, it is enough to titrate up to twice the concentration present in conditioned medium. Next, we assayed the effects of previously known mESC secreted proteins – Cystatin C, Clusterin, Osteopontin, TIMP-1, and FGF-4, and found that none of them improved growth in the relevant concentration ranges. Then we performed gel analyses and determined that mESCs also secrete Cyclophilin A and perhaps Thioredoxin. We assayed the effects of CypA on mESC growth and found that it increased mESC growth. Additionally, blocking/inhibition of the CypA receptor CD147 led to decreased growth. These results demonstrate that CypA is an autocrine growth factor in mESC cultures.

Chapter 6: Nutritional Aspects and Numerical Modeling of mESC growth

In chapter 4 we demonstrated that there is an optimal density for (2-day) growth of mESCs. Further, in chapters 4 and 5 we demonstrated that the increase in fold growth at low densities is at least partially due to the effects of an autocrine survival factor, and that Cyclophilin A is one such factor. In this chapter we will explore the role of nutrient depletion in the decrease in fold growth seen at higher densities. Finally, via numerical modeling we explore whether the growth supportive effect of autocrine factors combined with the growth-inhibitory effects of nutrient depletion can account for the observed optimal growth density.

6.1 Introduction: Modeling the growth of cells and communication between cells

As mentioned in chapter 1, numerical models have been used since the 1990s to optimize the yield of proteins from cells cultured in bioreactors[6]. Most of these models were Monod-type models incorporating the effects of nutrient depletion and metabolite production. In these models, the cells were assumed to be in a well-stirred bioreactor, thus there were no spatial gradients of nutrients.

As we have seen, a second important mechanism that is responsible for modulating the growth rate in cultures is autocrine signaling via growth factors. Cell-cell interaction via diffusible signaling has been investigated primarily by Doug Lauffenburger's group at MIT, and Shvartsman's group (Princeton). While it is reasonable that the production of a growth factor by cells should lead to a density-dependent increase in growth rate, this hypothesis was first quantitatively examined via numerical modeling by Lauffenburger and Cozens in 1989[43], and they demonstrated that such a process indeed leads to an increase in growth that is consistent with experimental data.

However, we are unaware of any efforts at combining the two above types of models so as to better understand the growth of mammalian cells in culture over longer periods of time. In the models and experiments by Lauffenburger's group[43], growth over short periods of time, typically < 24 hours, is examined such that nutrient depletion is not an issue. Additionally, a few studies have examined (via numerical modeling) the role of the competing effects of growth factor production and nutrient depletion in tumor growth[125, 126]. Byrne and Gourley[125] showed that such competition could lead to interesting effects such as oscillations in tumor size over time. Ferreira *et al*.[126] examined the role of growth factors in determining the fractal dimension of tumor boundaries. However, experimental testing of these models does not appear to have been performed. This is not surprising given the challenges associated with *in vivo* tumor imaging. Our models will be constrained by our cell culture data, which is relatively easy to obtain.

6.2 Materials and Methods

6.2.1 Nutrient analyses

Amino acid (AA) analyses were performed at the Molecular Biology Core Facility at the Dana Farber Cancer Institute (Boston, MA). The facility uses an Applied Biosystems model 420A Amino Acid Analyzer.

Approximately 20% of the liquid was found to evaporate in our experiments. Therefore we applied a correction factor of 0.8 to all AA concentrations.

Glucose consumption rate was measured using a commercially available kit (GAHK20 Sigma). 5e5 cells were plated in wells in a 96-well plate. After allowing them to attach overnight, the medium was replaced and then collected after 6 hours. The number of cells at the beginning and end of the incubation was counted using similarly plated wells. By fitting an exponential function to these values, the average number of cells during the incubation period was calculated. Glucose titration was performed in N2 medium by replacing DMEM/F-12 with glucose-free DMEM (Invitrogen) supplemented with non-essential amino acids (glucose-free neurobasal medium is not commercially available). Data shown is Day 2-3 data. Cells were plated in N2B27+LIF+BMP-4 and allowed to attach (24 hours). Then cells were placed in various concentrations of glucose and allowed to adapt for 24 hours. The assay was performed following this adaptation period; cell counts were performed before and after the assay period using two similarly plated plates. A 24 adaptation period appeared to be required for this assay;cells did not respond to altered glucose concentrations with a shorter adaptation period, perhaps due to intracellular reserves of glucose or downstream products.

Glutamine titration was performed by adapting cells for six hours to various concentrations of glutamine followed by a six hour assay period. The six hour adaptation period was chosen because the mESC lag phase is approximately six hours (chapter 4). The shorter assay period was chosen because glutamine is known to degrade at 37^{o}C.

6.2.2 Numerical modeling

Numerical modeling was performed using MATLAB (Mathworks). The equation system simulated was:

$$\dot{\boldsymbol{n}} = \left(\mathbf{r}_{\boldsymbol{basal}} * \boldsymbol{f}(\boldsymbol{c}) * \frac{(\boldsymbol{g} - \boldsymbol{g}_{\boldsymbol{min}})}{(\boldsymbol{g}_{\boldsymbol{0}} - \boldsymbol{g}_{\boldsymbol{min}})}\right)\boldsymbol{n}; \quad (1)$$

$$\dot{\boldsymbol{c}} = \boldsymbol{r}_{\boldsymbol{prod}} * \boldsymbol{n} - \boldsymbol{\gamma c}; \quad (2)$$

$$\dot{\boldsymbol{g}} = -\boldsymbol{k}_{\boldsymbol{n}} * \boldsymbol{n} * \boldsymbol{g} \quad (3)$$

Where n is the plating density (units of x1000 cells/cm^2),
c is the (dimensionless) concentration of the growth factor (GF),
g is the (dimensionless) nutrient concentration,
r_{basal} represents the growth rate in the absence of GF and nutrient depletion (units of hours^{-1}),
r_{prod} is the GF production rate (units of cm^{2}cell^{-1}hours^{-1}),
g_0 and g_{min} are respectively the dimensionless initial nutrient concentration (set to 1 (unity)), and the dimensionless minimum nutrient concentration required for mESC growth,
γ is the degradation rate (units of hours^{-1}) of the GF, and
k_n is the rate constant for nutrient consumption (units of cm^{2}cell^{-1}hours^{-1}).
$f(c)$ was set to be either $(1+ k_c c)$, or $[1 + k_c c/(1+c)]$.

Our system consists of coupled ordinary differential equations, and neglects the effects of gradients in the concentration of proteins and nutrients (see Discussion). The model with the sigmoidal f(c) is likely more realistic; Knauer *et al.*[127] have shown that the growth rate of fibroblast cells depends in a sigmoidal manner on the concentration of epidermal growth factor in the culture. The linear model is presented because the linear term represents the first term in a Taylor expansion for arbitrary functional forms.

Fitting was performed by computing solutions for a range of parameter values and determining the values that provided the least square error.

6.3 Results

6.3.1 Nutritional aspects of cell culture

6.3.1.1 Net effect of nutrient depletion and metabolite production on mESC growth

We first wanted to determine the net effect of nutrient depletion and metabolite production on mESC growth. For this assay we used D3 mESCs. In Figure 4.6b we showed that for D3 mESCs growth starts to decrease at a density of 20,000 cells/cm^2. We repeated this assay and found that for another batch of cells, the difference in fold growth on Day 1-2 between cells plated at 10,000 cells/cm^2 and 20,000 cells/cm^2 was 10.2 ± 1.6%. To assess the role of nutrients and metabolites i.e. the low MW components of the medium, in this decrease we used a complimentary strategy to that used in chapter 4. We collected Day 0-2 and Day 1-2 conditioned medium from cells plated at 20,000 cells/cm^2 (cells were from the same batch/passage as in the previous experiment). We then dialyzed this medium with a 3 kDa filter to separate out the low MW components and to control for protein secretion and depletion. Then we replenished these media with the required proteins. Our reason for trying both Day 0-2 CM and Day 1-2 CM is that the molecular profile of the medium is constantly changing with time, thus it is best to try medium from more than one period when assessing the effects of the media. Finally, we applied either 100% CM, or 50% CM to a fresh batch of cells, to simulate growth in a 20,000 cells/cm^2 culture or a 10,000 cells/cm^2 culture respectively. We found that growth was indeed slower in 100% CM for both Day 0-2 CM and Day 1-2 CM. The difference in fold growth between 50% and 100% CM for Day 0-2 CM was 7.9 ± 0.6%, while the difference in fold growth between 50% and 100% CM for Day 1-2 CM was 11.6 ± 1.5%. These values are consistent with the difference in growth between cells plated at 10,000 cells/cm^2 and 20,000 cells/cm^2 (10.2 ± 1.6%), suggesting that alterations in the low MW composition on the medium are indeed responsible for the decrease in growth at higher densities. Similar trends were obtained for CM obtained from cells grown at 40,000 cells/cm^2 (Appendix 4).

Cells require a variety of nutrients to grow in culture, primarily amino acids (AA), salts, energy sources (usually glucose and glutamine, sometimes additionally sodium pyruvate), and vitamins. In pioneering experiments in the 1950s, Harry Eagle at the NIH determined the dependence of cell growth on nutrient concentrations for the above nutrients, and developed a "minimal essential medium" (MEM)[128-130]. (I have only referenced a few of his multiple papers on this subject.) Using values measured by him and others, we tried to determine which nutrient(s) is (are) likely to be depleted below the threshold(s) required for maximal growth. Unfortunately, our survey of the literature, in combination with experiments, was not able to unearth which species is likely to be depleted in our system. Below, I

describe in detail our efforts in this regard. A complete characterization of depletion rates for all ~70 ingredients present in N2B27 is beyond the scope of this thesis.

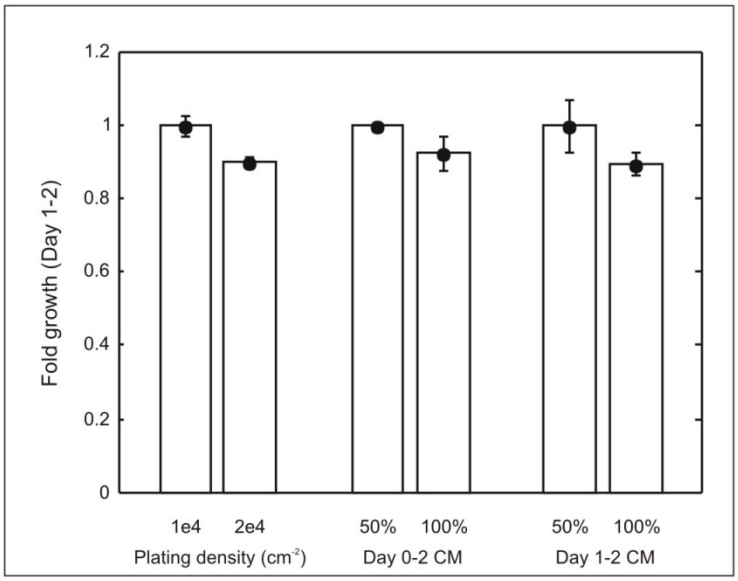

Figure 6. 1 (Left) Relative fold growth over Day 1-2 for cells plated at 10,000 and 20,000 cells/cm^2. (Center and Right) Relative fold growth over Day 1-2 for cells plated in 50% and 100% CM, for Day 0-2 and Day 1-2 CM respectively.

6.3.1.2 Amino Acids

There appears to still be some debate in the literature as to which amino acids are essential versus nonessential for the survival of humans (see, for e.g. Reeds[131]). However, of the twenty amino acids found in nature, nine cannot be synthesized by adult vertebrate animals and therefore must be obtained from their diet[8]. In addition, most cultured cells appear to require four other amino acids[132] which, in the intact animal, are synthesized by specialized cells such as liver or kidney cells[8]. Animal cells can synthesize the 7 remaining amino acids; thus these amino acids need not be present in the culture medium.

To determine whether AA may be limiting in our cultures, we measured the percent amino acid remaining in the culture for ABJ1 cells plated at 10,000 cells/cm^2, at the end of day 2, in serum containing medium. At this density, there is a decrease in growth rate on day 2 (chapter 4), suggesting that a nutrient is depleted. The reason for performing this measurement in serum-containing medium is that the serum-free medium we used for our experiments contained a modified form of L-glutamine (Glutamax, Invitrogen) that cannot be measured using standard amino acid analyzers. Assuming that AA uptake rates will be similar in the serum-free medium, we determined the final concentration of AA in the medium at the end of the culture and compared these values to the AA concentrations required for mammalian cell growth, as determined by Eagle[129] (Table 6.1). In fact, Eagle measured the AA requirements for several cell lines, as mentioned above, and we have reported below the highest values we could find, which are for a kidney cell line[129]. Additionally, more recent studies suggest that the values measured by Eagle may be somewhat high[133]. However, it is easy to see that the concentrations in our cultures are greater than (typically by a factor of 4-5) that required for optimal cell growth (as

measured by Eagle). This data indicates depletion of the AA listed below is likely not responsible for growth reduction in our experiments.

Table 6.1 Final concentrations of 10 essential amino acids in our experiments after two days of culture with cells at 10,000 cells/cm^2.

	Amino Acids	µM in N2B27	% consumed	µM (final)	µM required	Ratio of final to required concentrations
1	L-Arginine	550	23	424	100	4.2
2	L-Histidine	175	11	156	100	1.6
3	L-Isoleucine	600	14	516	100	5.2
4	L-Leucine	625	18	513	100	5.1
5	L-Lysine·HCl	650	4	624	100	6.2
6	L-Methionine	157.5	18	129	30	4.3
7	L-Phenylalanine	300	14	258	30	8.6
8	L-Threonine	625	33	419	100	4.2
9	L-Tyrosine	300	15	255	100	2.6
10	L-Valine	625	11	556	100	5.6

The following caveats must be noted: a) concentrations of cystine and tryptophan could not be measured at Dana Farber (see methods); b) all values for final AA concentrations have been corrected for evaporation (see methods). In other words, the actual final concentrations are about 20% higher than presented above due to concentration of molecules as a result of the evaporation of water.

We also measured the depletion of non-essential amino acids (Table 6.2). However, the concentration dependence of cell growth for these AA is not well studied. For serine, McKeehan *et al.* report a requirement of only 0.8 µM for half-maximal growth of lung fibroblasts[133], while Herzenberg and Roosa reported a requirement of 200 µM for lymphoma cells[134]. However, our final concentration of serine is higher than both these values. In the same paper, Herzenberg and Roosa report a glycine requirement of 200 µM, which is also lower than our measured concentration, and that asparagine, aspartic acid, glutamic acid and proline had no effect on the growth rate of lymphoma cells. Alanine is produced by most cell types and we also detected a small increase in alanine concentration in our media. Finally, asparagine and aspartic acid, and glutamine and glutamic acid are pooled for analysis in the Applied Biosystems 420A Amino Acid Analyzer. The pooled result for asparagines and aspartic acid are presented in the table below. The pooled analysis of glutamine and glutamic acid yielded that there was a net consumption of these AA of 14.6%.

Table 6.2 Final concentrations of 6 nonessential amino acids in our experiments

	Amino Acids	µM in N2B27	% consumed	µM (final)
1	L-Alanine	36.25	Produced	>36.25
2	L-Asparagine	27.5	14	23.7
3	L-Aspartic Acid	25		21.5
4	Glycine	325	21	256.75
5	L-Proline	108.5	7.5	100.3625
6	L-Serine	325	25	243.75

L-glutamine is an important energy source for most cell types[135] and is usually utilized more rapidly than other AA. As a result of this, basal media also contains much higher concentrations of glutamine relative to other kinds of AA. Still, L-glutamine or glucose are most often growth limiting in cell cultures, at least in the published data (reviewed by Portner and Schaffer[6]; interestingly, the authors mention that this may be, in part, because concentrations of glutamine and glucose are relatively easy to measure). Therefore we investigated the role of L-glutamine in further detail. Typical Monod constants for glutamine (K_{Gln}) are 60-150 µM[6], where the Monod constant is the concentration at which the growth rate decreases to half its maximal value. We determined that the Monod constant for glutamine, for ABJ1 mESCs, is 75 µM (Figure 6.2), with maximal growth achieved by ~400 µM.

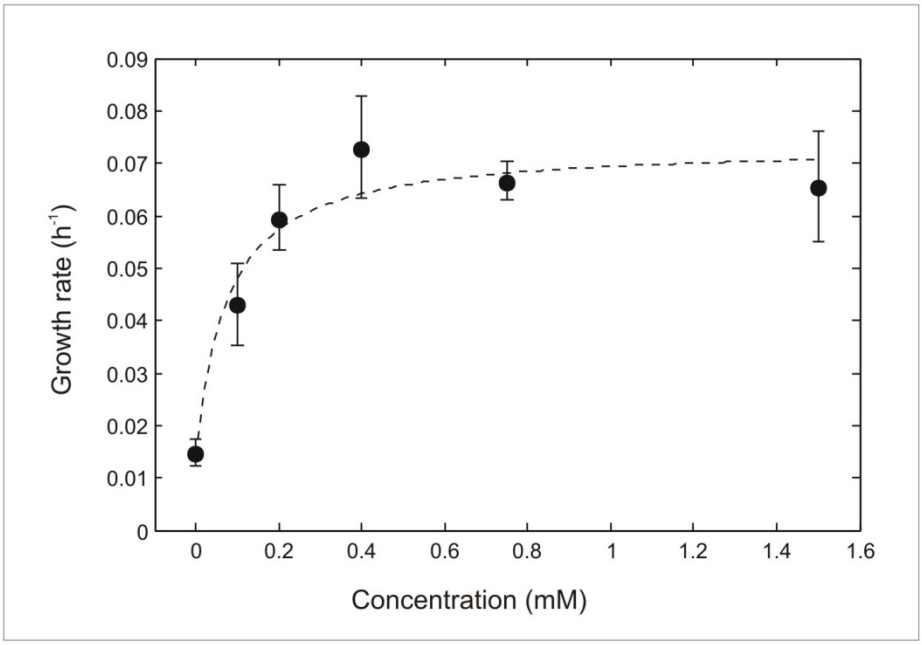

Figure 6.2 Measured growth rate as a function of L-Glutamine concentration for ABJ1 mESCs. The dotted line shows the best fit to the data using a Monod function.

The pooled analysis of glutamine and glutamic acid in our culture yielded that there was a net consumption of these AA of 14.6%. This suggests that the final glutamine concentration is approximately 1.2 mM, which is in the saturation regime of the above graph. To complement our analysis we looked at glutamine consumption rates measured by other authors[136, 137] are 40-60 nmol/10^6 cells/h. At our highest densities for ABJ1 cells (20,000 cells/cm^2), we have on average ~1.5e5 cells/well (24 well plates), which, in 50 h, at the highest measured rate of 60 nmol/10^6 cells/h would consume < 500 nmoles and resulting in a final glutamine concentration of > 1mM. Thus L-glutamine depletion is also not a likely source of growth reduction for ABJ1 cells.

In summary, the measured rates of consumption of AA agree well with values measured for other cell types (Appendix 4). Based on our measurements and data from the literature we find that amino acid depletion is not likely to be the cause underlying growth reduction in our experiments.

6.3.1.3 Glucose

Glucose is an important source of energy for most cell types. During glycolysis, glucose is converted to pyruvate, and then pyruvate is further metabolized to lactate (anaerobic respiration) or carbon dioxide and water (aerobic respiration)[8]. All these processes result in the generation of energy which is ultimately stored as ATP. Additionally, glucose serves as an intermediate for the synthesis of other compounds such as lipids and nucleotides.

Monod constants for glucose have been measured by several authors, and are in the range of 30-300 µM[6, 133, 138]. We measured the dependence of growth rate on glucose concentrations for ABJ1 mESCs (Figure 6.3) and determined the Monod constant to be 380 µM.

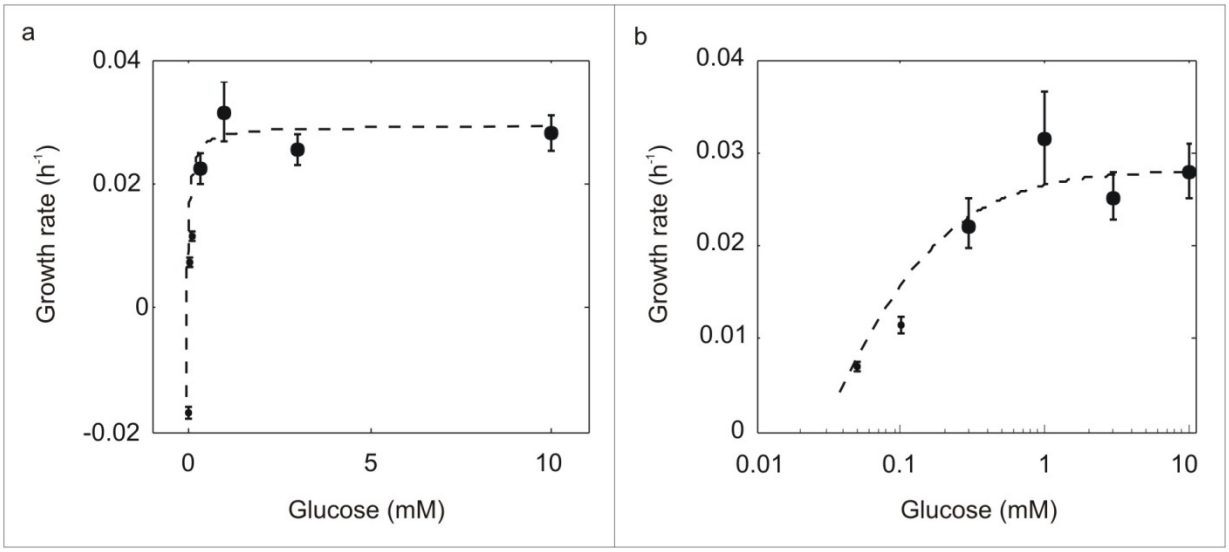

Figure 6.3 a. Measured growth rate as a function of L-Glutamine concentration for ABJ1 mESCs. The dotted line shows the best fit to the data using a Monod function. b. Linear-log plot of the same data as in (a).

Additionally, uptake rates for glucose are typically 1-4 x 10^{-10} mmoles/cell/h[6, 135]. While the glucose uptake rate is a function of the extracellular glucose concentration, the above measurements are

typically performed in the 10-25 mM range where the uptake rate is relatively independent of concentration. The glucose uptake rate for a mESC line was measured by Cochran *et al.* to be 3.3 x 10^{-10} mmoles/cell/h[139]. We measured the glucose uptake rate for ABJ1 mESCs to be 4.6 x 10^{-10} mmoles/cell/h. Since the initial concentration of glucose in our medium is 25 mM, the final concentration even at our highest cell densities will be greater than 15 mM, which is almost two orders of magnitude above the Monod constant for glucose. Thus glucose depletion is not responsible for the growth decrease in our experiments.

6.3.1.4 Vitamins and Salts

Uptake of vitamins does not appear to be commonly measured. We were only able to find one publication that tried to comprehensively measure uptake rates for most vitamin species. In this paper by Blaker and Pirt[140], they measure vitamin uptake rates for a mouse fibroblast cell line. However, values measured by them are comparable to the values for individual vitamins measured in other studies (Appendix 4). Where depletion was not measured by Blaker and Pirt, we have used values from other references (cited in the table below, Appendix 4). As shown in Table 6.3, the amount of vitamin taken up by cells is very little relative to the amount supplied, which may explain why uptake rates for vitamins are not typically measured for cell culture optimization purposes i.e. vitamin depletion is unlikely to be an issue for most cultures.

Table 6.3 Depletion of vitamins in our experiments, based on uptake values from the literature

Vitamin	µg in 1ml N2B27	µg consumed, 1e5 cells, 50 h	Cell type	% depleted	Comments
Thiamine·HCl (B1)	3	0.03	Retinal[141]	1	Depletion not detectable in LS
Riboflavin (B2)	0.3	0.00165	Fibroblast (LS)	0.55	
Niacinamide (B3)	3	0.07	Fibroblast (LS)	2.33	
D-Pantothenic Acid (B5)	3	0.0055	Fibroblast (LS)	0.18	
Pyridoxine·HCl (B6)	3	0.075	Fibroblast (LS)	2.5	
D-Biotin (B7)	3.65e-3	0.00002	Kidney[142]	0.55	See Appendix 4
Myo-Inositol (B8)	10	0.215	Fibroblast (LS)	2.15	
Folic Acid (B9)	3.3	0.033	Intestinal[143]	1	Depletion not detectable in LS
Cobalamin (B12)	0.5	3E-07	Fibroblast[144]	6e-5	Depletion not detectable in LS
Choline Chloride	6.44	1.7	Fibroblast (LS)	26.4	

Finally, the salt contents of mammalian cells are well described and typical intracellular concentrations are available in standard biology/biochemistry textbooks (for example from Molecular Cell Biology[8]). Based on such values DMEM contains several orders of magnitude more of salts than would be required by 10^5-10^6 cells.

6.3.1.5 Metabolites

Lactic acid and ammonia are the main metabolites in cell cultures, resulting from the decomposition of glucose and glutamine respectively. In section 6.3.1.2 we showed that glucose consumption rate for mESCs is in the range of 3-5 x 10^{-10} mmoles/cell/h. Based on our measured value of the consumption rate of 4.6 x 10^{-10} mmoles/cell/h for ABJ1 cells, the decrease in glucose concentration in our experiments is less than 5 mM for ABJ1 cells, which implies that the lactic acid concentration is less than 10 mM. We measured the growth of ABJ1 cells in various concentrations of lactic acid and found that a concentration of 13 mM did not decrease the growth of ABJ1 cells (Figure 6.4). At 26 mM lactic acid there was a ~10% decrease in fold growth that tended towards significance (p=0.06). Finally, at 40 mM lactic acid there was a significant decrease in growth rate (p=4e-8). These values agree with those measured by other investigators, who have shown that lactic acid concentrations of up to 60 mM do not decrease growth[6]. For D3 mESCs which grow faster than ABJ1 mESCs (Figure 4.6), the lactic acid concentration could exceed 13 mM and further measurements will be required to determine whether lactic acid could cause growth decrease in D3 cultures.

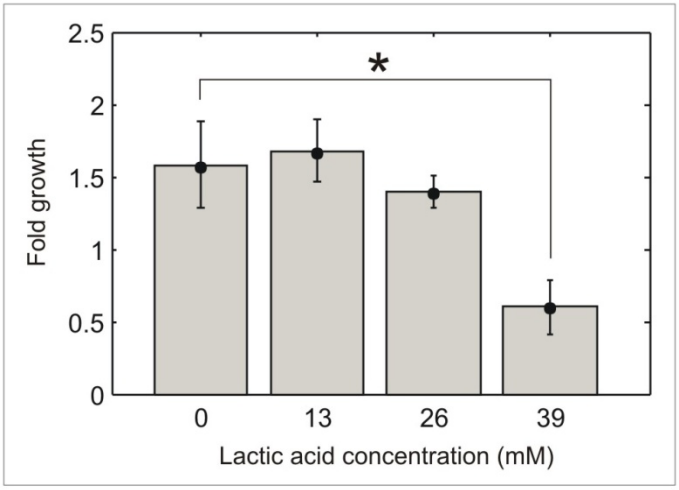

Figure 6.4 Effect of various concentration of lactic acid on the growth of ABJ1 mESCs.

Finally, the Monod constant for ammonia has been measured by several authors to be in the range of 5-6 mM. In our serum-free medium we use only 1.5 mM of an Alanine-Glutamine dipeptide (Glutamax, Invitrogen). Thus the ammonia concentration cannot exceed 1.5 mM, suggesting that the accumulation of ammonia is not likely to be the cause for decrease in growth for our cells. Additionally, the rate of decomposition of the Glutamax dipeptide is approximately 1/6th that of L-glutamine (Glutamax datasheet) suggesting that only small quantities of ammonia will be produced in our cultures.

6.3.2 Numerical modeling of mESC growth

Finally, we wanted to check whether the density-dependent growth of mESCs could, in principle, be caused by a combination of autocrine growth factor (GF) production and nutrient depletion, or whether the data are fundamentally inconsistent with a combination of only these two processes. To do this we

developed a numerical model of cell growth including the above two processes (methods) and fit the resulting behaviors to our data.

In Figure 6.5 we see that density-dependent growth over two days for ABJ1 mESCs is consistent with such models. The solid line shows the behavior of a model where growth is linearly dependent on GF concentration while the dashed line shows the behavior of a model where growth has a sigmoidal dependence on GF concentration. These models demonstrate that for mESCs, the optimal density for growth could indeed be determined by competition between the positive effects on growth of autocrine growth factors and the negative effect of nutrient depletion.

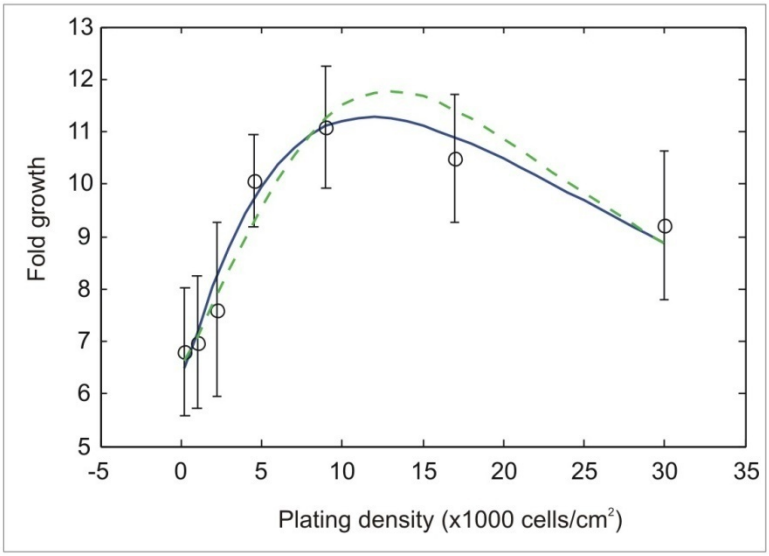

Figure 6.5 Comparison of growth data with numerical modeling results. The open circles show data from measurement of fold growth of ABJ1 mESCs in serum over two days. The dashed line represents best fit data from a model with a linear dependence of growth rate on growth factor concentration, while the solid line represents similar data from a model with sigmoidal dependence.

Fitting was performed by computing solutions for a range of parameter values and determining the values that provided the least square error. Our solutions represent local minima in the parameters space, and we cannot rule out the existence of other best-fit parameter values. For $f(c) = (1+ k_c c)$ we obtained a best-fit basal doubling time of 18 hours (r_{basal} = 0.0389 h^{-1}) and a factor half-life of 12 hours (γ = 0.0583 h^{-1}). For $f(c) = [1 + k_c c/(1+c)]$ we obtained a best-fit basal doubling time of 11 hours (r_{basal} = 0.0636 h^{-1}) and a factor half-life of 5 hours (γ = 0.14 h^{-1}). The doubling time values are within the range expected for mESCs. The factor half-lives appear to be within the physically acceptable range; while not much is known about the half lives of extracellular proteins, the half lives of intracellular proteins is in the range of minutes to hours[145]. Other best-fit parameters were as follows:

$f(c) = (1+ k_c c)$		$f(c) = [1 + k_c c/(1+c)]$	
r_{prod}	0.3 cm^2/cell/s	r_{prod}	0.6 cm^2/cell/s
g_{min}	0.4	g_{min}	0
k_n	0.1 cm^2/cell/s	k_n	0.1 cm^2/cell/s
k_c	1	k_c	1

6.4 Discussion

In this chapter I have presented our efforts at trying to determine the nutrient(s) that may be depleted in mESC cultures. While we have investigated the commonly studied components of media, our medium contains ~20 additional components. These components were presumably added to the medium by developers of the N2 and Neurobasal/B27 media because they were growth supportive. Thus, it is plausible that they would be growth-supportive for mESCs as well, and that depletion of one or more of these components is responsible for the decrease in growth seen at high densities in our experiments. In general nutrient development is currently performed at companies which have robotics for assaying the effects of titrating the 10s of ingredients that are included in media. This is an especially challenging exercise because different components may have synergistic effects on growth and other properties of cells. Thus determining what nutrient(s) is(are) depleted in cultures would also, in general, benefit from the use of high throughput equipment to determine the titration curves for the cell type of interest. These experiments will also be challenging because for each assay a medium will have to be made that lacks that particular ingredient.

Our model uses coupled ordinary differential equations and neglects the effects of gradients of soluble factors and nutrients. We have seen in Chapter 5 that gradients of soluble factors are not very large; therefore such an assumption is not unreasonable. However, efforts to model cell behaviors would certainly benefit from a more complete characterization of transport in culture dishes, and if required, subsequent modification of the model to include the effects of gradients in concentrations.

In our model we have not included the effects of cell-cell contact, but it is plausible that contact may play a role in modulating growth. Todorova *et al.*[42] have shown that inhibiting gap-junctional communication leads to a reduction in either attachment or growth (they did not distinguish between the two). But it is not known whether increasing the amount of contact or the number of gap junctions between mESCs will improve growth. Another common method by which cell contact influences growth is via a phenomenon called contact inhibition (chapter 1). Our data suggest that nutrient depletion is sufficient to account for the decrease in growth seen at high densities in our experiments. Indeed, for ES cells, the general perception in the field seems to be that ES cells do not possess contact inhibition[60]. This is because they form cancers when injected into mice, and tumor cells usually lack contact inhibition. Additionally, in the blastocyst, cells are generally dividing rapidly so as to form germ layers, even though they are in contact with other cells[36]. A third piece of evidence that is sometimes cited is that mESCs grow as multilayer colonies. It is thought that cells in the upper layer come from cell division in the lower layers. Thus cells in the lower layers appear to be able to divide even though these cells contact other cells. This implies that they are not contact inhibited. While these observations suggest

that ESCs do not experience contact inhibition, more conclusive evidence is required since (i) ESCs injected into mice do form teratomas, but they are no longer in a self-renewing environment, so it is not clear that they will not experience contact inhibition in self-renewal medium, (ii) ESCs are obtained from inner cell mass (ICM) cells via adaptation to *in vitro* culture. Thus it is possible that their properties and different from those of ICM cells, and (iii) it is possible to obtain clusters with multiple layers via motility of cells in the lower layer coupled with division of cells only in the outermost layer. Finally, while contact may not abolish growth, it is possible that contact may reduce the growth rate and sensitive assays will be required to discern such changes.

6.5 Summary

In this chapter I have presented our efforts at trying to determine the nutrient(s) that may be depleted in mESC cultures, and that may cause the decrease in growth seen at higher densities. We focused on glucose depletion in particular because it is one of the main energy sources for cells, and showed it is not likely to occur in our experiments. For amino acids we measured the levels present at the end of culture and compared these values to those required for optimal growth, as determined for other cell lines. We found that for those amino acids that were analyzed, none of them appear to be depleted below the required levels.

We have also developed a simple numerical model to check whether GF production and nutrient depletion can account for the density-dependent growth observed in our experiments. We found that our numerical model can provide a good fit to the data. Further characterization of autocrine processes and nutrient depletion will be required to constrain this model and determine whether these mechanisms are indeed sufficient to account for our growth curves.

Chapter 7: Conclusions

In this chapter I will conclude with the major contributions of this thesis. I will then give my outlook for future work that could be pursued to build upon the contributions that have been described in this thesis.

7.1 Thesis contributions

7.1.1 Workflow for investigating cell signaling

I believe that one of the major contributions of this thesis (in concert with other projects in our lab) is a workflow for investigating cell signaling. The first step in the process is screening for the presence of cell interactions in the process/phenotype of interest by using the BFC. While it is possible to screen for interactions by performing large-scale RNAi screens, these are expensive to perform and only a few laboratories appear to have access to the necessary reagents and robotics required to perform such screens. For example, as of this writing, an RNAi library for 464 proteases from Thermo Scientific costs $9558. While the fabrication of a mould for the BFC does need a special facility, the cost of a mould is typically <$100 and usually several 10s of chips can be made from a single mould. In addition, using a plastic molding technology developed in our lab[81], additional moulds can be developed from the original mould. The cost of a single chip is thus of O($10). Therefore the BFC is a cost-effective device for screening for the role of cell interactions (if any) in a phenotype/process of interest, which is the first step in the proposed workflow (Figure 7.1).

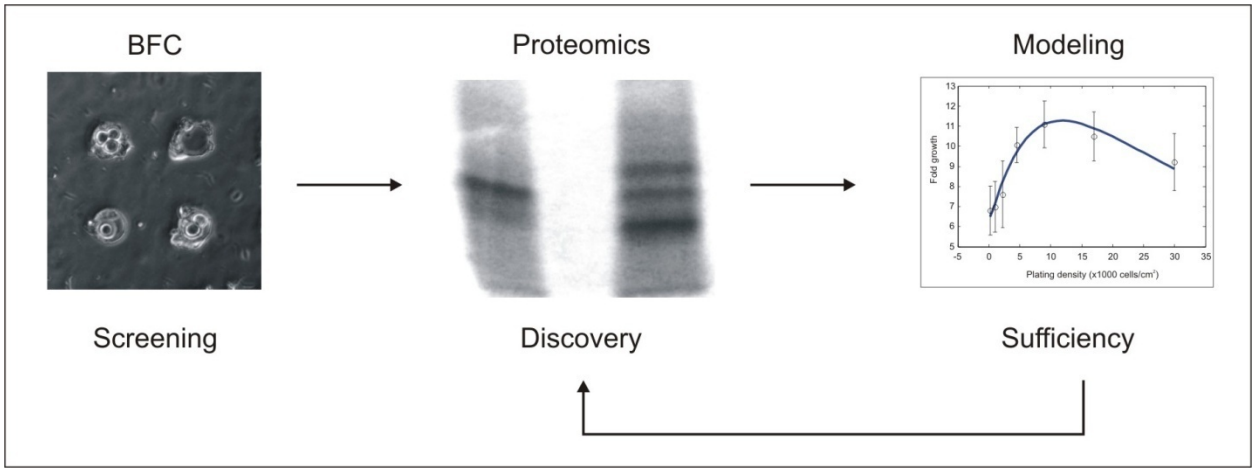

Figure 7.1 Workflow for investigating intercellular signaling

If the BFC indicates that signaling is involved in the phenotype of interest, a different BFC, or plating density variation in traditional culture (depending on the phenotype under study) could be used to investigate whether diffusible signaling affects the phenotype intensity. Further, a positive result from the BFC could justify the investment of greater resources into trying to discover the identity of the proteins involved. For example, in our study, BFC experiments suggested that cell interactions modulate cell survival in mESCs, and further that the interaction was at least partly diffusible. Since we were measuring colony-forming efficiency and did not want colonies to merge, we used a BFC to modulate

plating density, which enforced a minimum colony spacing (chapter 3). These results encouraged us to perform proteomic analysis of mESC conditioned medium to try to unearth the identity of growth factors in the medium.

Additionally, pre-screening with the BFC prior to an RNAi or similar screen could reduce the search space. For example, according to the Gene Ontology database only about 4% of currently annotated human genes consist of proteins that are directly involved in cell-cell signaling. This list includes all known ligands, receptors, connexins, and cadherins. If by using the BFC one were able to associate the development of a phenotype with cell interaction, then instead of screening the whole genome using RNAi one might choose to screen that 4% of genes that are known to be involved in cell –cell interaction.

Additionally, we have used numerical modeling to establish the range of protein concentrations that must be tested in biological assays downstream of proteomic efforts. The final step of the workflow has not been explored in depth in this thesis because of the process studied (growth) and the inability to identify the depleted nutrient(s) (or the metabolite(s) responsible for growth reduction at high densities). However, in general it may be possible to use numerical modeling in combination with quantitative experiments to assess the sufficiency of the discovered proteins in accounting for the phenotype/process under study. These last two steps could be used iteratively to obtain satisfactory, quantitative descriptions of cellular processes.

7.1.2 Discovery of Cyclophilin A as an autocrine survival factor in mESC cultures

The discovery of CypA as an autocrine survival factor in mESC cultures should be of interest to the biology and bio-engineering communities. Cyclophilin A also appears to be produced by human embryonic stem cells (hESCs; Bendall *et al*.[146], supplemental data), and the CD147 precursor protein was detected in the plasma membrane of hESCs via mass spectrometry[147], raising the possibility that Cyclophilin A plays a protective role in hESC cultures as well. This may have useful implications for improving the cloning efficiency of hESCs, which can be as low as 1%[39]. CypA addition may also prove useful for the improvement of serum-free media for the *in vitro* growth of embryos. For example, within reasonable limits, mouse, bovine, and porcine embryos show improved survival at higher densities[148-150], suggesting the presence of soluble survival signals in the culture.

7.1.3 Characterization of mESC growth in culture

Finally, we have performed a detailed characterization of mESC growth in culture including attachment rate, length of lag phase, percent apoptotic cells etc. These studies lay the foundation for similar studies in hESC and human induced pluripotent stem cell (hiPSC) cultures, which could be relevant for the development of cell-based therapies (chapter 1).

7.2 Future directions

In this section I outline my thoughts on future projects that would build on the contributions of this thesis.

7.2.1 nDEP Microwell Array

For making clusters of cells we found that the BFC was preferable to the nDEP microwell array. However, the array may be useful for other types of studies. For example, one group has shown some interest in using the array to study the effects of shear stress on non-adherent cells. To do this these cells must be held stationary against the flow, which is a function that our array can provide. Additionally, with the BFC ~50% of the array can typically be filled when loading single cells. With the nDEP microwells and our development of a technique for positioning cells we can reach loading efficiencies of ~90%. This additional functionality may have useful applications, for example for engineering neuronal networks *in vitro*. With regard to improving the operation of the device the following areas may be interesting to explore in the future:

i. **Including constraints resulting from the generation of reactive oxygen species (ROS) in device design**. We used modeling of the effects of the device on cell health as a design tool. However, we did not explore the role of ROS. Experimental studies by Wang *et al.*[80] as well as in our own lab[81] have demonstrated that AC electrical fields can lead to the generation of ROS, which can activate the stress-response in cells. These studies also demonstrated that the effect of ROS is lower at frequencies above 1 MHz which is the region we typically operate in. Nevertheless, the cellular response is dependent on voltage and frequency, and it may be useful to include the constraints resulting from ROS generation in future array designs.

ii. **Chip architecture and loading protocol**. In the current device design process, the primary emphasis was on the holding strength of the DEP traps[67, 76]. Subsequently, interdigitated electrodes (IDEs) were added to the device to mitigate the sticking of cells. While the influence of these additional electrodes on trapping strength has not been assessed quantitatively, we have observed that they are indeed able to trap cells against flowrates of ~10 µm/s. Future designs could focus on methods by which to improve the loading efficiency of the device. Currently, even using EHD flow, it is only possible to load ~25 out of the 100 traps in each array. This is why loading efficiency was calculated over 25-site regions. This happens because loading 25 traps takes approximately 30 minutes, by which time cells settle in the syringe, tubing, and device; thus there are no more cells available for filling the remaining traps. A simple fix for this may be to re-orient the syringe pump so that the syringe is vertical instead of horizontal. This technique has been used with yeast cells in our lab, and appears to work well. Additionally, it may be useful to incorporate bubble traps into the fluidics, since switching between the syringe containing the cell suspension and the one containing just medium (for washing away the untrapped cells) can lead to the formation of bubbles.

    Another way to improve the supply of cells may be to create a cell storage region in front of the array. Currently, most cells in the region upstream (and downstream) of the array stick to the device surface and are unable for loading into wells (Figure 7.2a). This makes it challenging to load especially the initial rows of the array. By either extending the IDEs to cover the entire chamber, or altering the surface chemistry outside the array to prevent the sticking of cells, these cells should become available for loading. This would also solve a second issue with the current design, which is that cells that stick outside the array currently proliferate into the array region (Figure 7.2b).

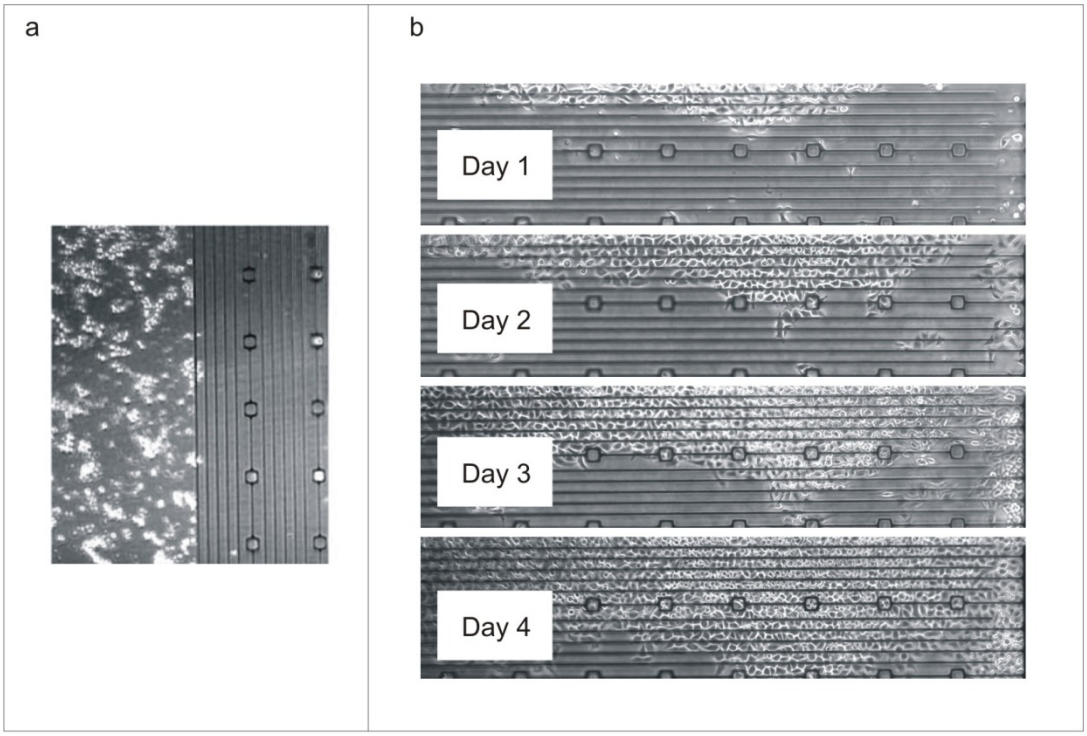

Figure 7.2 a. In the current design, cells stick to the substrate outside of the array. b. Cells that stick outside of the array expand over time into the array.

7.2.2 Bio Flip Chip

i. Studying other cell types. We have performed one demonstration of the utility of the Bio Flip Chip (BFC) in studying and screening for cell interactions. To establish the utility of the BFC for studying cell interactions more generally, it will be important to perform further demonstrations of the ability of the BFC method to detect cell interactions. It may be best to do assays with cell lines that are known to have specific interactions. It will be especially interesting to study systems where contact interaction is important; in principle diffusible interaction can be varied by changing the plating density (though as we have seen in chapter 3 that the BFC offers some advantages), but there are no widely accepted and easy methods for modulating contact interaction.

One cell type that we have identified that may be interesting to study with the BFC is human umbilical vascular endothelial cells (HUVECs). These cells are known to have contact inhibition of growth[168]. Additionally, data from one study suggests that they produce autocrine growth factors[151]. Anne Ouyang, an undergraduate researcher in our laboratory has made initial measurements of the growth of HUVEC cells as a function of the number of cell in the cluster over a 24 hour period. She imaged the cells at 3 hours and determined the number of cells that attached, and then again imaged the cells at 24 and 48 hours to determine the number of cells. In the 24-48 hour period we observed that cells moved considerably and did not retain contact with each other, therefore we present the result of growth over the first 24 hours only. Interestingly, we found that growth over this period shows an initial increasing trend with cell number, followed by a decreasing trend (Figure 7.3a). It is plausible that the increasing

trend is caused by effect of the autocrine diffusible factors, and that the decreasing trend is caused by contact inhibition. However, when we plot growth as a function of the average number of neighbors (Figure 7.3b), we see that for n~3 neighbors there is actually a wide range in fold growth. This suggests that other mechanisms such as local nutrient depletion may also be involved. Further work is required to assess whether contact effects can indeed be detected by the BFC method.

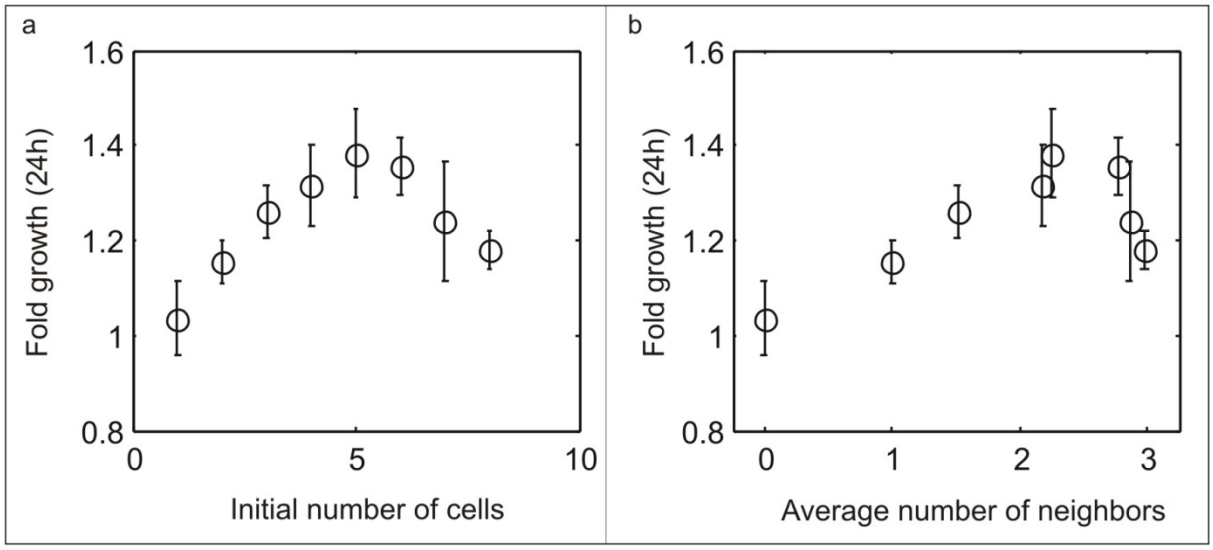

Figure 7.3 a. Fold growth (3-24 hours) versus the initial number of cells in a cluster for HUVECs. b. Fold growth (3-24 hours) versus the average number of neighbors for HUVECs.

Additionally, it would be interesting to study processes other than growth. In chapter 3 I described our use of the BFC for measuring the self-renewal potential of mESCs. It could be interesting to similarly measure the effects of interaction on the rate of differentiation by quantifying the effect of cell number variation on the expression level of differentiation markers such as Sox-1 etc.

ii. Active wells for studying heterotypic interactions. We have also shown proof-of-concept for a new system that contains "active wells", and could be used to study heterotypic interactions[163]. The microwells in this system have electrodes at the bottom that are used to provide a repulsive nDEP force which enables cells to be ejected from the microwells. By addressing these electrodes individually, we are able to selectively clear particular wells. We used this device to iteratively pattern two celltypes (Figure 7.4). However, this could be easily extended to more celltypes. This device could be used to study the effects of modulating interactions between two or more celltypes.

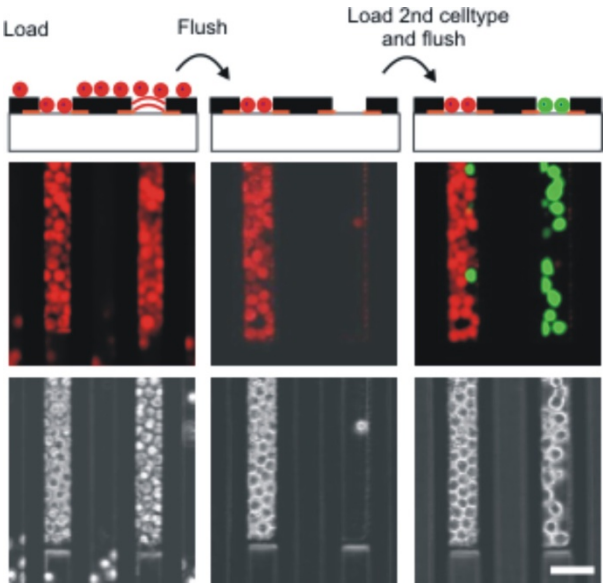

Figure 7.4 Patterning two celltypes. Schematic (top), fluorescence image (middle), and phase image (bottom), demonstrating the patterning of two celltypes using our device. With electrodes on, Ds-Red containing BA/F3 cells are introduced into the chamber. The chamber is then flushed, leaving cells only in the left well. Then gfp-expressing HeLa cells are introduced in the chamber. Since the well on the left is already filled, they can only populate the well on the right. The chamber is again flushed, which results in the final pattern.

iii. Combining the BFC with perfusion. In the BFC, by making clusters of cells we modulate both diffusible and juxtacrine signaling. It would be potentially useful if there was a way to isolate the effects of juxtacrine signaling alone. One way to do this would be to combine the BFC with perfusion, which can be used to wash away diffusible factors. Several current projects in our laboratory use perfusion to wash away diffusible factors and to thereby study the effects of diffusible signaling on mESC self-renewal and differentiation. However, in such devices it is important to distinguish between the effects of altered signaling and those associated with application of shear stress (such investigations are currently underway in our lab). Additionally, it will be important to ensure that diffusible signal from one cluster does not travel downstream to another cluster. One way to implement this is shown in Figure 7.5; by creating an inlet and outlet on opposite sides of a chamber and spacing cluster appropriately, it should be possible to create streamlines that only flow over one cluster.

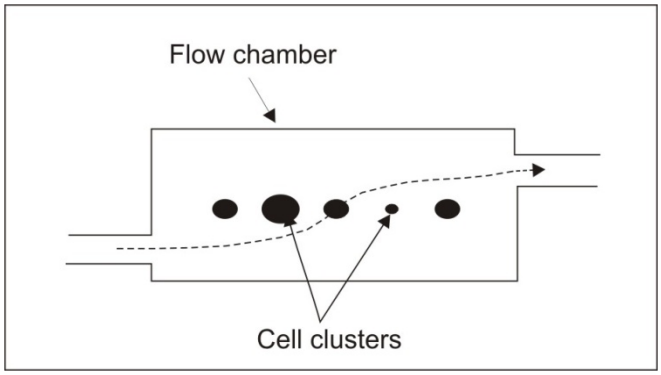

Figure 7.5 Schematic of a device for modulating contact signaling alone. By making clusters of cells one can modulate the amount of contact and diffusible signaling. By then flowing away diffusible factors one obtains a method for modulating contact signaling alone. It may be important to ensure that the factors swept away from one cluster do not travel downstream to another cluster. It may be possible to achieve this using the above design with inlets and outlets on opposite sides of a channel. The dotted line shows a (approximate) streamline that flows over only one cluster.

7.2.3 ESC signaling biology

Our study is the first study to examine the mESC secretome using gel analysis. While we used a simple 1-dimensional protein separation, it was sufficient to detect the presence of several proteins – Cyclophilin A, Cystatin C, Thioredoxin. While two previous studies have examined the mESC secretome[110, 161], they both used ELISA-based approaches, where one is limited to assaying the factors for which antibodies are available. However, it would certainly be better to use 2-dimensional protein separation techniques to further investigate the mESC secretome. Alternately, the SILAC method could be used (Stable Isotope Labeling by Amino Acids in Cell Culture). In this method, cells are grown in media lacking a standard essential amino acid but supplemented with a non-radioactive, isotopically labeled form of that amino acid. This amino acid will be incorporated into proteins made by the cell, and thus proteins made by the cell can be distinguished from proteins originally added to the medium.

We have found that Cyclophilin A is an autocrine survival factor in mESC cultures. Recent studies have found that CypA is also produced by human ESCs[146] and the CD147 (CypA receptor) precursor protein was detected in the plasma membrane of hESCs via mass spectrometry[147]. It would certainly be interesting to test whether CypA also acts as an autocrine survival factor in hESC cultures. This could have useful implications for improving the colony-forming efficiencies of hESCs which can be as low as 1%[39].

References

1. Richards, O.W. The growth of the yeast Saccharomyces cerevisiae. I. The growth curve, its mathematical analysis, and the effect of temperature on the yeast growth. *Annals of Botany* **42**, 271-283 (1928).
2. Monod, J. The Growth of Bacterial Cultures. *Annual Reviews of Micobiology* **3**, 371-394 (1949).
3. Sofos, J.N. Current Microbiological Considerations in Food Preservation. *Int. J. Food Microbiol.* **19**, 87-108 (1993).
4. *Various authors, Biotechnology and Bioengineering* **32**, 945-1078 (1988).
5. Leader, B., Baca, Q.J. & Golan, D.E. Protein therapeutics: A summary and pharmacological classification. *Nature Reviews Drug Discovery* **7**, 21-39 (2008).
6. Portner, R. & Schafer, T. Modelling hybridoma cell growth and metabolism a comparison of selected models and data. *Journal of Biotechnology* **49**, 119-135 (1996).
7. Sporn, M.B. & Todaro, G.J. Autocrine Secretion and Malignant Transformation of Cells. *New England Journal of Medicine* **303**, 878-880 (1980).
8. Lodish, H.F., et al. Molecular Cell Biology (2004).
9. Ramos, J.W. The regulation of extracellular signal-regulated kinase (ERK) in mammalian cells. *Int. J. Biochem. Cell Biol.* **40**, 2707-2719 (2008).
10. Manning, B.D. & Cantley, L.C. AKT/PKB signaling: Navigating downstream. *Cell* **129**, 1261-1274 (2007).
11. Kiger, A.A., White-Cooper, H. & Fuller, M.T. Somatic support cells restrict germline stem cell self-renewal and promote differentiation. *Nature* **407**, 750-754 (2000).
12. Mese, G., Richard, G. & White, T.W. Gap junctions: Basic structure and function. *J. Invest. Dermatol.* **127**, 2516-2524 (2007).
13. Jansen, J.A., van Veen, T.A.B., de Bakker, J.M.T. & van Rijen, H.V.M. Cardiac connexins and impulse propagation. *J. Mol. Cell. Cardiol.* **48**, 76-82.
14. Caveda, L. et al. Inhibition of cultured cell growth by vascular endothelial cadherin (Cadherin-5 VE-cadherin). *Journal of Clinical Investigation* **98**, 886-893 (1996).
15. Perrais, M., Chen, X., Perez-Moreno, M. & Gumbiner, B.M. E-cadherin homophilic ligation inhibits cell growth and epidermal growth factor receptor signaling independently of other cell interactions. *Mol. Biol. Cell* **18**, 2013-2025 (2007).
16. Martin, G.R. Isolation of a Pluripotent Cell-Line from Early Mouse Embryos Cultured in Medium Conditioned by Teratocarcinoma Stem-Cells. *Proceedings of the National Academy of Sciences of the United States of America-Biological Sciences* **78**, 7634-7638 (1981).
17. Evans M.J. & Kaufman M.H. Establishment in culture of pluripotential cells from mouse embryos. *Nature* **292**, 154-156 (1981).
18. Thomson, J.A. et al. Embryonic stem cell lines derived from human blastocysts. *Science* **282**, 1145-1147 (1998).
19. Ivanova, N.B. et al. A stem cell molecular signature. *Science* **298**, 601-604 (2002).
20. Ramalho-Santos, M., Yoon, S., Matsuzaki, Y., Mulligan, R.C. & Melton, D.A. "Stemness": Transcriptional profiling of embryonic and adult stem cells. *Science* **298**, 597-600 (2002).
21. We sampled 20 candidate pluripotency genes as found by Ramalha-Santos *et al*. who used stricter criteria than Ivanova *et al.* Of these, 65% (13/20) were also found to be enriched Ivanova *et al*. Typically, the non-overlapping genes showed lower expression - 3-4 fold as compared to the overlapping genes - 4-11 fold. Therefore it may be possible to obtain a greater overlap by using more stringent criteria. Similar observations have been made by others (Science 302 p. 393).

22. Lu, R. et al. Systems-level dynamic analyses of fate change in murine embryonic stem cells. *Nature* **462**, 358-U126 (2009).
23. Liu, N., Lu, M., Tian, X. & Han, Z. Molecular mechanisms involved in self-renewal and pluripotency of embryonic stem cells. *Journal of Cellular Physiology* **211**, 279-286 (2007).
24. Smith, A.G. et al. Inhibition of pluripotential embryonic stem cell differentiation by purified polypeptides. *Nature* **336**, 688-690 (1988).
25. Williams, R.L. et al. Myeloid-Leukemia Inhibitory Factor Maintains the Developmental Potential of Embryonic Stem-Cells. *Nature* **336**, 684-687 (1988).
26. Matsuda, T. et al. STAT3 activation is sufficient to maintain an undifferentiated state of mouse embryonic stem cells. *Embo Journal* **18**, 4261-4269 (1999).
27. Boeuf, H., Hauss, C., DeGraeve, F., Baran, N. & Kedinger, C. Leukemia inhibitory factor-dependent transcriptional activation in embryonic stem cells. *Journal of Cell Biology* **138**, 1207-1217 (1997).
28. Daheron, L. et al. LIF/STAT3 signaling fails to maintain self-renewal of human embryonic stem cells. *Stem Cells* **22**, 770-778 (2004).
29. Hay, D.C., Sutherland, L., Clark, J. & Burdon, T. Oct-4 knockdown induces similar patterns of endoderm and trophoblast differentiation markers in human and mouse embryonic stem cells. *Stem Cells* **22**, 225-235 (2004).
30. Avilion, A.A. et al. Multipotent cell lineages in early mouse development depend on SOX2 function. *Genes Dev.* **17**, 126-140 (2003).
31. Fong H., Hohenstein K.A. & Donovan P.J. Regulation of Self-Renewal and Pluripotency by Sox2 in Human Embryonic Stem Cells. *Stem Cells* **26**, 1931-1938 (2008)
32. Mitsui K. et al. The Homeoprotein Nanog Is Required for Maintenance of Pluripotency in Mouse Epiblast and ES Cells. *Cell* **113**, 631-642 (2003).
33. Chambers I. et al. Functional Expression Cloning of Nanog, a Pluripotency Sustaining Factor in Embryonic Stem Cells. *Cell* **113**, 643-655 (2003).
34. Hyslop, L. et al. Downregulation of NANOG induces differentiation of human embryonic stem cells to extraembryonic lineages. *Stem Cells* **23**, 1035-1043 (2005).
35. Orford, K.W. & Scadden, D.T. Deconstructing stem cell self-renewal: genetic insights into cell-cycle regulation. *Nat. Rev. Genet.* **9**, 115-128 (2008).
36. Stead, E. et al. Pluripotent cell division cycles are driven by ectopic Cdk2, cyclin A/E and E2F activities. *Oncogene* **21**, 8320-8333 (2002).
37. Lianguzova, M.S., Chuykin, I.A., Nordheim, A. & Pospelov, V.A. Phosphoinositide 3-kinase inhibitor LY294002 but not serum withdrawal suppresses proliferation of murine embryonic stem cells. *Cell Biol. Int.* **31**, 330-337 (2007).
38. Schratt, G. et al. Serum response factor is required for immediate-early gene activation yet is dispensable for proliferation of embryonic stem cells. *Molecular and Cellular Biology* **21**, 2933-2943 (2001).
39. Ware, C.B., Nelson, A.M. & Blau, C.A. A comparison of NIH-approved human ESC lines. *Stem Cells* **24**, 2677-2684 (2006).
40. Ogawa, K. et al. Activin-nodal signaling is involved in propagation of mouse embryonic stem cells. *Journal of Cell Science* **120**, 55-65 (2007).
41. Heo, J.S., Lee, Y.J. & Han, H.J. EGF stimulates proliferation of mouse embryonic stem cells: involvement of Ca2+ influx and p44/42 MAPKs. *American Journal of Physiology-Cell Physiology* **290**, C123-C133 (2006).
42. Todorova, M.G., Soria, B. & Quesada, I. Gap junctional intercellular communication is required to maintain embryonic stem cells in a non-differentiated and proliferative state. *Journal of Cellular Physiology* **214**, 354-362 (2008).

43. Lauffenburger D. & Cozens C. Regulation of mammalian cell growth by autocrine growth factors: Analysis of consequences for inoculums cell density effects. *Biotechnology and Bioengineering* **33**, 1365-1378 (1989).
44. Qi, W.T. et al. Optimization of the cell seeding density and modeling of cell growth and metabolism using the modified Gompertz model for microencapsulated animal cell culture. *Biotechnol. Bioeng.* **93**, 887-895 (2006).
45. McGowan Institute for Regenerative Medicine website.
46. Palsson, B. & Bhatia, S. Tissue engineering. (Pearson Prentice Hall, Upper Saddle River, N.J.; 2004).
47. Atala, A., Bauer, S.B., Soker, S., Yoo, J.J. & Retik, A.B. Tissue-engineered autologous bladders for patients needing cystoplasty. *Lancet* **367**, 1241-1246 (2006).
48. Cheng, M., Moretti, M., Engelmayr, G.C. & Freed, L.E. Insulin-like Growth Factor-I and Slow, Bi-directional Perfusion Enhance the Formation of Tissue-Engineered Cardiac Grafts. *Tissue Engineering Part A* **15**, 645-653 (2009).
49. Krampera, M., Pizzolo, G., Aprili, G. & Franchini, M. Mesenchymal stem cells for bone, cartilage, tendon and skeletal muscle repair. *Bone* **39**, 678-683 (2006).
50. Kuhn, N.Z. & Tuan, R.S. Regulation of Stemness and Stem Cell Niche of Mesenchymal Stem Cells: Implications in Tumorigenesis and Metastasis. *J. Cell. Physiol.* **222**, 268-277 (2010).
51. Mitjavila-Garcia, M.T., Simonin, C. & Peschanski, M. Embryonic stem cells: Meeting the needs for cell therapy. *Advanced Drug Delivery Reviews* **57**, 1935-1943 (2005).
52. Cheshier, S.P., Morrison, S.J., Liao, X.S. & Weissman, I.L. In vivo proliferation and cell cycle kinetics of long-term self-renewing hematopoietic stem cells. *Proc. Natl. Acad. Sci. U. S. A.* **96**, 3120-3125 (1999).
53. Suda, Y., Suzuki, M., Ikawa, Y. & Aizawa, S. Mouse Embryonic Stem-Cells Exhibit Indefinite Proliferative Potential. *J. Cell. Physiol.* **133**, 197-201 (1987).
54. Schatten, G., Smith, J., Navara, C., Park, J.H. & Pedersen, R. Culture of human embryonic stem cells. *Nat. Methods* **2**, 455-463 (2005).
55. Mannello, F. & Tonti, G.A. Concise review: No breakthroughs for human mesenchymal and embryonic stem cell culture: Conditioned medium, feeder layer, or feeder-free; Medium with fetal calf serum, human serum, or enriched plasma; Serum-free, serum replacement nonconditioned medium, or ad hoc formula? All that glitters is not gold! *Stem Cells* **25**, 1603-1609 (2007).
56. Zheng, X.Y. et al. Proteomic analysis for the assessment of different lots of fetal bovine serum as a raw material for cell culture. Part IV. Application of proteomics to the manufacture of biological drugs. *Biotechnology Progress* **22**, 1294-1300 (2006).
57. Mantel, C. et al. Checkpoint-apoptosis uncoupling in human and mouse embryonic stem cells: a source of karyotpic instability. *Blood* **109**, 4518-4527 (2007).
58. Okita, K., Nakagawa, M., Hong, H.J., Ichisaka, T. & Yamanaka, S. Generation of Mouse Induced Pluripotent Stem Cells Without Viral Vectors. *Science* **322**, 949-953 (2008).
59. Visvader, J.E. & Lindeman, G.J. Cancer stem cells in solid tumours: accumulating evidence and unresolved questions. *Nature Reviews Cancer* **8**, 755-768 (2008).
60. Takahashi, K., Murakami, M. & Yamanaka, S. Role of the phosphoinositide 3-kinase pathway in mouse embryonic stem (ES) cells. *Biochemical Society Transactions* **33**, 1522-1525 (2005).
61. Glick, B.R. & Pasternak, J.J. Molecular biotechnology : principles and applications of recombinant DNA, Edn. 3rd. (ASM Press, Washington, D.C.; 2003).
62. Fire, A. et al. Potent and specific genetic interference by double-stranded RNA in Caenorhabditis elegans. *Nature* **391**, 806-811 (1998).
63. Wang, P. & Heitman, J. The cyclophilins. *Genome Biology* **6**, - (2005).
64. Yurchenko, V. et al. Active site residues of cyclophilin A are crucial for its signaling activity via CD147. *Journal of Biological Chemistry* **277**, 22959-22965 (2002).

65. Rodriguez-Sinovas, A. et al. The modulatory effects of connexin 43 on cell death/survival beyond cell coupling. *Prog. Biophys. Mol. Biol.* **94**, 219-232 (2007).
66. Klaunig, J.E. & Shi, Y. Assessment of Gap Junctional Intercellular Communication. *Current Protocols in Toxicology* **Unit 2.17** (2009).
67. Rosenthal, A.D. Cell Patterning Technology for Controlling the Stem Cell Microenvironment. Ph.D. thesis, Massachusetts Institute of Technology (2007).
68. Huang, S., Chen, C.S. & Ingber, D.E. Control of cyclin D1, p27(Kip1), and cell cycle progression in human capillary endothelial cells by cell shape and cytoskeletal tension. *Molecular Biology of the Cell* **9**, 3179-3193 (1998).
69. Nath N., Hyun J., Ma H. & Chilkoti A. Surface engineering strategies for control of protein and cell interactions. *Surface Science* **570**, 98-110 (2004).
70. Ozkan, M. et al. Electro-optical platform for the manipulation of live cells. *Langmuir* **19**, 1532-1538 (2003).
71. Toriello, N.M., Douglas, E.S. & Mathies, R.A. Microfluidic device for electric field-driven single-cell capture and activation. *Analytical Chemistry* **77**, 6935-6941 (2005).
72. Chiou, P.Y., Ohta, A.T. & Wu, M.C. Massively parallel manipulation of single cells and microparticles using optical images. *Nature* **436**, 370-372 (2005).
73. Albrecht, D.R., Underhill, G.H., Wassermann, T.B., Sah, R.L. & Bhatia, S.N. Probing the role of multicellular organization in three-dimensional microenvironments. *Nat Methods* **3**, 369-375 (2006).
74. Ho, C.T., Lin, R.Z., Chang, W.Y., Chang, H.Y. & Liu, C.H. Rapid heterogeneous liver-cell on-chip patterning via the enhanced field-induced dielectrophoresis trap. *Lab Chip* **6**, 724-734 (2006).
75. Mittal, N., Rosenthal, A. & Voldman, J. nDEP microwells for single-cell patterning in physiological media. *Lab Chip* **7**, 1146-1153 (2007).
76. Rosenthal, A. & Voldman, J. Dielectrophoretic traps for single-particle patterning. *Biophysical Journal* **88**, 2193-2205 (2005).
77. Muller, T. et al. The potential of dielectrophoresis for single-cell experiments. *Ieee Engineering in Medicine and Biology Magazine* **22**, 51-61 (2003).
78. Heida, T., Wagenaar, J.B.M., Rutten, W.L.C. & Marani, E. Investigating membrane breakdown of neuronal cells exposed to nonuniform electric fields by finite-element modeling and experiments. *Ieee Transactions on Biomedical Engineering* **49**, 1195-1203 (2002).
79. Beebe, S.J. et al. Nanosecond pulsed electric field (nsPEF) effects on cells and tissues: Apoptosis induction and tumor growth inhibition. *Ieee Transactions on Plasma Science* **30**, 286-292 (2002).
80. Wang, X.J., Yang, J. & Gascoyne, P.R.C. Role of peroxide in AC electrical field exposure effects on Friend murine erythroleukemia cells during dielectrophoretic manipulations. *Biochimica Et Biophysica Acta-General Subjects* **1426**, 53-68 (1999).
81. Desai, S.P. Building Integrated Cell-based Microsystems – Fabrication Methodologies, Metrology Tools and Impact on Cellular Physiology. Ph.D. thesis, Massachusetts Institute of Technology (2009).
82. Neumann, E., Sowers, A.E. & Jordan, C.A. Electroporation and electrofusion in cell biology. (Plenum Press, New York; 1989).
83. Castellanos, A., Ramos, A., Gonzalez, A., Green, N.G. & Morgan, H. Electrohydrodynamics and dielectrophoresis in microsystems: scaling laws. *Journal of Physics D-Applied Physics* **36**, 2584-2597 (2003).
84. Bortvin, A., Goodheart, M., Liao, M. & Page, D.C. Dppa3 / Pgc7 / stella is a maternal factor and is not required for germ cell specification in mice. *BMC Developmental Biology* **4** (2004).
85. Driska, S.P. & Porter, R. Isolation of Smooth-Muscle Cells from Swine Carotid-Artery by Digestion with Papain. *American Journal of Physiology* **251**, C474-C481 (1986).

86. Hui, K.M. & Bidwell, J.L. Handbook of HLA typing techniques Page 276. (CRC Press, Boca Raton; 1993).
87. DiMilla, P.A., Stone, J.A., Quinn, J.A., Albelda, S.M. & Lauffenburger, D.A. Maximal migration of human smooth muscle cells on fibronectin and type IV collagen occurs at an intermediate attachment strength. *J Cell Biol* **122**, 729-737 (1993).
88. Dykstra, B. et al. High-resolution video monitoring of hematopoietic stem cells cultured in single-cell arrays identifies new features of self-renewal. *Proceedings of the National Academy of Sciences of the United States of America* **103**, 8185-8190 (2006).
89. Friedman, R.S., Jacobelli, J. & Krummel, M.F. Surface-bound chemokines capture and prime T cells for synapse formation (vol 7, pg 1101, 2006). *Nature Immunology* **7**, - (2006).
90. Jaenisch, R. & Young, R. Stem cells, the molecular circuitry of pluripotency and nuclear reprogramming. *Cell* **132**, 567-582 (2008).
91. Eggan, K. et al. Hybrid vigor, fetal overgrowth, and viability of mice derived by nuclear cloning and tetraploid embryo complementation. *Proceedings of the National Academy of Sciences of the United States of America* **98**, 6209-6214 (2001).
92. Nagy, A. et al. Embryonic Stem-Cells Alone Are Able to Support Fetal Development in the Mouse. *Development* **110**, 815-& (1990).
93. Liu, N., Lu, M., Tian, X.M. & Han, Z.C. Molecular mechanisms involved in self-renewal and pluripotency of embryonic stem cells. *Journal of Cellular Physiology* **211**, 279-286 (2007).
94. Davey, R.E. & Zandstra, P.W. Spatial organization of embryonic stem cell responsiveness to autocrine gp130 ligands reveals an autoregulatory stem cell niche. *Stem Cells* **24**, 2538-2548 (2006).
95. Davey, R.E., Onishi, K., Mahdavi, A. & Zandstra, P.W. LIF-mediated control of embryonic stem cell self-renewal emerges due to an autoregulatory loop. *Faseb Journal* **21**, 2020-2032 (2007).
96. Bottenstein, J.E. & Sato, G.H. Growth of a Rat Neuroblastoma Cell Line in Serum-Free Supplemented Medium. *Proceedings of the National Academy of Sciences of the United States of America* **76**, 514-517 (1979).
97. Brewer, G.J., Torricelli, J.R., Evege, E.K. & Price, P.J. Optimized Survival of Hippocampal-Neurons in B27-Supplemented Neurobasal(Tm), a New Serum-Free Medium Combination. *Journal of Neuroscience Research* **35**, 567-576 (1993).
98. Zwerner, R.K., Cox, R.M., Lynn, J.D. & Acton, R.T. Five-Year Perspective of the Large-Scale Growth of Mammalian Cells in Suspension Culture. *Biotechnology and Bioengineering* **23**, 2717-2735 (1981).
99. Slattery, M.G. & Heideman, W. Coordinated regulation of growth genes in Saccharomyces cerevisiae. *Cell Cycle* **6**, 1210-1219 (2007).
100. Brejning, J., Jespersen, L. & Arneborg, N. Genome-wide transcriptional changes during the lag phase of Saccharomyces cerevisiae. *Archives of Microbiology* **179**, 278-294 (2003).
101. Conrad, A.H. & Ruddle, F.H. Regulation of Thymidylate Synthetase-Activity in Cultured Mammalian-Cells. *Journal of Cell Science* **10**, 471-& (1972).
102. Watanabe, I. & Okada, S. Effects of Temperature on Growth Rate of Cultured Mammalian Cells (L5178Y). *Journal of Cell Biology* **32**, 309-& (1967).
103. Fattman, C.L., Schaefer, L.M. & Oury, T.D. Extracellular superoxide dismutase in biology and medicine. *Free Radical Biology and Medicine* **35**, 236-256 (2003).
104. Michiels, C., Raes, M., Toussaint, O. & Remacle, J. Importance of Se-Glutathione Peroxidase, Catalase, and Cu/Zn-Sod for Cell-Survival against Oxidative Stress. *Free Radical Biology and Medicine* **17**, 235-248 (1994).

105. Qi, X.X. et al. BMP4 supports self-renewal of embryonic stem cells by inhibiting mitogen-activated protein kinase pathways. *Proceedings of the National Academy of Sciences of the United States of America* **101**, 6027-6032 (2004).
106. Abu-Absi, N.R. & Srienc, F. Instantaneous evaluation of mammalian cell culture growth rates through analysis of the mitotic index. *Journal of Biotechnology* **95**, 63-84 (2002).
107. Hardy, K. Cell death in the mammalian blastocyst. *Molecular Human Reproduction* **3**, 919-925 (1997).
108. Hem, L.H. & Niemeyer, B. A novel correlation for protein diffusion coefficients based on molecular weight and radius of gyration. *Biotechnology Progress* **19**, 544-548 (2003).
109. Shvartsman, S.Y., Wiley, H.S., Deen, W.M. & Lauffenburger, D.A. Spatial range of autocrine signaling: Modeling and computational analysis. *Biophysical Journal* **81**, 1854-1867 (2001).
110. Singla, D.K. & McDonald, D.E. Factors released from embryonic stem cells inhibit apoptosis of H9c2 cells. *Am. J. Physiol.-Heart Circul. Physiol.* **293**, H1590-H1595 (2007).
111. Wilder, P.J. et al. Inactivation of the FGF-4 gene in embryonic stem cells alters the growth and/or the survival of their early differentiated progeny. *Developmental Biology* **192**, 614-629 (1997).
112. Kato, T. et al. A neurosphere-derived factor, cystatin C, supports differentiation of ES cells into neural stem cells. *Proceedings of the National Academy of Sciences of the United States of America* **103**, 6019-6024 (2006).
113. Morita-Fujimura, Y., Fujimura, M., Gasche, Y., Copin, J.C. & Chan, P.H. Overexpression of copper and zinc superoxide dismutase in transgenic mice prevents the induction and activation of matrix metalloproteinases after cold injury-induced brain trauma. *Journal of Cerebral Blood Flow and Metabolism* **20**, 130-138 (2000).
114. Lafon-Cazal, M. et al. Proteomic analysis of astrocytic secretion in the mouse - Comparison with the cerebrospinal fluid proteome. *Journal of Biological Chemistry* **278**, 24438-24448 (2003).
115. Abouzied, M.M. et al. Expression patterns and different subcellular localization of the growth factors HDGF (hepatoma-derived growth factor) and HRP-3 (HDGF-related protein-3) suggest functions in addition to their mitogenic activity. *Biochemical Journal* **378**, 169-176 (2004).
116. Renehan, A.G. et al. Circulating insulin-like growth factor II and colorectal adenomas. *Journal of Clinical Endocrinology & Metabolism* **85**, 3402-3408 (2000).
117. Jin, Z.G. et al. Cyclophilin A is a secreted growth factor induced by oxidative stress. *Circulation Research* **87**, 789-796 (2000).
118. Seko, Y. et al. Hypoxia followed by reoxygenation induces secretion of cyclophilin A from cultured rat cardiac myocytes. *Biochemical and Biophysical Research Communications* **317**, 162-168 (2004).
119. Boulos, S. et al. Evidence that intracellular cyclophilin A and cyclophilin A/CD147 receptor-mediated ERK1/2 signalling can protect neurons against in vitro oxidative and ischemic injury. *Neurobiol. Dis.* **25**, 54-64 (2007).
120. Colgan, J. et al. Cyclophilin A regulates TCR signal strength in CD4(+) T cells via a proline-directed conformational switch in Itk. *Immunity* **21**, 189-201 (2004).
121. Colgan, J., Asmal, M. & Luban, J. Isolation, characterization and targeted disruption of mouse Ppia: Cyclophilin A is not essential for mammalian cell viability. *Genomics* **68**, 167-178 (2000).
122. Intoh, A. et al. Proteomic analysis of membrane proteins expressed specifically in pluripotent murine embryonic stem cells. *Proteomics* **9**, 126-137 (2009).
123. Yang, H.R. et al. Cyclophilin A is upregulated in small cell lung cancer and activates ERK1/2 signal. *Biochemical and Biophysical Research Communications* **361**, 763-767 (2007).
124. Riethdorf, S. et al. High incidence of EMMPRIN expression in human tumors. *International Journal of Cancer* **119**, 1800-1810 (2006).
125. Byrne, H.M. & Gourley, S.A. The role of growth factors in avascular tumour growth. *Mathematical and Computer Modelling* **26**, 35-55 (1997).

126. Ferreira, S.C., Martins, M.L. & Vilela, M.J. A growth model for primary cancer (II). New rules, progress curves and morphology transitions. *Physica A* **272**, 245-256 (1999).
127. Knauer, D.J., Wiley, H.S. & Cunningham, D.D. Relationship between Epidermal Growth-Factor Receptor Occupancy and Mitogenic Response - Quantitative-Analysis Using a Steady-State Model System. *Journal of Biological Chemistry* **259**, 5623-5631 (1984).
128. Eagle, H. The Specific Amino Acid Requirements of a Mammalian Cell (Strain L) in Tissue Culture. *Journal of Biological Chemistry* **214**, 39 (1955).
129. Eagle, H., Freeman, A.E. & Levy, M. The Amino Acid Requirements of Monkey Kidney Cells in 1St Culture Passage. *J. Exp. Med.* **107**, 643-& (1958).
130. Eagle, H. The Minimum Vitamin Requirements of the L-Cells and Hela Cells in Tissue Culture, the Production of Specific Vitamin Deficiencies, and Their Cure. *J. Exp. Med.* **102**, 595-& (1955).
131. Reeds, P.J. Dispensable and indispensable amino acids for humans. *Journal of Nutrition* **130**, 1835S-1840S (2000).
132. Eagle, H. Nutrition Needs of Mammalian Cells in Tissue Culture. *Science* **122**, 501-504 (1955).
133. Mckeehan, W.L., Mckeehan, K.A. & Calkins, D. Extracellular Regulation of Fibroblast Multiplication - Quantitative Differences in Nutrient and Serum Factor Requirements for Multiplication of Normal and Sv40 Virus-Transformed Human-Lung Cells. *Journal of Biological Chemistry* **256**, 2973-2981 (1981).
134. Herzenberg, L.A. & Roosa, R.A. Nutritional Requirements for Growth of a Mouse Lymphoma in Cell Culture. *Experimental Cell Research* **21**, 430-438 (1960).
135. Eibl, R., Fussenegger, M. & Weber, W. Cell and tissue reaction engineering. (Springer, Berlin; 2009).
136. Griffiths, J.B. & Pirt S.J. The Uptake of Amino Acids by Mouse Cells (Strain LS) During Growth In Batch Culture and Chemostat Culture: The Influence Of Cell Growth Rate. *Proceedings of the Royal Society of London. Series B, Biological Sciences* **168**, 421-438 (1967).
137. Duval, D., Demangel, C., Munier-Jolain, K., Miossec, S. & Geahel, I. Factors controlling cell proliferation and antibody production in mouse hybridoma cells: I. Influence of the amino acid supply. *Biotechnol Bioeng* **38**, 561-570 (1991).
138. Zielke, H.R., Ozand, P.T., Tildon, J.T., Sevdalian, D.A. & Cornblath, M. Growth of Human Diploid Fibroblasts in Absence of Glucose-Utilization. *Proceedings of the National Academy of Sciences of the United States of America* **73**, 4110-4114 (1976).
139. Cochran, D.M., Fukumura, D., Ancukiewicz, M., Carmeliet, P. & Jain, R.K. Evolution of oxygen and glucose concentration profiles in a tissue-mimetic culture system of embryonic stem cells. *Annals of Biomedical Engineering* **34**, 1247-1258 (2006).
140. Blaker, G.J. & Pirt, S.J. Uptake of Vitamins by Mouse Fibroblast Cells (Strain LS) during Growth in a Chemically Defined Medium. *Journal of Cell Science* **8**, 701-& (1971).
141. Subramanian, V.S. et al. Vitamin B1 (thiamine) uptake by human retinal pigment epithelial (ARPE-19) cells: mechanism and regulation. *Journal of Physiology-London* **582**, 73-85 (2007).
142. Balamurugan, K., Vaziri, N.D. & Said, H.M. Biotin uptake by human proximal tubular epithelial cells: cellular and molecular aspects. *American Journal of Physiology-Renal Physiology* **288**, F823-F831 (2005).
143. Ariel, M., Eilam, Y., Jablonska, M. & Grossowicz, N. Effect of Phenytoin on Folic-Acid Uptake in Isolated Intestinal Epithelial-Cells. *Journal of Pharmacology and Experimental Therapeutics* **223**, 224-226 (1982).
144. Rosenblatt, D.S., Thomas, I.T., Watkins, D., Cooper, B.A. & Erbe, R.W. Vitamin-B12 Responsive Homocystinuria and Megaloblastic-Anemia - Heterogeneity in Methylcobalamin Deficiency. *American Journal of Medical Genetics* **26**, 377-383 (1987).

145. Bachmair, A., Finley, D. & Varshavsky, A. Invivo Half-Life of a Protein Is a Function of Its Amino-Terminal Residue. *Science* **234**, 179-186 (1986).
146. Bendall, S.C. et al. An Enhanced Mass Spectrometry Approach Reveals Human Embryonic Stem Cell Growth Factors in Culture. *Molecular & Cellular Proteomics* **8**, 421-432 (2009).
147. Dormeyer, W. et al. Plasma membrane proteomics of human embryonic stem cells and human embryonal carcinoma cells. *Journal of Proteome Research* **7**, 2936-2951 (2008).
148. Lane, M. & Gardner, D.K. Effect of Incubation Volume and Embryo Density on the Development and Viability of Mouse Embryos Invitro. *Hum. Reprod.* **7**, 558-562 (1992).
149. Khurana, N.K. & Niemann, H. Effects of oocyte quality, oxygen tension, embryo density, cumulus cells and energy substrates on cleavage and morula/blastocyst formation of bovine embryos. *Theriogenology* **54**, 741-756 (2000).
150. Stokes, P.J., Abeydeera, L.R. & Leese, H.J. Development of porcine embryos in vivo and in vitro; evidence for embryo 'cross talk' in vitro. *Developmental Biology* **284**, 62-71 (2005).
151. Labitzke, R. & Friedl, P. A serum-free medium formulation supporting growth of human umbilical cord vein endothelial cells in long-term cultivation. *Cytotechnology* **35**, 87-92 (2001).
152. Niwa, H., Miyazaki, J. & Smith, A.G. Quantitative expression of Oct-3/4 defines differentiation, dedifferentiation or self-renewal of ES cells. *Nature Genetics* **24**, 372-376 (2000)
153. Takahashi, K., Mitsui, K. & Yamanaka, S. Role of ERas in promoting tumour-like properties in mouse embryonic stem cells. *Nature* **423**, 541-545 (2003).
154. Kim, Y.H. & Han, H.J. Synergistic effect of high glucose and ANG II on proliferation of mouse embryonic stem cells: Involvement of PKC and MAPKs as well as AT1 receptor. *Journal of Cellular Physiology* **215**, 374–382 (2008).
155. Zhang, C.C., Kaba, M., Lizuka, S., Huynh, H. & Lodish, H.F. Angiopoietin-like 5 and IGFBP2 stimulate ex vivo expansion of human cord blood hematopoietic stem cells as assayed by NOD/SCID transplantation. *Blood* **111**, 3415-3423 (2008).
156. Gray, D.S. et al. Engineering amount of cell-cell contact demonstrates biphasic proliferative regulation through RhoA and the actin cytoskeleton. *Experimental Cell Research* **314**, 2846-2854 (2008).
157. Berrill, A. et al. Assessment of stem cell markers during long-term culture of mouse embryonic stem cells. *Cytotechnology* **44**, 77-91 (2004).
158. Prudhomme, W., Daley, G.Q., Zandstra, P. & Lauffenburger, D.A. Multivariate proteomic analysis of murine embryonic stem cell self-renewal versus differentiation signaling. *Proceedings of the National Academy of Sciences of the United States of America* 101, 2900-2905 (2004).
159. Ying, Q.L., Nichols, J., Chambers, I. & Smith, A. BMP induction of Id proteins suppresses differentiation and sustains embryonic stem cell self-renewal in collaboration with STAT3. *Cell* **115**, 281-292 (2003).
160. Keenan, J., Pearson, D. & Clynes, M. The role of recombinant proteins in the development of serum-free media. *Cytotechnology* **50**, 49-56 (2006).
161. Viswanathan, S., Benatar, T., Rose-John, S., Lauffenburger, D.A. & Zandstra, P.W. Ligand/receptor signaling threshold (LIST) model accounts for gp130-mediated embryonic stem cell self-renewal responses to LIF and HIL-6. *Stem Cells* **20**, 119-138 (2002).
161. Guo, Y., Graham-Evans, B. & Broxmeyer, H.E. Murine embryonic stem cells secrete cytokines/growth modulators that enhance cell survival/anti-apoptosis and stimulate colony formation of murine hematopoietic progenitor cells. *Stem Cells* **24**, 850-856 (2006).
162. Ying, Q.L., Stavridis, M., Griffiths, D., Li, M. & Smith, A. Conversion of embryonic stem cells into neuroectodermal precursors in adherent monoculture. *Nature Biotechnology* **21**, 183-186 (2003).
163. Mittal, N. & Voldman J. Patterning multiple heterogeneous cells using active microwells. *RLE Progress Report 2007* 11-7.

164. Li, Y. et al. Comparative study of mesenchymal stem cells from C57BL/10 and mdx mice. *BMC Cell Biology* **9** (2008).
165. Ong SE et al. Stable isotope labeling by amino acids in cell culture, SILAC, as a simple and accurate approach to expression proteomics. *Molecular and Cellular Proteomics* 1, 376-86 (2002).
166. Li, Z.Y. et al. Proteomics Identification of Cyclophilin A as a Potential Prognostic Factor and Therapeutic Target in Endometrial Carcinoma. *Molecular & Cellular Proteomics* **7**, 1810-1823 (2008).
167. Li, M. et al. Cyclophilin A is overexpressed in human pancreatic cancer cells and stimulates cell proliferation through CD147. *Cancer* 106, 2284-2294 (2006).
168. Suzuki, E. et al. Reentry into the Cell Cycle of Contact-inhibited Vascular Endothelial Cells by a Phosphatase Inhibitor. *Journal of Biological Chemistry* **275**, 3637-3644 (2000).
169. Jones, T.B. Electromechanics of Particles (1995).
170. Nelson, C.M. & Chen, C.S. Cell-cell signaling by direct contact increases cell proliferation via a PI3K-dependent signal. *FEBS Letters* 514, 238-242 (2002).
171. Lee, P.J. et al. Microfluidic application-specific integrated device for monitoring direct cell-cell communication via gap junctions between individual cell pairs. *Applied Physics Letters* **86**, 223902 (2005).
172. Kim, L. Y. Microfluidic perfusion culture for controlling the stem cell microenvironment. Ph.D. thesis, Massachusetts Institute of Technology (2008).

Appendix 1: Dielectrophoresis (DEP)

DEP refers to the force on a cell in a spatially non-uniform electric field. When a cell is placed in any electric field, an electric dipole is induced in the cell. When this field is spatially non-uniform, the electrical forces pulling on each half of the cell are unbalanced, resulting in a net force that propels the cell to either the maximum electric field intensity (positive DEP or p-DEP) or minimum field intensity (negative DEP or n-DEP).

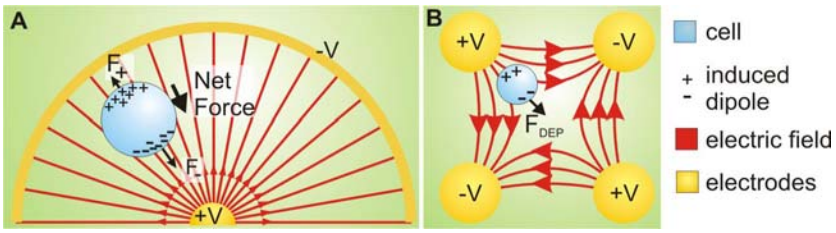

Figure A1.1 Dielectrophoresis. **(A)** A cell in an electric field feels a Coulomb force (F_+, F_-) on its induced dipole. Spatial non-uniformity in the electric field causes a net force, in this case toward the field maximum—positive DEP (p-DEP). **(B)** In a negative DEP (n-DEP) trap, the induced dipole is oriented oppositely. In this case, four electrodes create an electric field that imparts a force toward the center of the trap, trapping the cell.

The DEP force (F_{DEP}) on a spherical particle is given by

$$F_{DEP} = 2\pi\varepsilon_m R^3 Re\{CM\}.\nabla E^2$$

where ε_m is the electrical permittivity of the surrounding media, R is the radius of the particle, and E is the applied electric field. CM is the Clausius-Mossotti (CM) factor, which describes the electrical properties of the particle and the medium, and is given by[169]:

$$CM = \frac{\underline{\sigma}_p - \underline{\sigma}_m}{\underline{\sigma}_p + 2\underline{\sigma}_m}$$

where $\underline{\sigma}_p$ and $\underline{\sigma}_m$ are the complex effective conductivities of the particle and the medium respectively. For the medium this is given by

$$\underline{\sigma}_m = \sigma_m + j\omega\varepsilon_m$$

where σ_m is the conductivity of the medium, ε_m is the permittivity of the medium, ω is the radian frequency, and j is $\sqrt{-1}$. For cells with a membrane (but no cell wall), the effective permittivity is given by

$$\underline{\sigma}_p = \frac{\underline{C}_m R \underline{\sigma}_c}{\underline{C}_m R + \underline{\sigma}_c},$$

where the membrane is described as a shell with a complex surface capacitance $\underline{C}_m = C_m + G_m/j$. C_m and G_m are the surface capacitance and conductance, respectively, given by $C_m = \varepsilon_s/t$ and $G_m = \sigma_s/t$, where t is the membane thickness and the ε_s and σ_s are the permittivity and conductivity of the membrane. R is the radius of the cell. $\underline{\sigma}_c$ is the complex permittivity of the cytoplasm. Values for HL60 cells have been measured by Huang *et al.* (*Biophysical Journal*, 1997, **73**, 1118):

C_m	$1.6*10^{-2}$ F/m^2
G_m	2200 S/m^2
ε_c	75 ε_0
σ_c	0.75 S/m

t is typically ~5nm[8]. Given these values, it is possible to simplify the above equation to obtain the effective permittivity and conductivity of a cell.

$$Re(\underline{\sigma_p}) \cong \varepsilon_s \frac{R}{t}\left(\frac{\varepsilon_s \varepsilon_c R}{t} + \left(\frac{\sigma_c}{\omega}\right)^2\right) / \left(\left(\frac{\varepsilon_s R}{t}\right)^2 + \left(\frac{\sigma_c}{\omega}\right)^2\right)$$

$$Imag(\underline{\sigma_p}) \cong -\frac{\sigma_c}{\omega}\frac{R}{t}\left(\frac{{\varepsilon_s}^2 R}{t} + \frac{\sigma_s \sigma_c}{\omega^2}\right) / \left(\left(\frac{\varepsilon_s R}{t}\right)^2 + \left(\frac{\sigma_c}{\omega}\right)^2\right)$$

The plot below gives the behavior of $Re(\underline{\sigma}_p)$ and $Imag(\underline{\sigma}_p)$, for R = 10μm. In particular, the effective permittivity shows a transition from a higher to a lower value. It can be shown that the numerator of $Re(\underline{\varepsilon}_p)$ decays more slowly than the denominator, and as a result, the frequency of the transition is given by $\omega \cong \sigma_c \frac{t}{\varepsilon_s R}$.

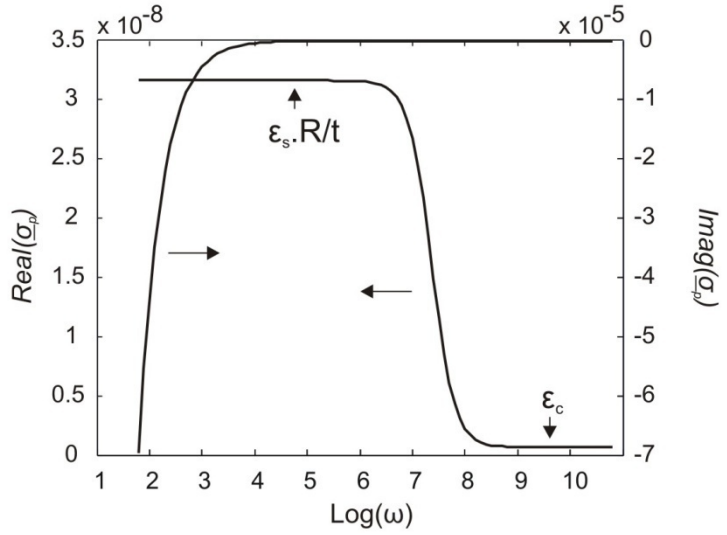

Figure A1.2 Graphs of $Re(\underline{\sigma}_p)$ and $Imag(\underline{\sigma}_p)$ versus frequency using parameters for HL60 cells measured by Huang *et al.*

One way to gain some intuition into this phenomenon is to use a circuit model for the cell (Figure A1.3). At frequencies in the MHz range, the membrane is primarily capacitive i.e. its impedance is dominated by its capacitive reactance, which is much smaller than its resistance (since the two are in parallel), $\chi_s \sim j\, t/\omega\varepsilon_s$ (per unit area). Similarly, in this frequency range, the cytoplasm is mainly resistive, $\chi_c \sim R/\sigma_c$. This frequency represents the frequency at which the cell impedance as a whole switches from primarily capacitive, to primarily resistive. The impedance of the cell as a whole is the sum of these two

impedances. The frequency at which the cell impedance switches from being primarily capacitive to primarily resistive can be obtained by solving

—— —,

which yields ——, as above. Numerically, this frequency is ~10 MHz. The inverse of this frequency is called the Maxwell-Wagner relaxation time.

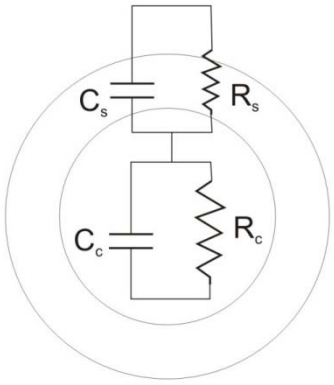

Figure A1.3 Electrical model of the cell. The model consists of two capacitor-resistor pairs in series representing the cell membrane and the cytoplasm.

The direction of the force depends on the sign of the CM factor. Importantly, cells in conductive media such as saline or DMEM *only* experience n-DEP. For such media, conductivity is 1.5 S/m and dielectric constant is 80. The graph below shows CM values versus frequency for a cell in such media. Note that there are now two "dispersions" i.e. regions where the CM factor varies strongly with frequency, corresponding to the two interfaces in the system – one between the cytoplasm and the cell membrane, and the other between the membrane and the medium.

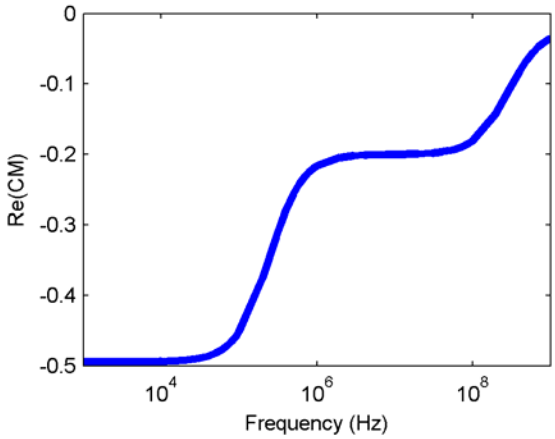

Figure A1.4 Graph of the real part of the CM factor versus frequency.

Appendix 2: Supplementary Data for Chapter 3

This appendix contains additional data pertaining to the BFC experiments described in chapter 3.

Patterning cells with the BFC

In Figure 3.2 we show patterning of mESCs using the BFC. In Figure A2.1 we show clusters of another cell type – human umbilical vein endothelial cells (HUVECs). Clusters of 1-8 HUVECs could easily be made using the BFC.

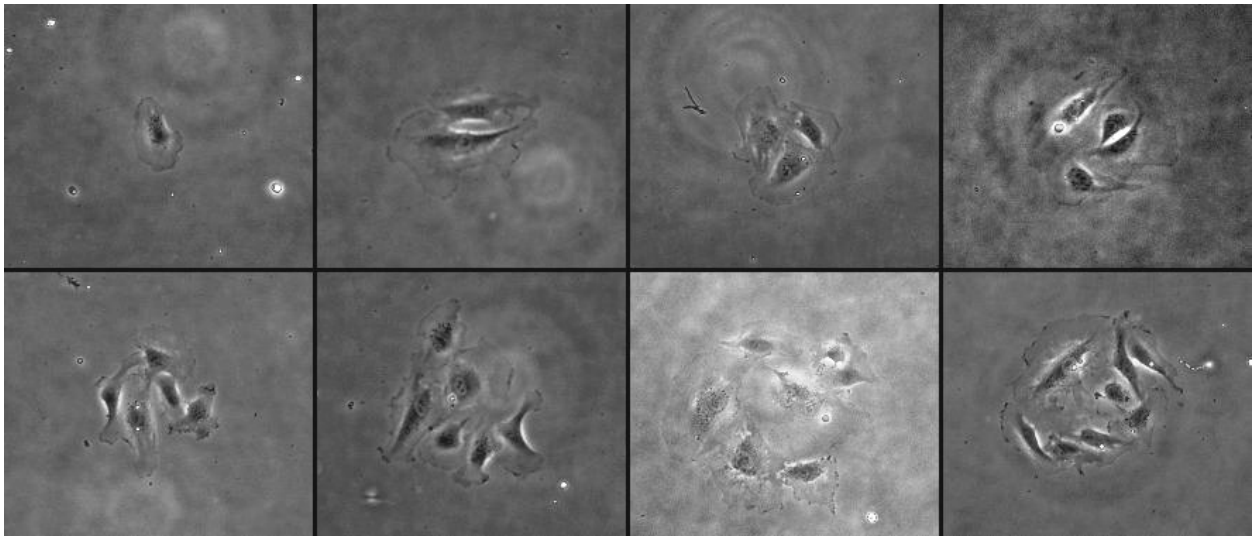

Figure A2.1 1-8 HUVECs can be easily patterned using the Bio Flip Chip.

Biocompatibility of the BFC

Biocompatibility was assessed by comparing the survival probability (colony-forming efficiency) of single mouse ES cells plated in the device, or in a culture dish at a low density of 100 cells/cm^2. Figure A2.2 shows that these survival probabilities are similar, demonstrating that the BFC does not reduce cell viability. In Figure A2.4 we further show that mESCs in our device express Oct-4 indicating that they maintain a pluripotent state.

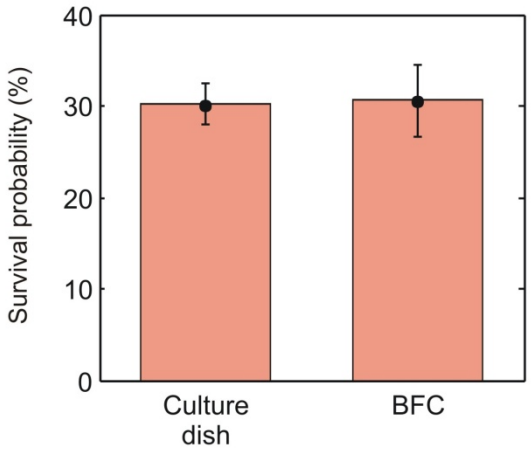

Figure A2.2 Survival probability of single CCE mESCs plated in a culture dish and in a BFC.

Colony area versus initial number of cells

Figure A2.3 shows that larger initial clusters of cells lead to larger colonies. This data, in combination with colony speed data suggest that clusters do not move rapidly from their initial location, allowing us to assign colonies with high confidence to the initial clusters they arose from. As described in chapter 3, colony areas were measured using Metamorph (Molecular Devices). Data presented below are from a single experiment with 5-10 colonies per initial number of cells.

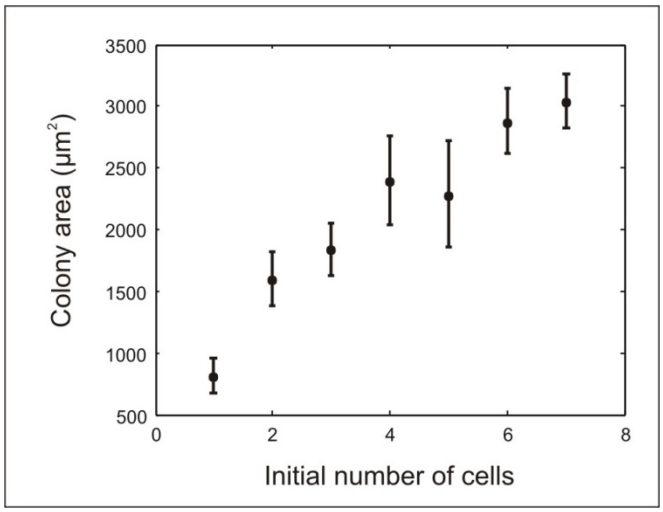

Figure A2.3 Colony area versus the initial number of cells in the cluster

Self-renewal potential experiments

Figure A2.4 shows some typical images of colonies of the Oct4-GFP expressing ABJ1 mouse ES cell-line used for measuring the SRP of clusters of cells.

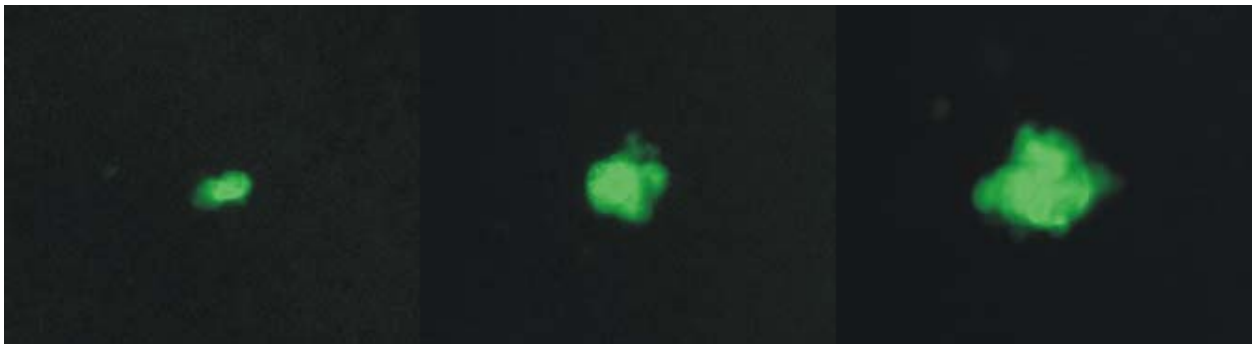

Figure A2.4 Some typical fluorescence images of colonies of the Oct4-GFP expressing ABJ1 cell-line (stitched image). From left to right, these colonies arose from 1, 4, and 7 cells respectively.

In Figure A2.5a we have plotted log(SRP per cell) for 1-4 cells initially in the cluster, which have similar SRP per cell (Figure 3.7a, the deviation from linear growth only starts after n = 5). This graph shows that there is a spatial bias to the SRP data (p=0.003). At distances of more than 4 mm (60 well spacings) from the center of the BFC, the SRP starts to decrease. In Figure A2.5b we show that if we only consider data within 60 well spacings from the center of the BFC, this bias is eliminated. Therefore we only considered data in this spatial range for further analysis. We are unsure as to the cause of this spatial bias. It could arise from the diffusible signaling suggested by the data obtained by varying the seeding density of cells (Figure 3.9, chapters 4-6), or from edge effects due to adsorption of proteins to the gasket.

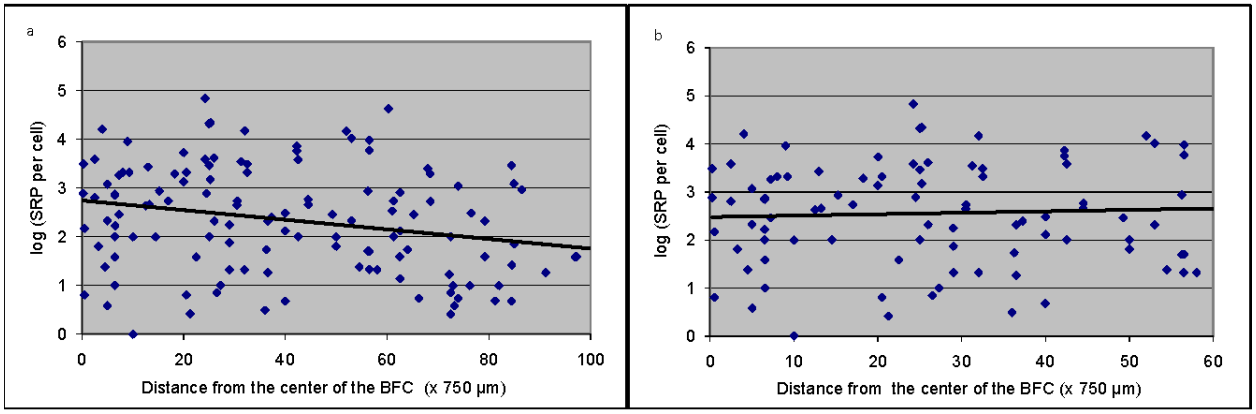

Figure A2.5 a) The SRP starts to decrease at a distance of approximately 60 sites from the center of the BFC (sites are spaced by 750 µm). b) By only including data within 60 sites from the center, we avoid this bias.

Additionally, because the droplet of cells placed on the BFC is convex, wells towards the edge typically collect less cells and as a result have smaller clusters. Thus one obtains more data for larger clusters within the unbiased region described above. In the future it would be a good idea to use a mixture of smaller and larger wells to eliminate this bias in data collection.

Seeding density experiments

In Table A2-1 below we present the detailed data from our BFC experiments where we varied the seeding density of cells, for ABJ1 cells. The areas were measured for all colonies on Day 2. In Table A2-2 we present similar data for CCE mESCs.

Table A2-1

Seeding Density	Expt #	Chip #	Number of cells (Day 0)	Number of colonies (Day 2)	Colony forming efficiency (%)
High	1	1	153	90	58.8
High	2	1	143	89	62.2
High	2	2	67	39	58.2
Low	1	1	43	18	41.9
Low	1	2	57	26	45.6
Low	2	1	75	37	49.3

Table A2-2

Seeding Density	Expt #	Chip #	Number of cells (Day 0)	Number of colonies (Day 2)	Colony forming efficiency (%)
High	1	1	150	88	58.7
High	2	1	199	129	64.8
High	2	2	146	104	71.2
Low	1	1	25	13	52.0
Low	2	1	43	24	55.8
Low	2	2	30	15	50.0

In Figure A2.6 a-b below, we show images of portions of the BFC used to pattern cells at high and low densities. In c and d we show images of cells taken shortly after inverting the BFC, clearly showing a large difference in the plating density. Images e and f show the resulting colonies in the same region of the chip on Day 2. Several such images were analyzed for each chip to obtain the data for CFE and colony area described previously.

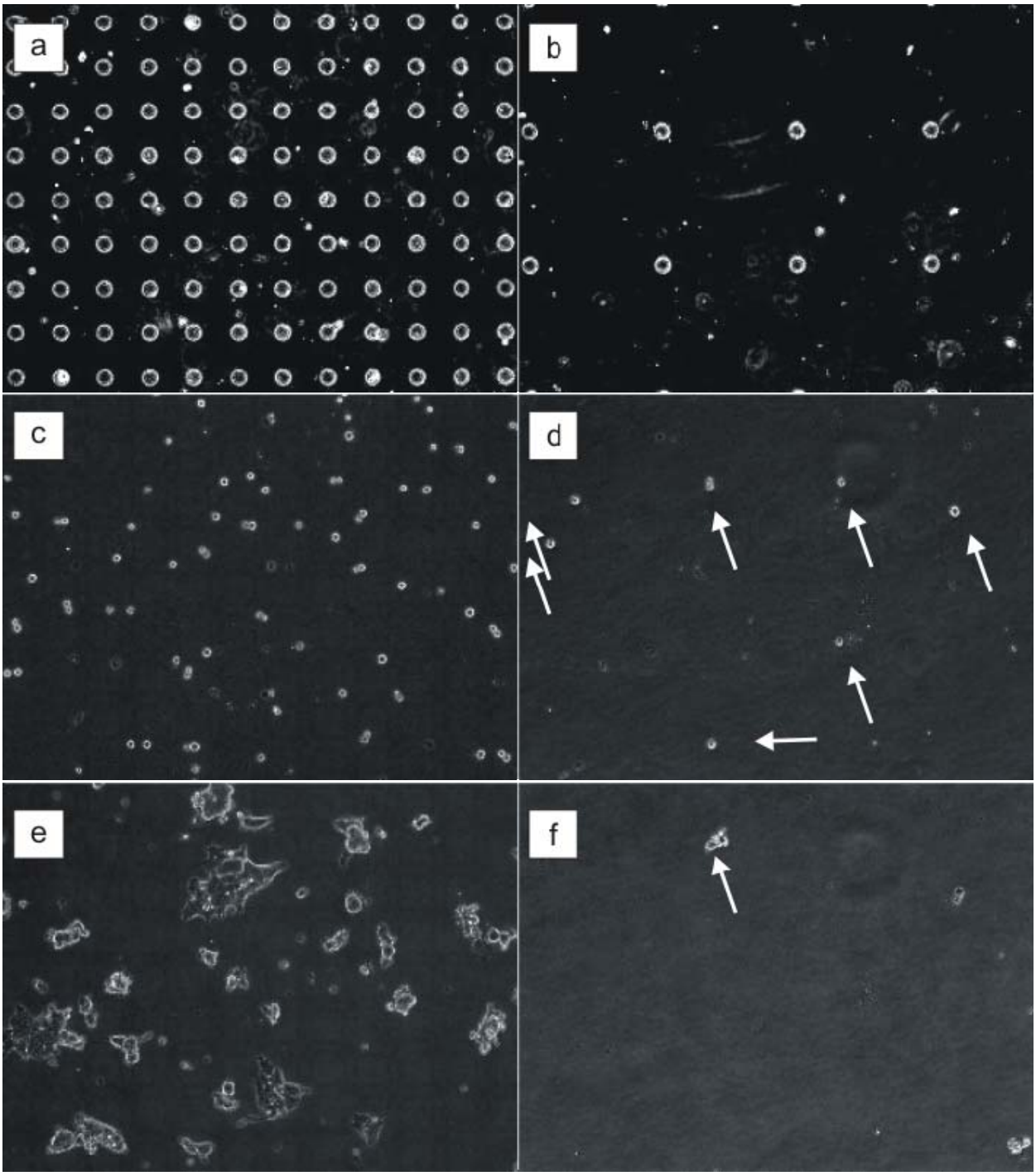

Figure A2.6 (a & b) Phase contrast images of portions of the BFC chip used to pattern cells at low and high densities respectively. The spacing between the wells is 50 and 150 μm respectively. (c & d) Images of cells shortly after plating, and (e & f) images of the resulting colonies on Day 2.

Appendix 3: Supplementary Data for Chapter 5

Determining protein concentrations in cell cultures using numerical modeling

In Figure 5.2c we showed the time-dependence of the ratio (α) of the secreted protein concentration at the surface of the cell to the average concentration in the culture. Those values were obtained from a model where the number of receptors per cell was fixed at 1e5/cell and the off-rate was neglected. We have also briefly investigated a model with receptor dynamics. For the model, we used values from Shvarstman *et al.*[109], which correspond to the epidermal growth factor system:

Surface complex dissociation rate (commonly called k_{off}) = 2e-3 s^{-1}
Endocytosis rate for bound receptors = 1e-3 s^{-1}
Internalization rate for unbound receptors = 1e-4 s^{-1}
Receptor production rate = 1e-12 moles/m^2/s

To model the receptor dynamics, in addition to the Diffusion module in COMSOL Multiphysics, we used two Weak form (boundary) modules to simulate the dynamics of bound and unbound receptors. In our simulation we actually found that the unbound receptor number varied over the duration of the simulated culture (48 hours). In this regard the results of Shvartsman *et al.*[109] are somewhat confusing because while they provide values for receptor production and internalization rates, in the text they often say "1e5 receptors per cell", suggesting that they used a constant for the number of free receptors.

Figure A3.1 shows that the presence of receptor dynamics provides only a small correction to the values of α at least for the density we are interested in (1e4 cells/cm^2). For these simulations we used k_{on}=1e8 $M^{-1}min^{-1}$ and r = 5e-13 moles/m^2/s.

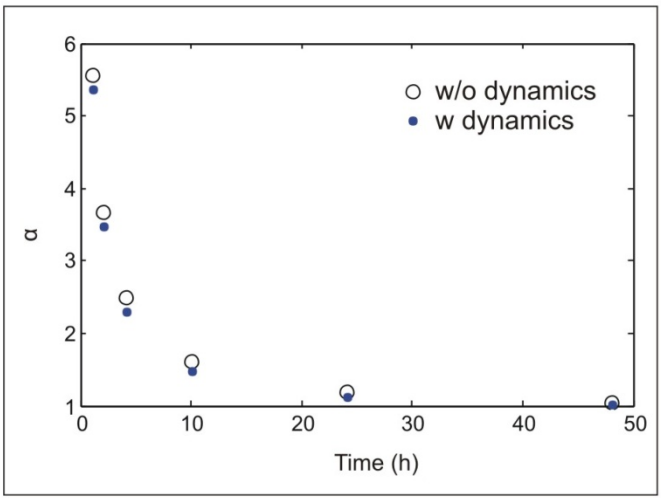

Figure A3.1 Graph of α versus time from models with (solid circles) and without (open circles) receptor dynamics.

Mass spectrometry data

In the table below, we list the various proteins detected in our LC/MS analysis of CM collected from cells grown in N2 medium alone, sorted by the bands that they likely contribute to (bands 1 and 2 were analyzed separately, bands 3-10 were analyzed as a pool). For some of the more abundant proteins, we have mentioned their apparent MW, by looking up datasheets for corresponding antibodies at SCBT/Abcam. For comparison, we show the number of peptides of the same proteins detected in an MS analysis of mESC lysate: Molecular & Cellular Proteomics 5:1261-1273, 2006. A comparison of their and our results reveals that ~ 75% of the highly abundant (>15 peptides detected), intracellular, non-ribosomal proteins in the range of 19.5-30 kDa seen in their study, were also detected in our analysis, and they must have come from dying cells in our cultures in N2 medium.

Band	Uniprot MW	#Peptides Us	#Peptides MCB '06	Apparent MW
Band 1 in addition to Profilin, Cystatin C and Thioredoxin				
Ubiquitin-conjugating enzyme E2 N	16104	1	8	
Eukaryotic translation initiation factor 5A-1	17049	3	9	
Fatty acid-binding protein, heart	14810	1	9	
Tubulin-specific chaperone A	12807	1	4	
Small ubiquitin-related modifier 3 precursor	12593	3	-	
Transcription elongation factor B polypeptide 1	13219	1	4	
Band 2 in addition to Cyclophilin A				
Eukaryotic translation initiation factor 5A-1	17049	3	9	
Small ubiquitin-related modifier 3 precursor	12593	3	-	
Ubiquitin-conjugating enzyme E2 variant 1	16458	1	4	
Ubiquitin-conjugating enzyme E2 L3	18033	1	9	
Band 3				
CNBP Cellular nucleic acid-binding protein	19578	4	10	20
TCTP Translationally-controlled tumor protein	19449	2	14	
PARK7 Protein DJ-1	20008	1	12	
Band 4				
PRDX1 Peroxiredoxin-1	22162	2	35	22
DUTP Dutp protein	21238	2	10	
CBX1 Chromobox protein homolog 1	21404	1	7	
LSM12 Protein LSM12 homolog	21687	1	-	
YKT6 Synaptobrevin homolog YKT6	22300	1	5	
Band 7				
TPIS Triosephosphate isomerase	26695	8	19	26

HMGB2 High mobility group protein B2	24146	5	24	~27
CYBP Calcyclin-binding protein	26493	3	18	
CPSF5 Cleavage and polyadenylation specificity factor subunit 5	26223	2	10	
IDI1 Isopentenyl-diphosphate Delta-isomerase 1	26272	2	5	
AK2 Adenylate kinase 2, mitochondrial	26451	2	9	
UCHL4 Ubiquitin carboxyl-terminal hydrolase isozyme L4	26433	1	-	
EFHD1 EF-hand domain-containing protein D1	26982	1	-	
Band 8-9				
PGAM1 Phosphoglycerate mutase 1	28813	7	19	29-30
GDIR1 Rho GDP-dissociation inhibitor 1	23392	7	14	29
YHWAZ 14-3-3 protein zeta/delta	27753	5	22	30
TIMP1 Metalloproteinase inhibitor 1	22613	3	-	29
HMGB1 High mobility group protein B1	24878	3	12	29
TPM3 tropomyosin 3, gamma	28840	2	20	
CAH2 Carbonic anhydrase 2	29014	2	6	
NIT2 Nitrilase homolog 2	30482	1	11	
HAGH Hydroxyacylglutathione hydrolase	28882	1	-	
DNJC8 DnaJ homolog subfamily C member 8	29794	1	5	
CN166 Protein C14orf166 homolog	28134	1	9	
Band 10				
TPM1 Tropomyosin alpha-1 chain	32660	2	8	
CPIN1 Anamorsin	33407	1	5	
SPEE Spermidine synthase	33972	1	10	
Do not appear to correspond to any band				
HDGF Hepatoma-derived growth factor	26252	3	6	40
IBP2 Insulin-like growth factor-binding protein 2	32740	3	3	35
KLK8 Kallikrein-8	28505	2	-	Unknown

Appendix 4: Supplementary Information for Chapter 6

Net effect of changes in the low MW composition of the medium

As in section 6.3.1.1, we collected either Day 1-2 or Day 0-2 CM from D3 mESCs grown at 40,000 cells/cm^2. We also collected control medium that had been incubated for the identical length of time in a similar dish. We dialyzed both media to obtain the <3kDa fraction and replenished the proteins. We applied either 25% CM or 100% CM to a fresh batch of cells and measured growth over a 24 hour period. In a separate experiment with the same set of cells, we measured growth over Day 1-2 for cells plated at 10,000 cells/cm^2 and 40,000 cells/cm^2 (Figure A4.1). We observed that relative Day 1-2 fold growth for cells plated at 40,000 cells/cm^2 (0.62 ± 0.03) lay between the value for relative fold growth in Day 0-2 CM (0.57 ± 0.06, p=.03) and the value for Day 1-2 CM (0.77 ± 0.03, p=1.6e-4). This data suggests that changes in the low MW composition of the medium are primarily responsible for the decrease in the growth of mESCs at high plating densities.

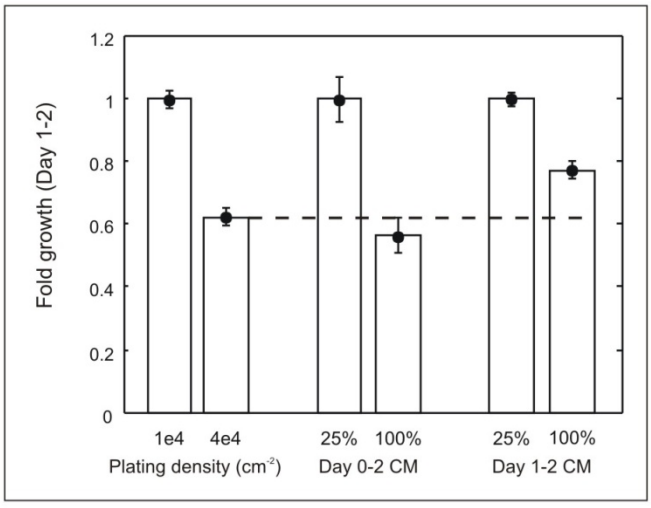

Figure A4.1 (Left) Relative fold growth over Day 1-2 for cells plated at 10,000 and 40,000 cells/cm^2. (Center and Right) Relative fold growth over Day 1-2 for cells plated in 25% and 100% CM, for Day 0-2 and Day 1-2 CM respectively.

Amino acid uptake in cell cultures

Of the three cell types described in Griffiths *et al.*[136] and Duval *et al.*[137], the 6H2 hybridoma cell line described by Duval[137] has the highest amino acid uptake rate for most species. We used the uptake rate of this cell type to determine the amount of amino acids taken up by $1.5.10^5$ cells in 50 hours. $1.5.10^5$ cells corresponds to the approximate average number of cells per well for the density used in our AA depletion experiment. From this, we determined the percentage of amino acid consumed for each species (Table 1), and the residual amount of AA in the medium at the end of the culture. It is easy to see that the amount of AA remaining is typically 4-5 more than that required by cells for optimal growth (see chapter 6). Additionally, values measured for 6H2 cells and our measurements for mESCs are comparable.

Table 1: Consumption of essential amino acids by $1.5.10^5$ 6H2 hybridoma cells in 50 hours

Amino Acid	% consumed	µM remaining	µM required	% consumed mESC
L-Arginine	17	459	100	23
L-Cystine	31	34	10	
L-Glutamine	31	1038	300	
L-Histidine	7.5	162	100	11
L-Isoleucine	12.4	525	100	14
L-Leucine	14	537	100	18
L-Lysine·HCl	8	600	100	4
L-Methionine	12	140	30	18
L-Phenylalanine	7.6	277	30	14
L-Threonine	6	588	100	33
L-Tryptophan	13.5	54	10	
L-Tyrosine	9	273	100	15
L-Valine	8	576	100	11

More vitamin uptake rate references

In this section we provide further references that contain data on the uptake rate of vitamins, to support the data and references already provided in Table 6.3.

Thiamine (B1)

1. Uptake was not measurable in LS fibroblast cells.
2. *J Physiol* 582 (2007) pp 73–85
   Vitamin B1 (thiamine) uptake by human retinal pigment epithelial (ARPE-19) cells: mechanism and regulation
   ~ 1 pmol/mg protein/minute
3. *Am J Physiol. Gastrointest Liver Physiol* 60 (2009) pp G825-G833
   Enteropathogenic Escherichia coli inhibits intestinal vitamin B 1 (thiamin) uptake: studies with human-derived intestinal epithelial Caco-2 cells
   ~ 0.4 pmol/mg protein/minute

Uptake rates from the two citations above are comparable.

Riboflavin (B2)

For Riboflavin, a wide range of uptake rates have been measured.

1. LS cells: ~ 5e-2 pmol/mg protein/minute
2. *J Pharmacol Exp Ther* 298 (2001) pp 264-271
   Riboflavin Uptake in Human Trophoblast-Derived BeWo Cell Monolayers: Cellular Translocation and Regulatory Mechanisms
   ~ 6e-3 pmol/mg protein/minute
3. *Am. J. Physiol. Cell Physiol.* 278 (2000) pp C270–C276
   Riboflavin uptake by human-derived colonic epithelial NCM460 cells
   ~ 1 pmol/mg protein/minute

D-Pantothenate (B5)

1. LS cells: ~ 70 pmol/mg protein/minute
2. *Placenta* 18 (1997) pp 527-33
Characterization of a sodium-dependent vitamin transporter mediating the uptake of pantothenate, biotin and lipoate in human placental choriocarcinoma cells.
~ 34 pmol/mg protein/minute
3. *J Bacteriol* 162 (1985) pp 1156–1161
Pantothenate transport in Escherichia coli
~ 45 pmol/mg dry weight/minute

Uptake rates in all citations are comparable.

Pyroxidine (B6)

1. LS cells: ~ 2 pmol/mg protein/minute
2. *Nut Metab* (1993) pp 85-89
Pyridoxine-5'-0-D-Glucoside competitively inhibits uptake of Vitamin B-6 into isolated rat liver cells
~ 1 pmol/mg protein/minute at physiological concentrations (i.e. not Vmax)

Uptake rates in both citations are comparable.

D-Biotin (B7)

1. LS cells: ~40 fmol/mg protein/minute
2. *J Nutr* (2003) pp 2703-2706
Monocarboxylate transporter 1 mediates biotin uptake in human peripheral blood mononuclear cells
~ 40 amol/mg protein/minute
3. *Am J Physiol Renal Physiol* 288 (2005) pp 823-831
Biotin uptake by human proximal tubular epithelial cells: cellular and molecular aspects
~ 200 amol/mg protein/minute at 0.01 µM biotin

Uptake rates are comparable in 2 and 3. The uptake rate for LS cells is 3 orders of magnitude higher and hence we assume that there is some error in the measurement or reporting. I used the higher of 2 & 3 (i.e. 3) in the calculation.

Myo-inositol (B8)

1. LS cells: ~ 40 pmol/mg protein/minute
Biochem J 254 (1988) pp 95-100
2. Uptake and metabolism of myo-inositol by L1210 leukaemia cells
~ 4 pmol/mg protein/minute for 50 µM myoinositol
3. *Invest Ophthalmol Vis Sci* 3 (1994) pp 1223-1235
Osmoregulatory Alterations in Myo-Inositol Uptake by Bovine Lens Epithelial Cells
~ 8 pmol/mg protein/minute for 50 µM myoinositol

Uptake rates in LS cells seem to be a little high, but nevertheless, expected percent uptake is only 2.5% for our experiments.

Folic Acid (B9)

J Pharmacol Exp Ther 233 (1982) pp 224-226
Effect of phenytoin on folic acid uptake in isolated intestinal epithelial cells
~ 2 pmol/mg protein/minute
Am J Clin Nutr 86 (2007) pp 159-166
Effect of folate oversupplementation on folate uptake by human intestinal and renal epithelial cells
~ .01 pmol/mg protein/minute

Even at the higher uptake rate (1), folic acid depletion is expected to be only 1% in our experiments.

Cobalamin (B12)

J Clin Inv 61 (1978) pp 133-141
Binding and Uptake of Transcobalamin II by Human Fibroblasts
~ 5 amol/mg protein/minute

Choline Chloride

1. LS cells: ~ 200 pmol/mg protein/minute
2. *J Nutr* 114 (1984) pp 2217-2220
   Choline Uptake by Isolated Enterocytes of Guinea Pig
   ~ 200 pmol/mg protein/minute
3. *J Lipid Res* 27 (1986) pp 1205-1213
   Effect of ethanolamine on choline uptake and incorporation into phosphatidylcholine in human Y79 retinoblastoma cells
   ~ 50 pmol/mg protein/minute

Uptake rates in all citations are comparable.

Appendix 5: Our Cell Lines

We have assessed the pluripotency of two of the cell lines used in this thesis via *in vitro* differentiation assays.

Methods: Total RNA was extracted from cell cultures using Guanidinium thiocyanate-phenol-chloroform extraction (using TRIzol from Invitrogen). Then contaminating genomic DNA was degraded by incubating with DNAase I (Invitrogen). We prepared cDNA using SuperScript II Reverse Transcriptase (Invitrogen) and Oligo$(dT)_{20}$ primer (Invitrogen). Primers were designed using PCR3, and the PCR reactions were performed using Taq DNA polymerase (Invitrogen). Annealing temperature was 55^{o}C for all primers except Brachury, for which we used 50^{o}C. 30 cycles were performed for all reactions, except Brachury, for which 35 cycles were performed. The PCR products were run on 1.5% agarose gels with 0.4 µg/ml ethidium bromide and visualized with UV.

The primers used were:

Oct-4:	ACCATGTTTCTGAAGTGCCCGAAG
	TGCCTCAGTTTGAATGCATGGGAG
Nanog:	TGAGACTTACGCAACATCTGGGCT
	TCAGGAGGCAAAGATAAGTGGGCA
Sox-2:	CGCGCGCATGTATAACATGATGGA
	TCCGGGAAGCGTGTACTTATCCTT
Gapdh:	CACTGAGCATCTCCCTCACA
	GTGGGTGCAGCGAACTTTAT
Fgf-5:	ACCCTTTGAGCTTTCTACCC
	CCGTCTGTGGTTTCTGTTGAGG
Brachury:	GCCAAAGAAAGAAACGACCA
	TGACCGGTGGTTCCTTAGAG
Gata-4:	CACTATGGGCACAGCAGCTCC
	TTGGAGCTGGCCTGCGATGTC

Results:

We performed PCR reactions as listed in the methods, with cDNA (obtained from RNA) collected from either undifferentiated cells, or cells at day 7, 15, or 40 of differentiation. The original undifferentiated cells had been cultured in N2B27 + LIF + BMP-4 for 15 generations. As can be seen below, undifferentiated cells expressed transcripts for Oct-4, Nanog and Sox-2, and the relative numbers of transcripts decreased with increasing differentiation. Gata-4, Brachury, and Fgf-5 were chosen as primitive markers of endoderm, mesoderm, and ectoderm germ layers respectively. Undifferentiated cells expressed very low levels of these transcripts. Fgf-5 and Brachury expression was visible on day 7 (Day 10 for Brachury expression in D3s), while Gata-4 expression was observed on Day 15.

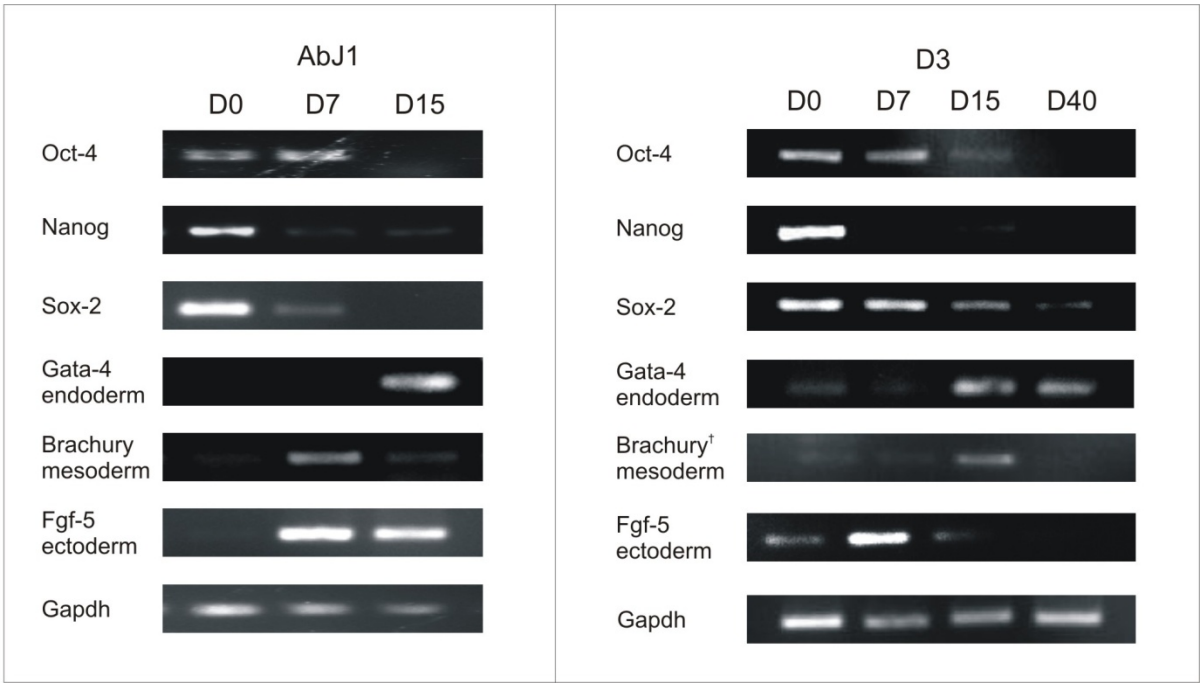

† This panel shows PCR products from RNA collected on days 0, 7, 10, and 30.

Acknowledgements

I would like to start by thanking Joel for taking me on as a graduate student in his lab, for advising me over the course of my PhD, and for letting me go where the science took me. Many thanks also to all members of the Voldman lab (May 2005- May 2010) who contributed critiques and suggestions during our weekly group meetings. Special thanks to those who trained me on the use of various techniques – Katarina Blagovic, Laralynne Przybyla, Brian Taff, Adam Rosenthal, and Stephanie Flavin. Also a special thanks to Mike Vahey for many consults on numerical analysis/techniques.

I would also like to acknowledge the contribution of the Biopolymers Laboratory at the Koch Center for Integrative Cancer Research at MIT, namely, performing the mass spectrometric analysis, and especially thank Dr. Ioannis Papayannopoulos for additional support with the gel-MS analysis. Thanks also to Hari Jayaram for initially loaning us a silver staining kit.

Last, but certainly not least, I must acknowledge the love, support, and encouragement offered by my family and friends, especially Manisha.